Universitetet i Stavanger

Faculty of Science and Technology

MASTER'S THESIS

Study program/ Specialization:	**Spring semester, 2018**
Offshore Technology/Subsea and Marine technology	Open / Restricted access
Writer: Yuri Egorov	…… (Writer's signature)

Faculty supervisor: Ove Tobias Gudmestad

External supervisor: Anatoly Borisovich Zolotukhin

Thesis title: Feasibility study of the concept of the Dolginskoye field development with subsea production systems.

Credits (ECTS): 30

Key words: marine operations, marine design, installation of the subsea templates, wave load, ice load, subsea production systems.	**Pages:** 100 + enclosure: 14 **Stavanger**

Abstract

This master`s thesis is dedicated to the Dolginskoye oil field development concept comprising of a gravity base structure with subsea production systems. This field is located in the central part of the Pechora Sea. The ice cover in the Dolginskoye field area is formed in September and remains until July, which seriously complicates the develop ment process. Application of subsea production systems in such an environment enables all-year production from the field substantially reducing the risk of operations in adverse climatic conditions.

One of the challenging problem is the installation process. What kind of vessels is required for the Dolginskoe area environment? Different types of vessels have been reviewed when trying to answer this question. It is known that heave is most important for vertical operations. Therefore, the heave periods are calculated and compared with the wave periods to avoid the resonance.

Moreover, the load on the gravity base structure is one of the key factors in the conceptual analysis. What type of load will prevail in this environmental condition? Two types of gravity base structures were considered in this study: (1) a monopod platform with vertical walls and (2) a platform with sloped walls. For calculations, the Monte Carlo method was implemented in the MATLAB software.
Different concepts of development and evaluation of reliability and quality (issues of HSE) of each of the concepts and cost-effectiveness were considered.

Key words: marine operations, marine design, installation of the subsea templates, wave load, ice load, subsea production systems.

Acknowledgement

I would like to thank those persons who helped during writing this thesis. I am very grateful to Professor Anatoly Borisovich Zolotukhin and Professor Ove Tobias Gudmestad for their support, advice, wisdom and patience. Also I would like to express my sincere gratitude to Vladimir Pavlovich Balitsky for his support in all endeavors. In addition, I would like to express my appreciation to Professor Svejnun Löset and Alexei Shestov for conducting the course "Arctic Technologies" in the Svalbard, which became the basis for this work. Also, I am grateful for the advices and support to the following people: Andrey Ponomarev, Pavel Liferov, Urysheva Marya, Igor Koptsov and many other good people!

List of figures

Figure 1-1 Location of the Dolginskoye oil field……8
Figure 1-2 Monthly extreme minimum and average daily minimum air temperatures in North Kolguyev and Varandey, Pechora Sea….12
Figure 1-3 Histograms of dates of ice clearance, ice formation, and ice free days in the Pechora Sea……14
Figure 1-4 Probability distribution of ice thickness in the Pechora and Kara Seas (April)……..16
Figure 1-5 Geological map of the Dolginskoye field……18
Figure 2-1 Hibernia……21
Figure 2-2 Hebron……..22
Figure 2-3 Piltun-Astokhskoye-B……..23
Figure 2-4 Sketch of the monopod platform……..25
Figure 2-5 Side view on the monopod platform……26
Figure 2-6 Sketch of the monocone platform……26
Figure 2-7 Side view on the monocone platform……..27
Figure 2-8 Wave force result when H=4.7 m……31
Figure 2-9 The probability density function of the wave load……..34
Figure 2-10 The exceedance distribution function……..35
Figure 2-11 Wave force result when H=4.7 m……37
Figure 2-12 The probability density function of the wave load……..38
Figure 2-13 The exceedance distribution function……..38
Figure 2-14 Ice load on a monopod structure……..40
Figure 2-15 Probability distribution of compressive strength of ice in the Pechora and Kara Seas (April)……..43
Figure 2-16 Probability distribution of ice thickness in the Pechora and Kara Seas (April))…….……...44
Figure 2-17 The probability density function of the ice load (Global ice action)……...44
Figure 2-18 The exceedance distribution function (Global ice action)…..…..45
Figure 2-19 The probability density function of the ice load (Korzhavin)……45
Figure 2-20 The exceedance distribution function (Korzhavin)……..45
Figure 2-21 The probability density function of the ice load (ISO 19906)…..46
Figure 2-22 The exceedance distribution function (ISO 19906)……..46
Figure 2-23 The probability density function of the ice load……51
Figure 2-24 The exceedance distribution function ……..51
Figure 3-1 Arctic subsea facilities…….42
Figure 3-2 Proposed Glory Hole Protective Structure with Gravel/Rock Fill and Protective Dome with Access Ports and Doors for Drilling and Maintenance…….44
Figure 3-3 Top view of the subsea facilities…….……..46

List of tables

Table 1-1 Average monthly wind speeds and directions (U , m/s) wind speed standard deviations (σ U , m/s), average frequencies during month (n ,%) of these speeds at Kolguyev Island.…….....10

Table 1-2 Ice drift speeds in the Pechora Sea.……..15

Table 2-1 Structure type and terms of their application ……..20

Table 2-2 Probability distribution of ice thickness in the Pechora and Kara Seas (April)……..24

Table 2-3 The annual maximums of wave periods and wave heights …….34

Table 2-4 Wave force results from MATLAB ……35

Table 2-5 Wave force results from MATLAB…….38

Table 2-6 Ice load results (for ice: $\sigma_c = 1.415$ MPa, h = 1.2 m, I = 1.1)……...42

Table 2-7 Ice load results from MATLAB…….……..47

Table 2-8 Ice load on the monocone (for ice: $\mathbf{D = 66\ m, \sigma_f = 0.52\ MPa, h = 1.2\ m}$)……..50

Table 2-9 Ice load on the monocone …….51

Table 2-10 Comparison of wave loads on the platforms…….52

Table 2-11 Comparison of ice loads on the platforms (Global ice action – ISO 19906)……...52

Table 2-12 Comparison of ice loads on the platforms (Korzhavin – ISO 19906)……...52

Table 2-13 Comparison of ice loads on the platforms (ISO 19906)……52

Table 3-1 Subsea projects located in the similar conditions with Dolginskoye field ……..…41

Table 3-2 The heave period of the installation vessels…….……58

Content

Abstract 2
Acknowledgement 3
List of figures 4
List of tables 5
Content 6
1. Introduction 9
1.1 Geography and resources of the Pechora Sea 9
1.2 Meteorological and hydrological parameters of the Pechora Sea 11
1.2.1 Wind 11
1.2.3Air temperature 12
1.2.4 Current 13
1.2.5 Waves 13
1.3 Ice Conditions in the Pechora Sea 14
1.3.1 Ice formation 14
1.3.2 Landfast ice 15
1.3.3 Drift ice 16
1.3.4 Ice thickness 16
1.3.5 Shear zone 17
1.3.6 Ridges 17
1.3.7 Grounded hummocks (stamukhas) 18
1.4 Field geology 19
2. Design of the gravity base structure 21
2.1 Challenges associated with the Arctic 21
2.2 Best practices 22
2.3 Possible GBS concepts 25
2.1.1 Monopod platform with vertical walls 26
2.1.2 Monocone structure 27
2.2 Wave load 29
2.2.1 Wave load on the monopod platform 32

2.2.2 Wave load on the monocone platform 38
2.3 Ice load 41
2.3.1 Ice load on the monopod structure 41
2.3.2 Ice load on the monocone structure 49
2.3.3 Preliminary conclusions 53
3. Main Subsea Projects 56
3.1 Subsea production and transportation 56
3.2 Protection of subsea equipment 58
3.3 Subsea processing 59
3.4 Best practice - the Goliat 59
3.4.1 General information 60
3.4.2 Subsea Concept 60
3.4.3 Special Features 62
3.4.4 Alternative Subsea Solution 64
3.4.5 Key Risks Identification Related to Subsea Development 65
3.5 Preliminary conclusion 66
3.6 Analysis of possible vessels for the template installation 66
3.6.1 Multipurpose service vessels 67
3.6.2 Heavy lift vessels 67
3.6.3 Construction vessel 67
3.6.4 Barges 68
3.6.5 Heave period calculation 68
3.6.6 Selection of vessel 73
4.1 Scenario A 77
4.1.1 Drilling and maintenance of the wells 77
4.1.2 Oil production, processing and storage 79
4.1.3 Production profile 81
4.1.4 Transportation 84
4.1.5 Economic Efficiency 84
4.2 Scenario B 89

4.2.1 Drilling and maintenance of the wells 89
4.2.2 Oil production, processing and storage 91
4.2.3 Production profile 92
4.2.4 Transportation 93
4.3 Economic Efficiency 94
Summary 95
References 96
Appendix 101
A: Data for calculations 101
B: MATLAB transcripts 102
Wave load on the monopod platform 102
Wave load on the monocone platform 104
Ice load on the monopod structure (Global ice action) 106
Ice load on the monopod structure (Korzhavin equation) 108
Ice load on the monopod structure (ISO 19906) 110
Ice load on the monocone structure (ISO 19906) 112

1. Introduction

1.1 Geography and resources of the Pechora Sea

The Dolginskoye oil field is located in the central part of the Pechora Sea in 120 km to the south from the archipelago of Novaya Zemlya and in 110 km to the north from the continental coast as it is illustrated in Figure 1-1. In the administrative relation, the field belongs to the Nenets national Autonomous Okrug (NAO) of the Arkhangelsk region of the Russian Federation (RF), the district center - the city of Naryan-Mar.

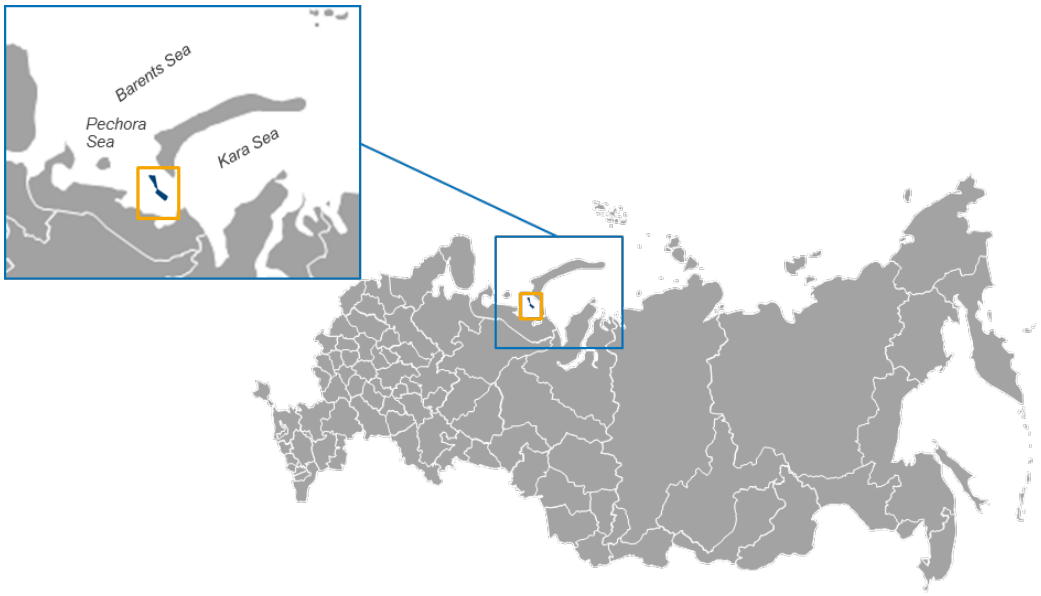

Figure 1-1. Location of the Dolginskoye oil field (Gazpromneft-Sakhalin internal data, n.d.)

According to the Gazpromneft-Sakhalin, the distance to Murmansk is about 960 km. The nearest ports are Naryan-Mar, Arkhangelsk and Murmansk. Murmansk is the main port of the European North of Russia. This is the largest non-freezing port available for vessels with any draft. Murmansk is connected with the central areas of the European part of the country by rail, air and road transport.

The Dolginskoye oil field was discovered by prospecting well 1YD in 1999. According to Fadeev (2014), four exploratory wells are drilled at the field - №1-SD,

№2-D, №1-YD and №3-SD. The oil-bearing capacity of the Lower Permian-Carboniferous deposits is established on the deposit (two oil deposits in the II + III upper Carboniferous-Lower Permian and Middle IV reservoir) have been identified and the oil content of the Upper Permian terrigenous sediments (beds I, II, III, IV). The Central Commission on Reserves of the Ministry of Natural Resources approved the oil reserves of the Dolginskoye field in 2000 in the amount (geological / recoverable): C1 category - 2,976 / 892 thousand tons, C2 category - 783,083 / 234,924 thousand tones.

There are a lot of oil and gas fields across the Timan-Pechora Basin and most of them have not been developed yet. Many fields have been discovered in sedimentary cover of various ages. The reservoirs are divided into two categories: riftal and post-riftal. The reservoirs that are belonging to the first category have been found in Ordovician, Devonian, Silurian and Fransian layers. Those belonged to the second category are laid in Upper Devonian, Tournaisian, Carboiferous (Visean), Permian and Triassic layers (Gazpromneft-Sakhalin internal data, n.d.).

1.2 Meteorological and hydrological parameters of the Pechora Sea

In this section, the metaocean data is considered according to the Gudmestad et al. (1999). Meteorological and hydrological data are needed to ensure that the offshore structures can be designed for endurance to combined loads when calculating. Several meteorological stations are located on the coast of the Pechora Sea. On one of them, located in the northern part of the island of Kolguev, regular observations have been carried out since 1945. At the Varandey and Khodovarich meteorological stations, statistics have been accumulating since 1945 and 1940, respectively.

1.2.1 Wind

The prevailing wind direction depends on the season. In winter, the south-west wind prevails. During summer, the winds are temperate and inconstant with the prevailing north or north-west direction. The duration of the storm during this period in 80-85% of cases does not exceed 12 hours. According to the Russian territory division (SNIP, 1986), the examined region onshore falls under district zone, characterized by 10 min mean wind speeds in winter up to 37 m/s (return period, R_p = 5 years).

The 50-year extreme wind speed (R_p = 50 years) lasting 6-7 hours (long-term period averaging) is equal to 26 m/s. The frequency of wind speeds higher than 16 m/s is close to 12 %. The greatest wind speeds occur from December to February. The highest wind speed is observed from December to February. The values of wind speed at an altitude of 10 m in different seasons based on data from 30-year observations are given in Table 1-1 (observation period 1945-1951, 1953-1977, Kolguev Island):

Table 1-1. Average monthly wind speeds and directions (U , m/s) wind speed standard deviations (σ_U, m/s), average frequencies during month (n ,%) of these speeds at Kolguyev Island. Periods of observation: 1945-1951, 1953-1977 (Gudmestad et al., 1999)

Month	Parameter	Wind direction							
		N	NE	E	SE	S	SW	W	NW
January	$\overline{U}$	10.0	9.4	9.9	8.5	8.8	10.1	9.4	10.5
	σ_U	5.5	4.6	4.6	4.4	5.2	5.2	5.0	5.4
	$\overline{n}$	7	11	9	15	31	32	11	8
May	$\overline{U}$	7.5	7.4	8.1	8.2	7.1	7.2	6.5	7.2
	σ_U	4.3	3.9	4.3	4.6	3.8	3.6	3.4	4.1
	$\overline{n}$	17	15	16	10	10	17	19	20
July	$\overline{U}$	7.2	6.1	6.4	6.7	6.6	7.0	6.0	6.9
	σ_U	4.1	3.5	3.4	3.4	3.5	3.5	3.1	3.8
	$\overline{n}$	2.1	17	18	14	11	10	14	19
October	$\overline{U}$	10.8	10.3	9.3	7.9	6.9	7.7	7.9	10.4
	σ_U	5.6	4.9	4.9	4.4	4.3	4.4	4.1	5.0
	$\overline{n}$	16	14	9	16	21	22	12	14

1.2.3Air temperature

The number of days with an air temperature below 0 ° C is about 230 per year. February is the coldest month with an average temperature in the Varandey area of -18.3 ° C and an absolute minimum of observed temperatures of -48 ° C. The change in average temperature from December to March is small. The variation of the mean temperature from December to March is small. Figure 1-2 shows a substantial decrease in the air temperature from the west (North Kolguyev) to the eastern location, Varandey. The annual mean temperature is - 2.9°C for the North Kolguyev location while it is -5.6°C for Varandey.

Figure 1-2. Monthly extreme minimum and average daily minimum air temperatures in North Kolguyev and Varandey, Pechora Sea. The data derives from the period 1936-1979 for the North Kolguyev Site and 1940-1980 for Varandey (Gudmestad et al., 1999)

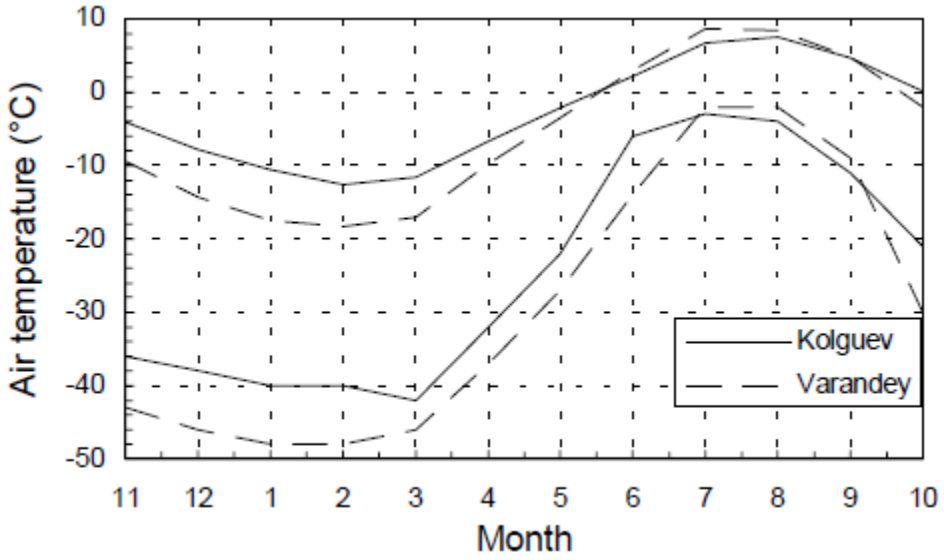

1.2.4 Current

The main direction of movement of water masses (currents) during tides from the southeast to the northwest. During low tide - on the contrary. The speed of the tidal current (in spring) can reach 0.4 m / s. The maximum velocity of wind currents is 1 m / s (Gudmestad et al., 1999).

1.2.5 Waves

The wave regime is substantially influenced by the bordering shorelines, the region is fully protected from the north, east and south, and the water depths are relatively small. The highest waves enter from the northwest and the intensity falls from west to east. The storm season usually starts in October and causes occasionally extreme waves up to 11.5 m at water depths of 20-30 m in October-November. However, the maximum wave height detected in the Dolginskoye field of 4.7 m (Novikov, 2014).

1.3 Ice Conditions in the Pechora Sea

The presence of mainly one-year-old ice of local origin is one of the characteristic features of the Pechora Sea. However, sometimes from the Kara Sea through the Kara gates and the White Sea through the Pomor strait, the ice drifts into the eastern part of the Pechora Sea. The ice season lasts from the end of October - the middle of November to the end of July - the beginning of August. Ice conditions in the eastern part of the Pechora Sea are more severe than in the western part. In particular, the average duration of the ice season in the western part is 185 days, while in the eastern part - 240 days (maximum 300 days). The longest ice cover is observed in March-April, when 10/10 of the surface of the water is covered with ice.

1.3.1 Ice formation

There is a great scatter in the times of ice freeze and melt/retreat. The ice-free period can vary from 0 to 130 days. For instance, the ice-free period for the Prirazlomnoye Field is about 110 days. Histograms of the dates of ice clearance in the area and associated dates of ice formation as well as ice-free duration in the Pechora Sea are shown in Figure 1-3.

During the last 54 years, 4 significant periods and 4 short periods of ice cover were observed. Three different ice zones are formed in the Pechora Sea: the zone of fast ice, the zone of drift ice, and the intermediate zone (interaction zone) where the drifting ice and fast ice interact.

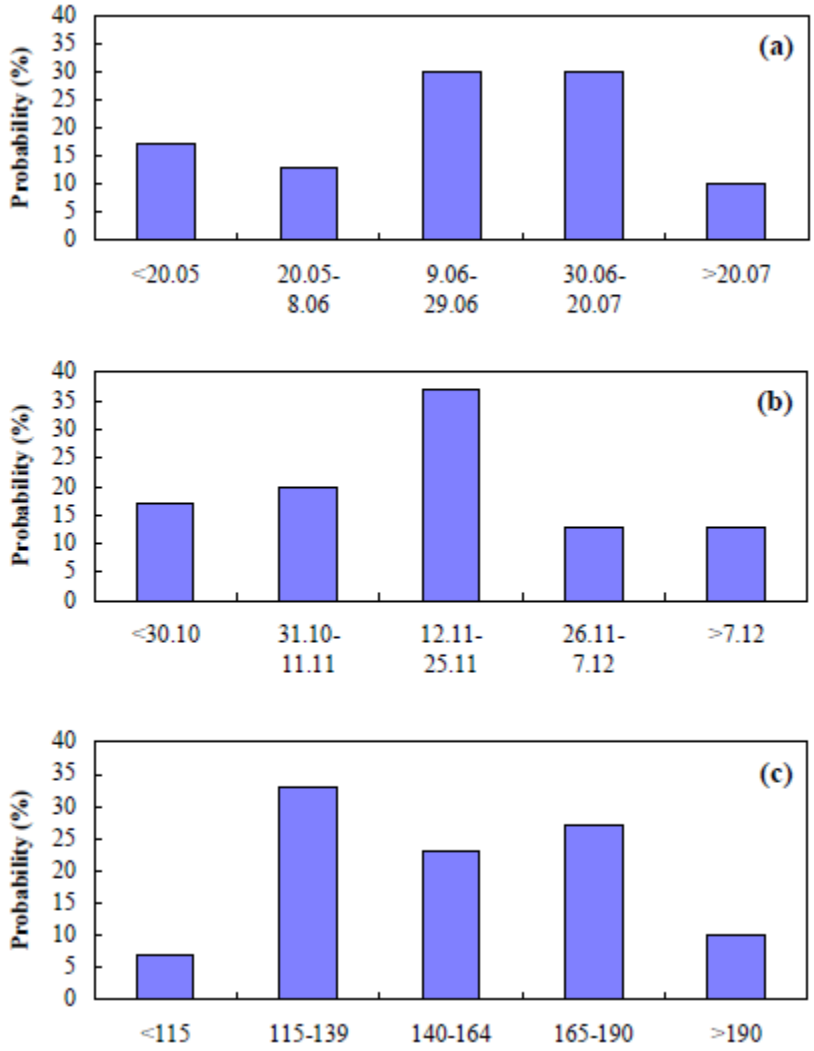

Figure 1-3. Histograms of dates of a) ice clearance, b) ice formation, and c) ice free days in the Pechora Sea (Gudmestad et al., 1999).

1.3.2 Landfast ice

The landfast ice zone during the extreme years extends 10-15 km offshore, reaching depths at 12-15 m. Its formation occurs before the end of February, fracturing starts in April-May in the western part of the sea and in the end of June - in the eastern part. The same trend yields zones located closer to the external fast ice boundary.

The fast ice is not stable, and often its breaking occurs during the winter. This can lead to the formation of hummocks and 60-80% of the entire sea surface can be occupied by hummocks (hummocking is 3-4 points, ie 1 point indicates that 20% of

the sea surface is covered with ice). The average ice thickness is 0.8-1.1 m. On the boundary of fast ice zones and drifting ice, there is an intense process of ice hummocking. As a result, ridges of hummocks and stamukha are formed. Stamukha shield coastal ice, protecting it from destruction.

1.3.3 Drift ice

In general, the drift of ice is caused by the action of wind and current. The predominant direction of ice drift in winter is northern, and in the spring - west and south-west. Wind drift can be characterized by a drift coefficient that relates the speed of wind and ice. Table 1-2 presents ice drift speeds in the Pechora Sea. When including currents and waves, the drift speed will normally be higher.

Table 1-2 Ice drift speeds in the Pechora Sea (Gudmestad et al., 1999).

Region	*Ice drift speed due to win (m/s)*	
	Average	*Maximum*
East	*0.09*	*0.6*
West	*0.15*	*1.0*

1.3.4 Ice thickness

The maximum average thickness of the sea ice in the eastern part of the Pechora Sea is 1.1 m, but the absolute maximum amounts to 1.6 m. Figure 1-4 illustrates the probability distribution function of ice thickness for April (the month with maximum ice thickness).

Formation of rafted ice at a thickness up to 2.5 m is considered to be possible in the conditions of dynamic interaction of ice fields, but the probability of such phenomena is not defined. In the majority of cases, the area of drift ice fields is approximately 0.2-4 km^2 but sometimes ice floes with area more than 78 km^2 can be found.

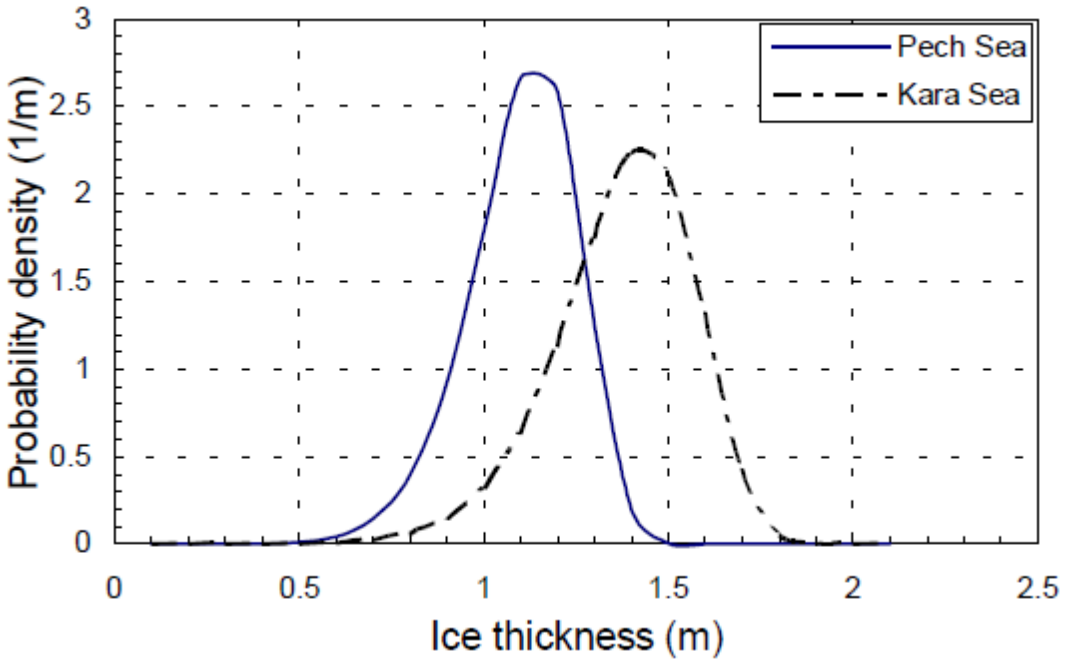

Figure 1-4. Probability distribution of ice thickness in the Pechora and Kara Seas (April) (Gudmestad et al., 1999).

1.3.5 Shear zone

This zone is located between the zones of coastal and drifting ice and is characterized by the most intensive interaction of ice fields. A large number of hummocks, ridges hummocks and stamukha formed in the intermediate zone. The width of the zone can vary from several hundred meters to several kilometers.

1.3.6 Ridges

The frequency of ice ridges (ridge density) increases from the shore to the external fast ice boundary and from the west to the east. In the drifting ice zone, the number of hummocks decreases with distance from the interaction zone. In the Varandey headland region, the ridging intensity (sea surface covered by hummocks) in February can reach 60-80 %, and in April, 80-100%. In the landfast ice zone, the ridging intensity can be equal to 60-80% and in some local areas, a few kilometres long, up to 100% (total).

The ridges of the area consist of blocks 0.3-0.6 m thick (sometimes up to 1.1 m) and 2-4 m long. The sail height is in the range of 0.5 to 2.5 m in 80 % of the cases, while in 10 % of the occasions it exceeds 2.5 m. The maximum ridge height of 4.6 m was observed in the southern part of the Pechora Sea. The consolidated ridge layer thickness is twice (according to some sources 2.5 times) as large as that for level ice thickness. On the other hand, some authors affirm that ridge consolidation in the winter is very low. The ridge keel depth in the Pechora Sea is on the average up to 3-6 m, but can sometimes reach 12 m and more (Gudmestad et al., 1999).

1.3.7 Grounded hummocks (stamukhas)

Grounded hummocks usually form at the edge of the fast ice. They are located at water depths of 7-15 m. Stamukhas were not observed at water depths exceeding 20 m. Very often, stamukhas form a chain at the same place from year to year. In the Pechora Sea they are located mainly in the vicinity of the Matveev and Dolgy Islands and along the southern extremity of Novaya Zemlya. Stamukhas consist mostly of ice blocks that are not consolidated. Their porosity is 30-35 %. The sail height can reach 7-12 m while the length can be hundreds of metres. The prevailing length is 30-150 m (Gudmestad et al., 1999).

1.4 Field geology

In this section the main features of the Dolginskoye filed geology is considered. The main part of the Arctic shelf is a platform area having a sedimentary cover up to 10-20 km thick that forms basins favorable for accumulation of oil and gas. In general, Arctic natural reservoirs have heterogeneous geological structure. The Dolginskoye field belongs to the Timan Pechora Basin that is a part of the Arctic shelf oil and gas-bearing basins (OGB) together with the Barents Sea Basin, the Southern Kara Basin and the Laptev Sea Basin (Gudmestad et al., 1999). The geological map of the field is shown in Figure 1-5.

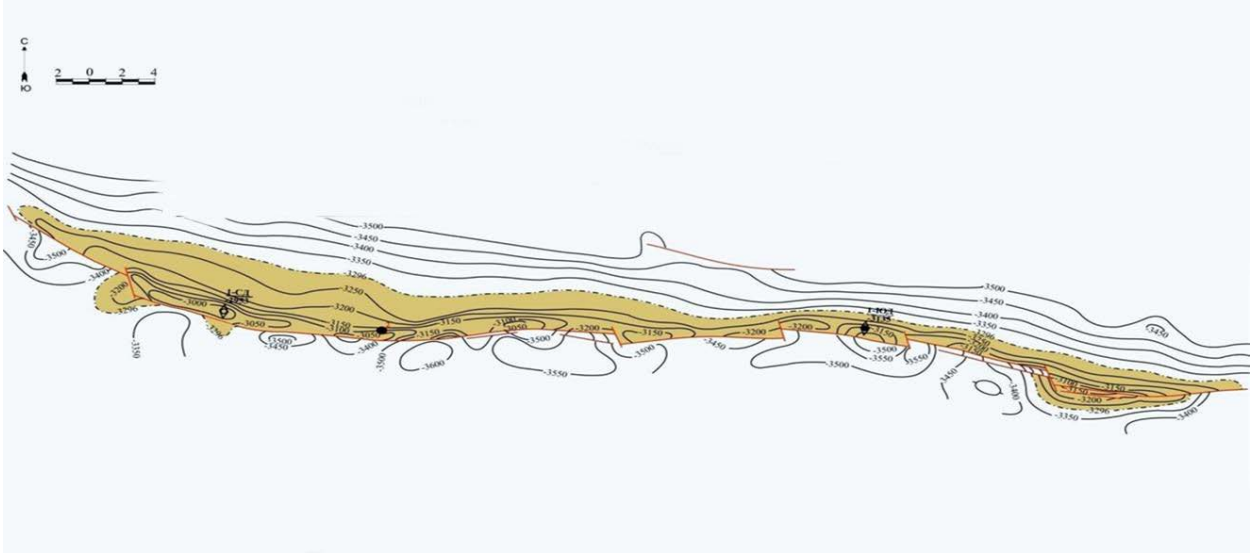

Figure 1-5. Geological map of the Dolginskoye field (Gazpromneft-Sakhalin internal data, n.d.)

The size of the Dolginskoye field along its long axis is approximately from 75 to 90 km depending on depth of the field. The field is almost equally divided into two parts, the South Dolginskaya and the North-Dolginskaya positive structures.

The general thickness of the sedimentary cover in the region of the Dolginskoye field is about 6-8 km. Currently, five exploration well: "№1-SD, №2-D, №1-YD and №3-SD have been drilled by LLC «Gazflot» at the South-Dolginskaya and the North-Dolginskaya structures respectively (Fadeev, 2014). According to geological

oil and gas zonation, the Dolginskoye field belongs to the Varandey-Adzvinskaya oil-and-gas bearing region, within which five oil-bearing zones are found. The zones are following (Gazpromneft, 2014):

- Silurian - Lower Devonian carbon-bearing;
- Mid-Devonian - Fransian terrigenous;
- Upper Devonian - Lower Fransian carbon-bearing;
- Permian - Carboniferous carbon-bearing;
- Lower Triassic terrigenous.

Estimation of C1+C2 categories of the Dolginskoye field's recoverable reserves gives the value of about 235.8 mln. tonnes (C1 – 0,9 mln. tonnes). According to the VNIIGAZ (2008), 92.4 % of recoverable reserves are in the North-Dolginskaya structure, 78.2 % of which related to the Upper Permian terrigeneous deposits. Moreover, based on the welllog survey data the reservoirs of the North-Dolginskaya structure have better quality (porosity and permeability) than the South-Dolginskaya.

2. Design of the gravity base structure

It is still a big challenge to design a GBS for the Arctic continental shelf because of severe condition and high loads on the structure. In order to understand and choose the type of platform, it is necessary to understand what problems and challenges can arise during the development and consider the best world practices associated with this topic. The challenges associated with the Arctic, best practice, possible GBS concepts, load calculations and platform selection are discussed further.

2.1 Challenges associated with the Arctic

To get a broad understanding of the conditions at some of the fields located in cold climate or Arctic regions such as Hibernia, Hebron, Sakhalin and Goliat, it is useful to discuss the environmental conditions at these sites. The main challenges encountered in these regions are listed in the following table:

Table 2-1. List of the challenges (Egorov, 2017)

Challenge	
Metaocean	Wind
	Waves
	Current
	Weather forecast
	Visibility
	Low temperature
	Icing
Sea ice	Level ice
	Ice ridges
	Icebergs
	Short open water period
Ecological	“Fragile” ecosystem
	Elimination of the consequences
Technological	Undeveloped infrastructure
	Complexity of logistics
	Uniqueness of technologies and equipment
	High qualification requirements for personal
	Absence of standards

2.2 Best practices

Several GBS structures were applied in the regions of the Arctic and the subarctic cold climate. One example is the world's largest oil platform: Hibernia is illustrated in Figure 2-1. Located 315 km east of southeast of St. John's, New Base in Canada. The height of the platform is 224 m and water depth in this area is 80 m. It witnesses some of the harshest conditions observed on Earth, including extreme fog (~ 124 days / year), snow, rain and wind. The jagged edges allow the platform to withstand the loads of sea ice and iceberg, which makes it possible to produce year-round production.

Figure 2-1. Hibernia (KBR, 1997)

The GBS, which sits on the ocean floor, is 111 meters high and has storage capacity for 1.3 million barrels of crude oil in its 85-metre-high caisson, it is considered the largest of its kind in Arctic conditions. Although return period for such large icebergs reaching Hibernia is down to 10^{-4}, the structure has been designed to resist them sustaining only repairable damage. The number of icebergs within the Hibernia ice-monitoring zone has been 45 per year since the installation of the platform in 1997 (Jacques Whitford Ltd, 2009). Standby support vessels have to-date managed to tow away all icebergs encountered near the platform (Hibernia, n.d.).

Another example of the Arctic design of GBS structure is Hebron. The GBS for the Hebron Project is a reinforced concrete structure designed to withstand impacts from sea ice and icebergs and the meteorological and oceanographic conditions at the Hebron Field. The GBS is designed to store 190,000 m^3 of crude oil in multiple separate storage compartments (Hebron project, 2011).

According to Widianto et al. (2016), the Hebron offshore oil development project consists of the following major components:

- Reinforced concrete gravity-based structure (GBS) consists of a base, a caisson, and a single shaft supporting the topsides structure;
- Topsides structure with all systems and equipment required to support drilling, processing, utilities, and living quarters; and
- Offshore oil loading system (OLS) with a looped pipeline and two separate loading stations about 2 km (1.2 miles) from the GBS.

The platform is installed in a water depth of approximately 93 m on the Grand Banks, 340 km from St. John's, NL, Canada, and close to the existing Terra Nova, White Rose, and Hibernia platforms.

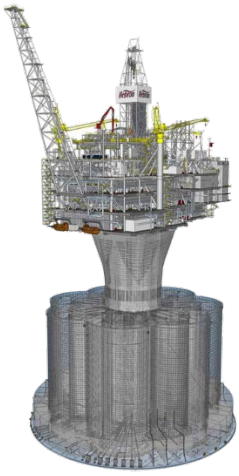

Figure 2-2. Hebron platform illustration (Hebron project, n.d.)

Other examples of GBS structure Arctic developments are Piltun-Astokhskoye-B (PA-B) and Lunskoye-A (LUN□A) off the east coast of Sakhalin Island in Russia. Although PA□B is shown in Figure 2-3 is a production and export platform, LUN□A is mainly used for drilling with limited processing capacity.

Figure 2-3. Piltun-Astokhskoye-B (Sakhalin Energy, n.d.)

The climatic conditions on Sakhalin are extreme. The northern end of Sakhalin is characterized by cold windy winters with minimum recorded temperatures of -48°C, although in January it is around -22.8°C , and a foggy summer with temperatures above 14°C in August. The icing is extreme in the region, where ships and offshore objects are pouring from November to May, and in some cases even in June, September and October. The combination of these harsh conditions with the formation of sea ice since November and the development of migratory ridges along the shoreline creates complex design work for pipelines, onshore approaches and platforms.

2.3 Possible GBS concepts

According to Bellendir and Toropov (2000), the possible types of GBS or pile-type structures for shallow are caisson, monocone, multi-column (2-4 columns) and truss type. Table 2-2 lists the conditions and specific features for application of the above types.

Table 2-2. Structure type and terms of their application (Bellendir and Toropov, 2000)

Type	Water	Terms of application	Loading specific features
Caisso	Less	Superstructure weight > 30000t. Presence of oil storage. Large amount of wells (>50).	The wall is almost vertical (angle α with the horizon > 60°). Extreme global ice load (4÷5 MN per one linear meter) exceeds wave load. The effect of ice and wave impacts on soil foundation is comparable due to wave dynamic effect.
Mo	Up	Superstructure weight 15000÷30000t. Large amount of wells up to 50.	The wall is inclined 45°> α >60 °. The values of extreme global and wave loads are comparable. Due to slamming, the integrated deck must be considerably elevated above MSL.
Multi-	Up to		Column walls are vertical or inclined in MSL zone. The values of extreme global wave load is less than ice load. The ice load may be considerable, especially for depths less than 20 m. Integrated deck slightly elevated above MSL.
Truss	Up to	Superstructure weight < 2000 t. Number of wells <20.	Ice toad surpassing wave load.

The water depth in the field location varies from 20-25 m in Southeast part to 40-45 m in North-West part. The first part has flat bench-like surface, while the second is slightly sloped in North-West direction (Novikov, 2014). Taking into account the water depth limitations the caisson and truss type structures can only be used in the

Southeastern part of the field. The monocone and multi-columns are preferable in the Northwestern part.

In this chapter, the two concepts of the GBS are considered such as the monopod platform with vertical walls and the monocone structure. However, the caisson structures also could be used in the Arctic area, for instance Ice Resistant Gravity Base Structure (IRGBS) “Prirazlomnaya” is used for the oil production in the Pechora Sea near the Dolginskoye oil field. The truss type is neglected due to the number of wells limitations, because the Dolginskoye field development requires a large number of the wells, approximately 100 (*Gazpromneft-Sakhalin internal data, n.d.*). In case of the multi-column platforms there is a challenge regarding to the ice accumulation between the supports and this problem should be considered in the future work.

2.1.1 Monopod platform with vertical walls

The following Figure 2-4 is a sketch of the structure made in Autodesk Inventor in accordance with best practices – Hebron platform. A more detailed drawing of the platform is shown in Figure 2-5. GBS is consist of three main parts:

- Basement – diameter is 110 m and 5 m high;
- Leg – diameter is 35 m and height is 75 m;
- Caisson comprises of eight capacities – each 30 m high and 32 m in diameter.

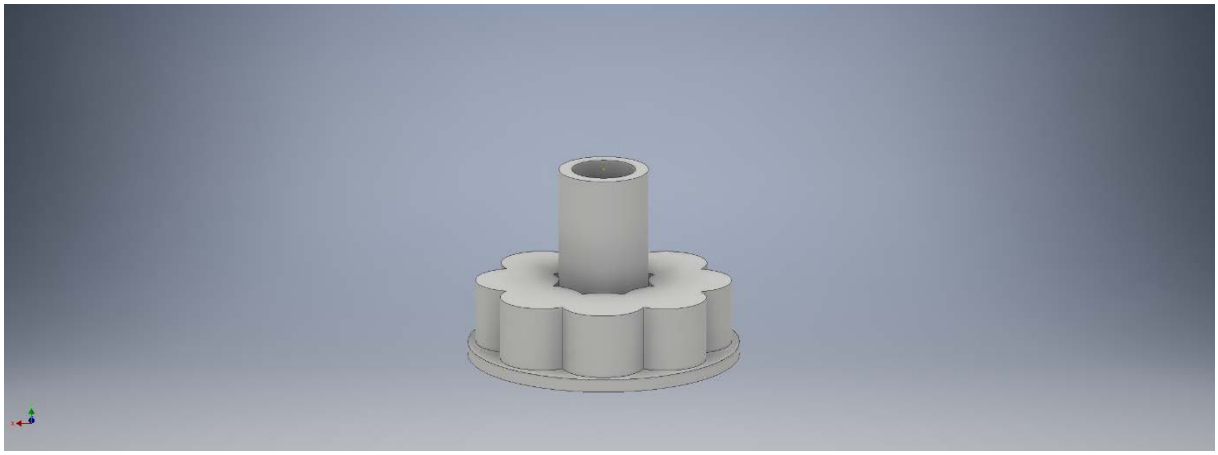

Figure 2-4. Sketch of the monopod platform

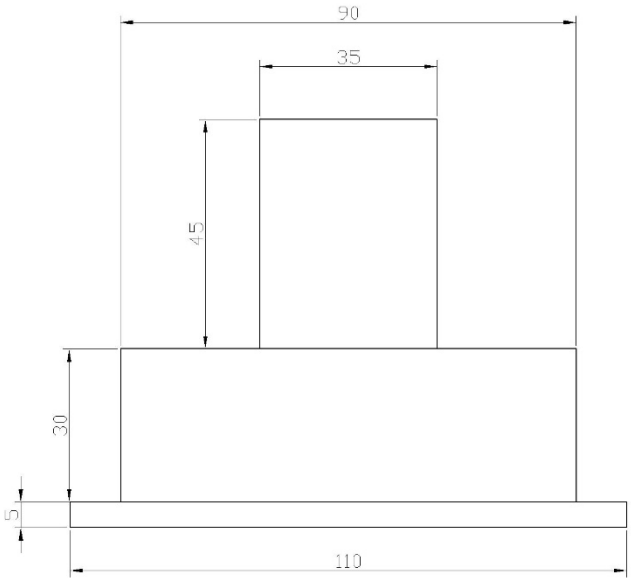

Figure 2-5. Side view on the monopod platform

2.1.2 Monocone structure

In this case, the platform is an upward cone as shown in the Figure 2-6. It is consist of four parts:

- Basement – diameter is 105 m and 5 m high;
- Leg – diameter is 35 m and height is 10 m;
- Upward cone – diameter of base is 90 m and top one is 35 m;
- Caisson – cylinder of diameter 90 m and height of 30 m.

A more detailed drawing of the platform is shown in Figure 2-7.

Figure 2-6. Sketch of the monocone platform

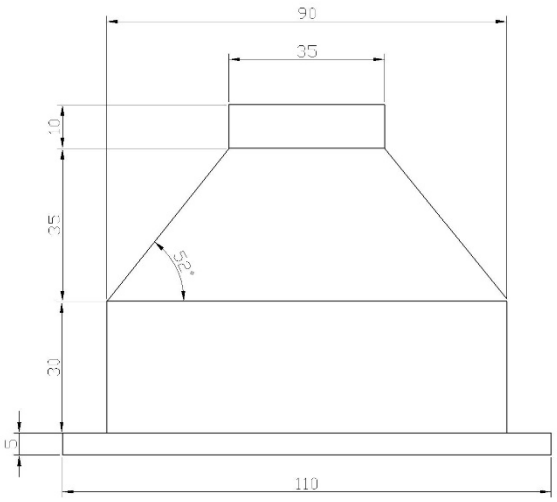

Figure 2-7. Side view on the monocone platform

The diameter of the cone at the water level of 50 m can be computes as:

$$D_{50} = D_{top} + 2(\cot(\alpha) \cdot H) \quad (2.1)$$

Where

D_{top}– diameter at the top of cone

α – angle of slope

H – height of the cone above water level

$$D_{50} = 35 + 2(\cot(52) \cdot 20) = 66.25\ m \quad (2.2)$$

Based on the calculations this diameter was assumed equal to 66.25 m.

2.2 Wave load

The resulting force on a vertical cylinder can be determined using Morison's Equation, which is a combination of an inertial term and a drag term. Gudmestad (2015):

$$F(t) = \int_{-d}^{surface} f(z,t)dz = \int_{-d}^{\xi} f_M(x,t)dz + \int_{-d}^{\xi} f_D(x,t)dz \qquad (2.3)$$

Where

f – total force acting on a unit length of a cylinder in a wave

f_M – mass force per unit length

f_D – drag force per unit length

ξ – wave amplitude

d – water depth

Mass force per unit length can be defined as follows:

$$f_M = \rho \frac{\pi D^2}{4} C_M \dot{U} \qquad (2.4)$$

Where

ρ – water density

D – cylinder diameter

C_M – mass coefficient

$\dot{U}$– horizontal water particle acceleration

Drag force per unit length is:

$$f_D = \frac{1}{2}\rho C_D U|U| \qquad (2.5)$$

Where

C_D –drag coefficient

U– horizontal water particle velocity

According to the Krogstad et al (2000), water is considered to be intermediate water when the criterion $\frac{1}{20} < \frac{d}{L} < \frac{1}{2}$ is satisfied. Wave length in the Pechora Sea is approximately 150 m and water depth is 50 m. Hence condition $\frac{1}{20} < \frac{50}{150} < \frac{1}{2}$ is satisfied. Below are the formulas for the case of intermediate water.

The horizontal velocity is given as:

$$U = \frac{\xi_0 kg}{\omega} \frac{\cosh(k(z+d))}{\cosh(kd)} \sin(wt - kx) \tag{2.6}$$

Where

ω – angular velocity

k – wave number

z – vertical coordinate

x – direction of propagation

The horizontal water particle acceleration is:

$$\dot{U} = \xi_0 kg \frac{\cosh(k(z+d))}{\cosh(kd)} \cos(wt - kx) \tag{2.7}$$

The wave number can be calculated from the dispersion relation:

$$\omega^2 = gk \tanh(kd) = \left(\frac{2\pi}{T}\right)^2 \tag{2.8}$$

Where

T – wave period

$k = 0.0415$

According to the Recommended Practice DNV-RP-C205 (2010):

$$C_A = \begin{cases} 0.2 \ \ rough\ cylinder \\ 0.6\ smooth\ cylinder \end{cases} \tag{2.9}$$

$$C_M = 1 + C_A = 1 + 0.2 = 1.2 \tag{2.10}$$

$$C_D = \begin{cases} 0.65 & smooth\ cylinder \\ 1.05 & rough\ cylinder \end{cases} = 1.05 \tag{2.11}$$

It is necessary to understand in what case the load will be maximum. Check if there is a dominating term:

- If $\frac{D}{H} < 0.1$ then the drag term will dominate.
- The mass term will dominate for $0.5 < \frac{D}{H} < 1.0$.
- In between, both drag and mass terms should be taken into account.
- If $\frac{D}{H} > 1.0$ then parts of the wave will be reflected.

The diameter of the platform is 35 m for monopod and 66.26 m for cone shaped structure and the maximum wave height is 4.2 m (Dymov et al., 2012), hence $\frac{D}{H} = \frac{35}{4.2} > 1.0\ and\ \frac{D}{H} = \frac{50}{4.2} > 1.0$.

The resulting force can be rewritten as:

$$\begin{aligned} F(t) = \int_{-d}^{\xi} f_M(x,t)dz + \int_{-d}^{\xi} f_D(x,t)dz = \int_{-d}^{\xi} \rho \frac{\pi D^2}{4} C_M \dot{U}\, dz + \int_{-d}^{\xi} \frac{1}{2}\rho C_D U|U| dz = \\ = \int_{-d}^{\xi} \rho \frac{\pi D^2}{4} C_M \xi_0 kg \frac{\cosh(k(z+d))}{\cosh(kd)} \cos(wt - kx)\, dz + \\ \int_{-d}^{\xi} \frac{1}{2}\rho C_D U \frac{\xi_0 kg}{\omega} \frac{\cosh(k(z+d))}{\cosh(kd)} \sin(wt - kx) \\ \left| \frac{\xi_0 kg}{\omega} \frac{\cosh(k(z+d))}{\cosh(kd)} \sin(wt - kx) \right| dz \end{aligned} \tag{2.12}$$

2.2.1 Wave load on the monopod platform

In this section, the two main methods of the design of the monopod platform are considered: Working Stress Design (WSD) (DNV, 2012) and Limit State Design (LSD) or Load Resistance Factor Design (LRFD) (DNV, 2011).

Working Stress Design

According to Karunakaran (2017), the method is defined as working stress method, as the loads for the design of structures are the service loads or the working loads. The failure of the structure occurs at a much higher load. Therefore, it is necessary to use a factor of the safety also known as design factor. It is equal to the ratio of the failure loads to the working loads. Accordingly, the stresses of concrete and steel in a structure designed by the working stress method are not allowed to exceed certain values of stresses known as permissible stresses.

The equation (2.12) was solved with the help of the MATLAB with assumption that 100-year wave height is 4.7 m and period is 10.2 (Novikov, 2014). The result is plotted in Figure 2-8 and the extreme value of wave force is 28.73 MN.

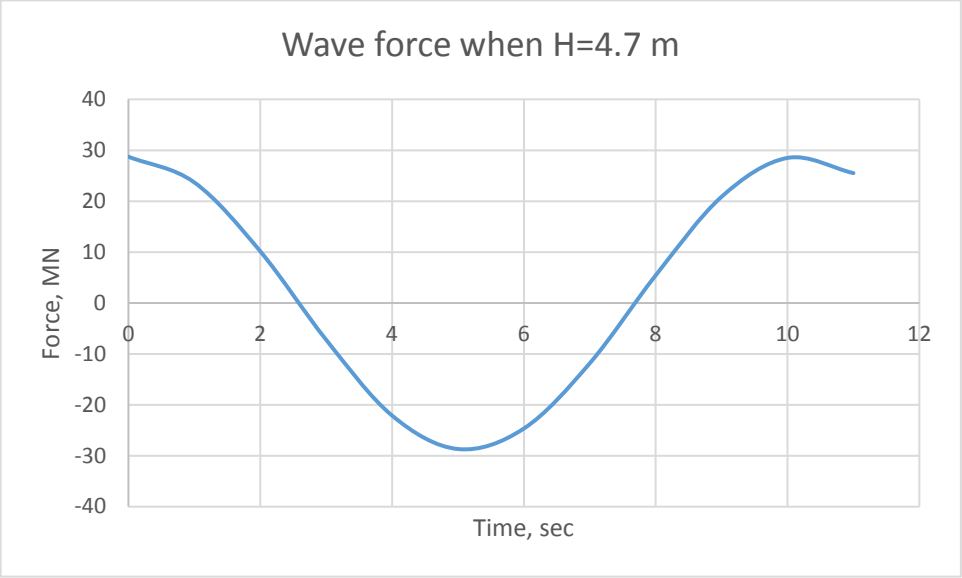

Figure 2-8. Wave force result when H=4.7 m

This force corresponds to the stress which could be written as:

$$\sigma_{100-year} = \frac{F_{100-year}}{A} = \frac{28.73}{A}\ MPa \tag{2.13}$$

Where

A – area

Therefore, the monopod structure should be designed in such a way as to withstand stress equal or less than stress due to 100-year wave force.

$$\sigma_{100-year} \leq f_d\ \sigma_{required}$$

$$\frac{28.73}{A}\ MPa \leq f_d\ \sigma_{required} \tag{2.14}$$

Where

f_d – design factor

$\sigma_{required}$ – required yield stress

Limit State Design and Load Resistance Factor Design

According to the DNV-OS-C101 (2011), the design by the LRFD method is a design method by which the target safety level is obtained as closely as possible by applying load and resistance factors to characteristic reference values of the basic variables. The basic variables are, in this context, defined as:

- Loads acting on the structure
- Resistance of the structure

The level of safety of a structural element is considered to be satisfactory if the design load effect S_d does not exceed the design resistance R_d:

$$S_d \leq R_d \tag{2.15}$$

A design load is obtained by multiplying the characteristic load by a given load factor:

$$F_d = \gamma_k F_k \tag{2.16}$$

Where

F_d – design load

γ_k – load factor

F_k – characteristic load

A design load effect is the most unfavourable combined load effect derived from the design loads and may be expressed by $S_d = f(F_d)$, but in this particular case, the design load is equal to the design load divided by the area:

$$S_d = \frac{F_d}{A} \tag{2.17}$$

The design resistance R_d is determined as follows:

$$R_d = \varphi R_k \tag{2.18}$$

Where

φ – resistance factor

R_k – characteristic resistance

The equation (2.12) was solved with the help of the MATLAB. Calculations were carried out for the time when the wave crosses the mean water level, because at this time the mass term is dominate and the load is maximum.

Applying the Monte Carlo method, the probability density function of the wave load on the monopod platform in the Pechora Sea was obtained. Statistical data of annual maximums of wave periods and wave heights in the period from 1949 to 2005 were used to calculate the probability density function. Statistical data are presented in the Table 2-3 (Dymov et al., 2012).

Table 2-3. The annual maximums of wave periods and wave heights (Dymov et al., 2012)

Year	H_{max}, m	T_{max}, s	Year	H_{max}, m	T_{max}, s	Year	H_{max}, m	T_{max}, s
1949	3.8	10.1	1970	3.6	7.7	1991	2.9	10.5
1950	2.4	10.3	1971	3.7	9.3	1992	3.4	9.6
1951	3.1	10.5	1972	3.3	7.3	1993	3.4	8
1952	2.3	8.3	1973	3.2	8.2	1994	3.2	8.2

Year	H_{max}, m	T_{max}, s	Year	H_{max}, m	T_{max}, s	Year	H_{max}, m	T_{max}, s
1953	2.6	8.2	1974	3.4	9.8	1995	3.9	11.1
1954	3.3	11	1975	3.7	9.8	1996	3.4	9.8
1955	3.1	10.3	1976	2.9	11	1997	3.7	7.7
1956	3	8.9	1977	2.7	10.2	1998	3.2	8.4
1957	3	8.2	1978	3.3	7.8	1999	2.8	8.3
1958	2.6	10.5	1979	2.9	9.9	2000	2.9	10.2
1959	3.2	8.4	1980	3.4	9.6	2001	2.6	10.7
1960	2.9	8.9	1981	3.7	9.4	2002	3.4	10.4
1961	2.9	9.5	1982	3.8	7.3	2003	3.3	9.4
1962	3.2	10.5	1983	3.1	9.1	2004	2.9	8
1963	3.2	10.2	1984	3	7.3	2005	2.9	9.6
1964	4.2	7.4	1985	2.7	8.8			
1965	2.8	9.3	1986	2.8	9.6			
1966	3.8	10.8	1987	2.9	9.5			
1967	3.7	9.2	1988	2.9	10			
1968	3.7	7.9	1989	3.4	10.5			
1969	2.5	9.2	1990	3.4	8.5			

The results from the MATLAB are plotted in Figures 2-9 and 2-10. The Table 2-4 shows the load values for different limit states.

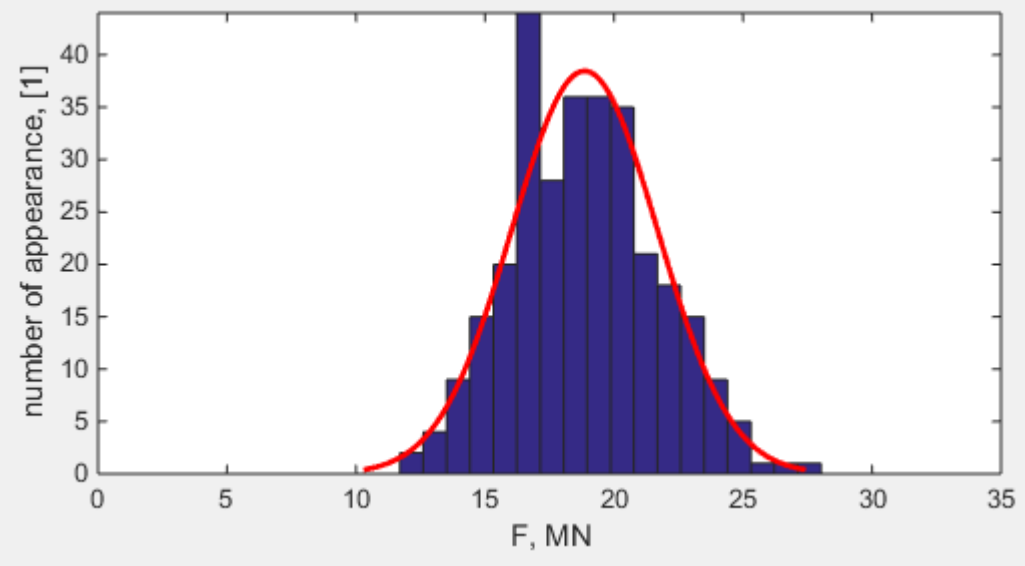

Figure 2-9. The probability density function of the wave load

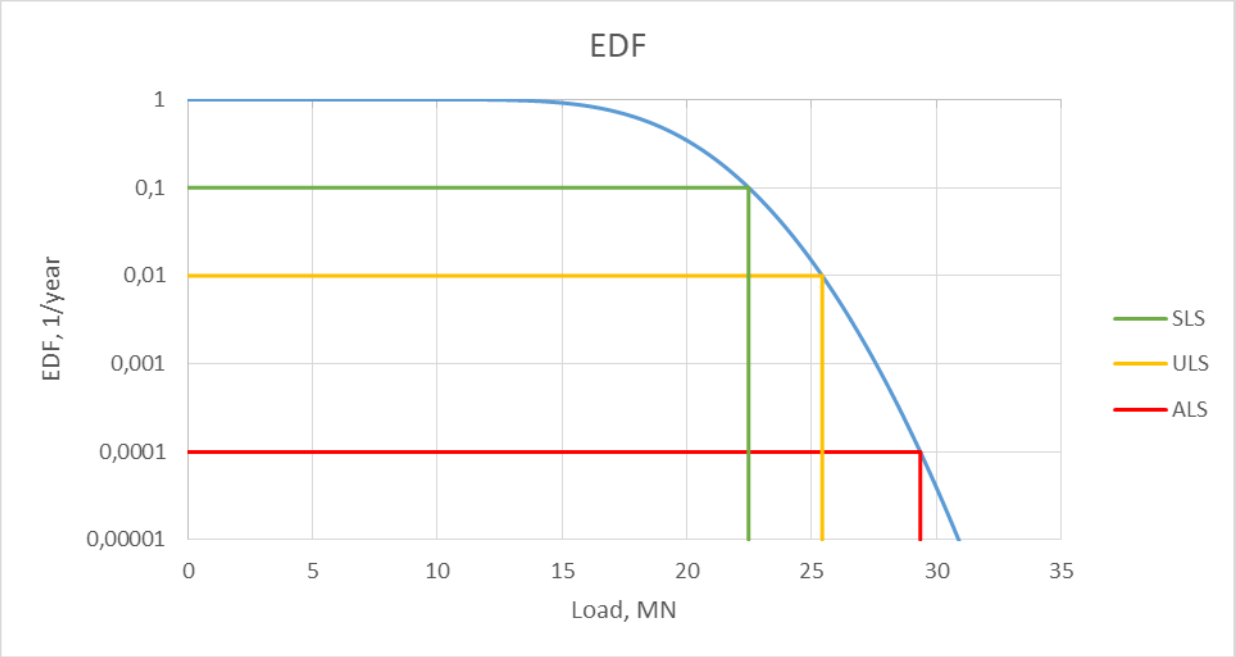

Figure 2-10. The exceedance distribution function

Table 2-4. Wave force results from MATLAB

Limit State	**Proportion**	**Load, MN**
Serviceability	Once in ten years	22.48
Ultimate	Once in a hundred years	25.43
Accidental	Once in ten thousand years	29.36

The design load effects corresponding to the design loads could be written as:

$$S_{d\ SLS} = \frac{F_{SLS}}{A} = \frac{22.48}{A} MPa \tag{2.19}$$

$$S_{d\ ULS} = \frac{F_{SLS}}{A} = \frac{25.43}{A} MPa \tag{2.20}$$

$$S_{d\ ALS} = \frac{F_{SLS}}{A} = \frac{29.36}{A} MPa \tag{2.21}$$

Due to lack of data, it is not possible to calculate the area, therefore it is assumed that stress corresponding to the design load could be written as in equations (2.19-2.21). According to the data obtained from calculations, the design load effects S_d should not exceed the design resistances R_d:

$$S_{d\ SLS} \leq R_{d\ SLS}$$

$$\frac{22.48}{A} MPa \leq R_{d\ SLS} \tag{2.22}$$

$$S_{d\ ULS} \leq R_{d\ ULS}$$

$$\frac{25.43}{A} MPa \leq R_{d\ ULS} \tag{2.23}$$

$$S_{d\ ALS} \leq R_{d\ ALS}$$

$$\frac{29.36}{A} MPa \leq R_{d\ ALS} \tag{2.24}$$

2.2.2 Wave load on the monocone platform

For the calculations, it was assumed that the cone is a set of cylinders with a height dh. Hence, the equation (2.12) could be used to compute the wave load on the cylinder of thickness dh and diameter D at the water level. Based on the calculations this diameter was assumed equal to 43.83 m.

Working Stress Design

The result of computing the equation (2.12) is plotted in Figure 2-11 and the extreme value of wave force is 39.067 MN.

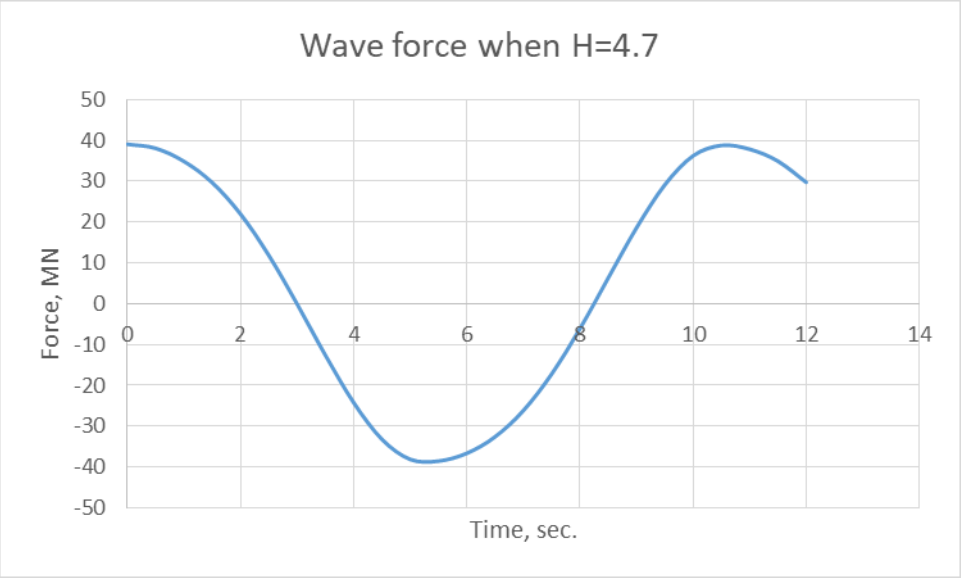

Figure 2-11. Wave force result when H=4.7 m

The stress corresponding to the force is given by:

$$\sigma_{100-year} = \frac{F_{100-year}}{A} = \frac{39.067}{A} MPa \tag{2.25}$$

Therefore, the monocone structure should be designed in such a way as to withstand stress equal or less than stress due to 100-year wave force.

$$\sigma_{100-year} \leq f_d \, \sigma_{required}$$
$$\frac{39.067}{A} MPa \leq f_d \, \sigma_{required} \tag{2.26}$$

The results of the Monte Carlo simulation from the MATLAB are plotted in Figures 2-12 and 2-13. The Table 2-5 shows the load values for different levels.

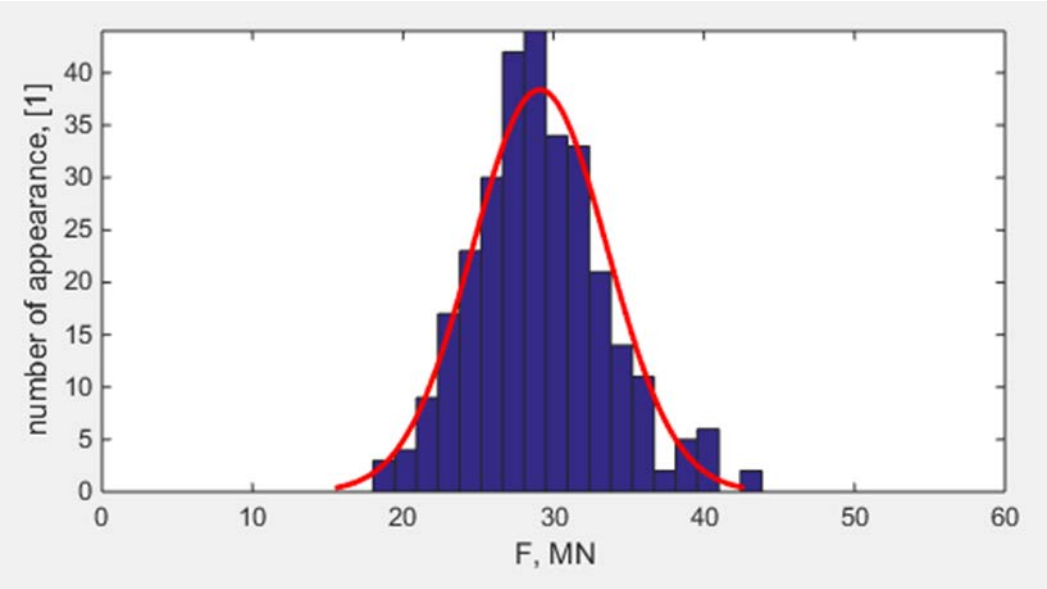

Figure 2-12. The probability density function of the wave load

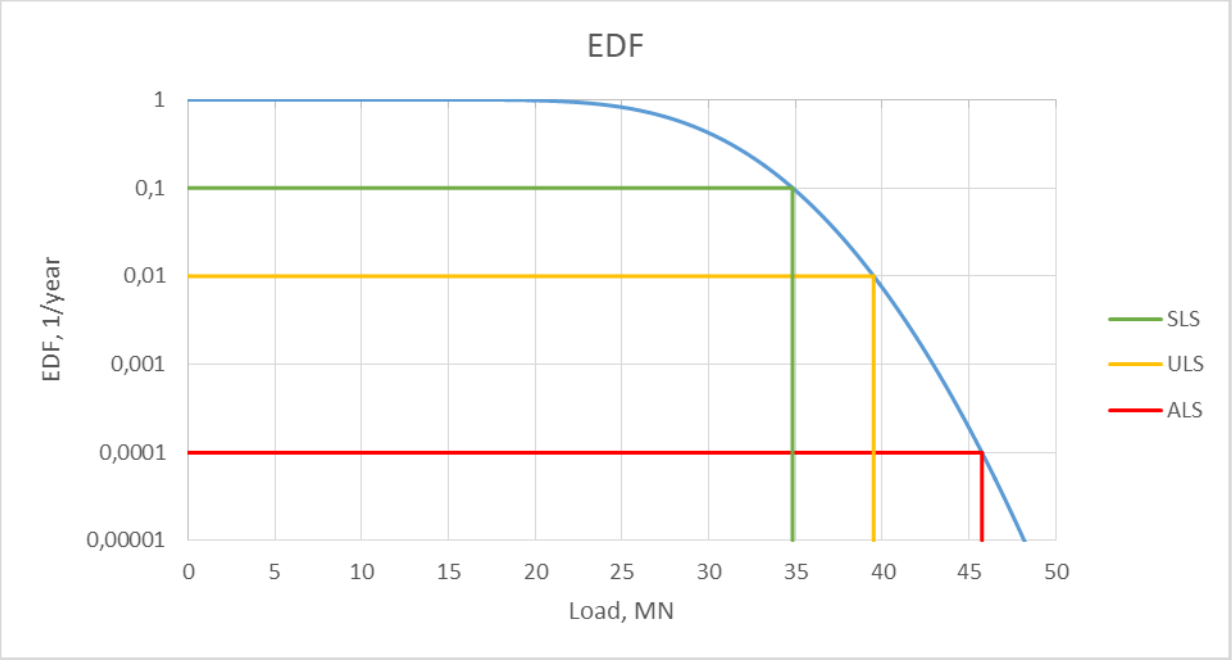

Figure 2-13. The exceedance distribution function

Table 2-5. Wave force results from MATLAB

Limit State	**Proportion**	**Load, MN**
Serviceability	Once in ten years	34.83
Ultimate	Once in a hundred years	39.50
Accidental	Once in ten thousand years	45.74

The design load effects corresponding to the design loads could be written as:

$$S_{d\ SLS} = \frac{F_{SLS}}{A} = \frac{34.83}{A} MPa \tag{2.27}$$

$$S_{d\ ULS} = \frac{F_{SLS}}{A} = \frac{39.50}{A} MPa \tag{2.28}$$

$$S_{d\ ALS} = \frac{F_{SLS}}{A} = \frac{45.74}{A} MPa \tag{2.29}$$

According to the data obtained from calculations, the design load effects S_d should not exceed the design resistances R_d:

$$S_{d\ SLS} \leq R_{d\ SLS}$$
$$\frac{34.83}{A} MPa \leq R_{d\ SLS} \tag{2.30}$$

$$S_{d\ ULS} \leq R_{d\ ULS}$$
$$\frac{39.50}{A} MPa \leq R_{d\ ULS} \tag{2.31}$$

$$S_{d\ ALS} \leq R_{d\ ALS}$$
$$\frac{45.74}{A} MPa \leq R_{d\ ALS} \tag{2.32}$$

2.3 Ice load

In this section, the ice loads on the monopod and monocone platforms are considered. The global ice action is considered the most important for structural design. It is the action exerted on the structure at any instant time. This global ice action is important when the stability, overturning moment or the overall strength of the structure are considered (Loset et.al., 2006).

2.3.1 Ice load on the monopod structure

The maximal global ice action on the monopod corresponds to the formula (Loset, 2017):

$$F = h\int_{-\pi/2}^{\pi/2} \sigma_c \cos\varphi \, R d\varphi = h\sigma_c 2R = \sigma_c D h \tag{2.33}$$

Where

D, R – diameter and radius of the monopod

h – ice thickness

σ_c – unconfined compressive strength

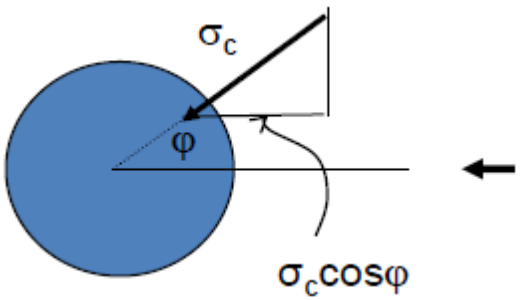

Figure 2-14. Ice load on a monopod structure

This equation is based on the following assumption: the local normal stresses is distributed evenly over the entire contact area and reach simultaneously a certain limiting level. This assumption is a drawback of this method. A more exact equation is the Korzhavin equation, which can be written in the following form (Loset et.al., 2006):

$$F = IKm\sigma_c D h \tag{2.34}$$

Where

I – indentation factor

K – contact factor

m – shape factor

The indentation factor I takes into account different parameters such as:

- crystallographic structure of the ice and its properties
- correlation between the diameter and the ice
- influence of the stress/strain field on strength.

According to the Selvadurai and Boulon (1995), indentation factor can be defined as follows:

$$I = \sqrt{5\frac{h}{D} + 1} \tag{2.35}$$

The imperfect contact between the structure and the ice is taken into account by the contact factor K. The factor m varies in limits between 0.9–1 where 0.9 corresponds to a cylinder and 1.0 to a flat contact surface.

According to the ISO 19906 (2010), the global ice pressure and the global ice action can be determined as given in equation:

$$P_g = C_R \left(\frac{h}{h_1}\right)^n \left(\frac{w}{h}\right)^m$$
$$F_g = hwP_g \tag{2.36}$$

Where

P_g – global average ice pressure

C_R– ice strength coefficient

h – thickness of the ice sheet

h_1– reference thickness of 1 m

w – projected width of the structure

n – empirical coefficient equal to -0.50 + h/5 for h <1.0 m and to -0.30 for h >1

m – empirical coefficient equal to -0.16

Working Stress Design

The result of computing the equations (2.33-2.35) is given in Table below:

Table 2-6.Ice load results (for ice: $\sigma_c = 1.415\ MPa, h = 1.2\ m, I = 1.1$)

Ice load, MN		
Global ice action Equation (2.33)	Korzhavin Equation (2.34)	ISO 19906 Equation (2.35)
59.45	58.84	32.80

According to Palmer and Croasdale (2013), Global ice action and Korzhavin equation are enticingly seductive because of their simplicity, but they are incorrect and deeply misleading. Hence, it is preferable to use the equation (2.36).

The stress corresponding to the force is given by:

$$\sigma = \frac{F}{A} = \frac{32.80}{A} \tag{2.37}$$

Therefore, the monopod structure should be designed in such a way as to withstand stress equal or less than stress due to ice force.

$$\sigma \leq f_d\ \sigma_{required}$$
$$\frac{32.80}{A} MPa \leq f_d\ \sigma_{required} \tag{2.38}$$

Applying the Monte Carlo method, the probability density function of the ice load on the monopod platform in the Pechora Sea was obtained. The distributions of annual maximums of ice height and compressive strength were used to calculate the probability density function. The distributions are presented in the Figures 2-15 and 2-16.

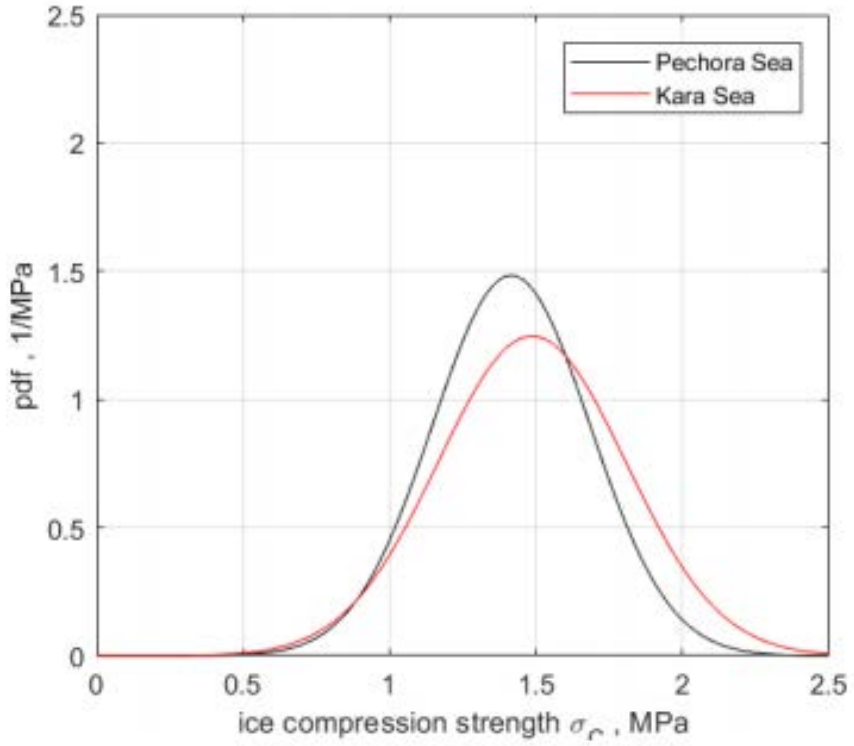

Figure 2-15. Probability distribution of compressive strength of ice in the Pechora and Kara Seas (April) (Shestov, 2017)

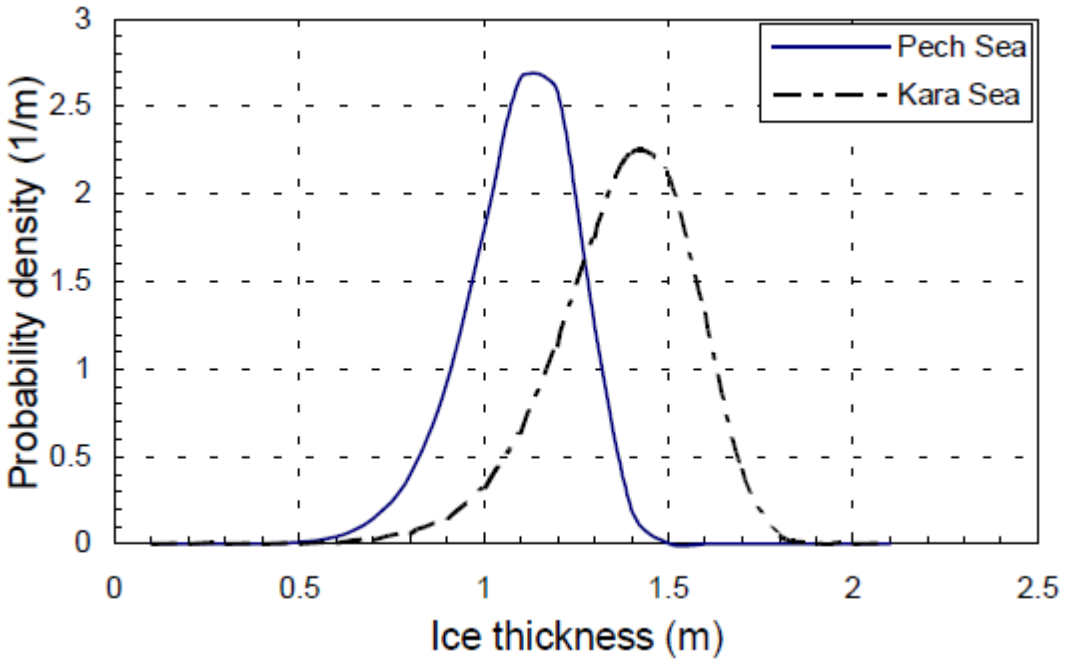

Figure 2-16. Probability distribution of ice thickness in the Pechora and Kara Seas (April) (Gudmestad et al., 1999).

The results of the Monte Carlo simulation from the MATLAB are plotted in Figures 2-17 - 2-22. The Table 2-17 shows the load values based on different equations and for three ice events such as serviceability, extreme and abnormal.

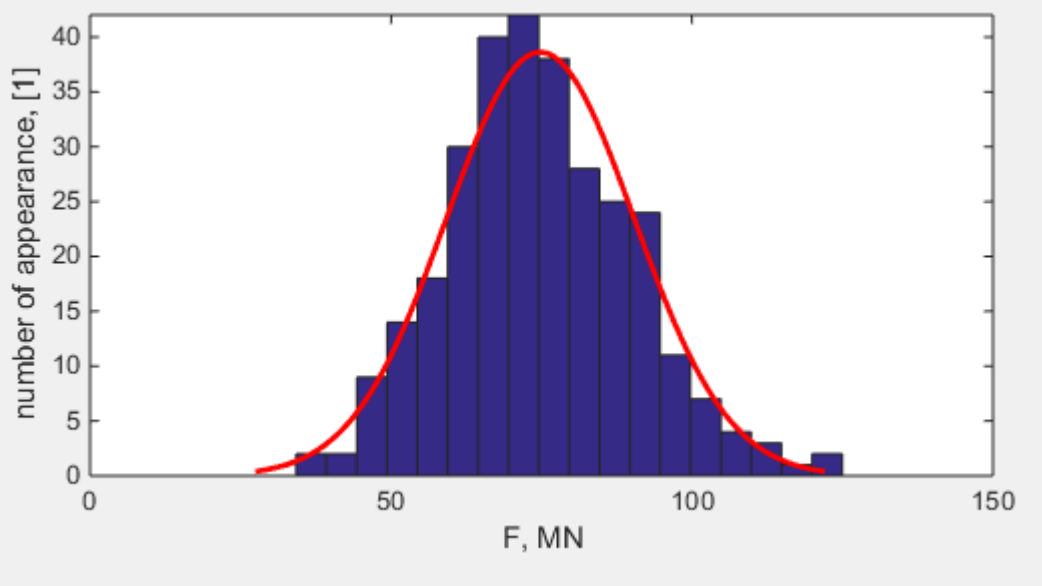

Figure 2-17. The probability density function of the ice load (Global ice action)

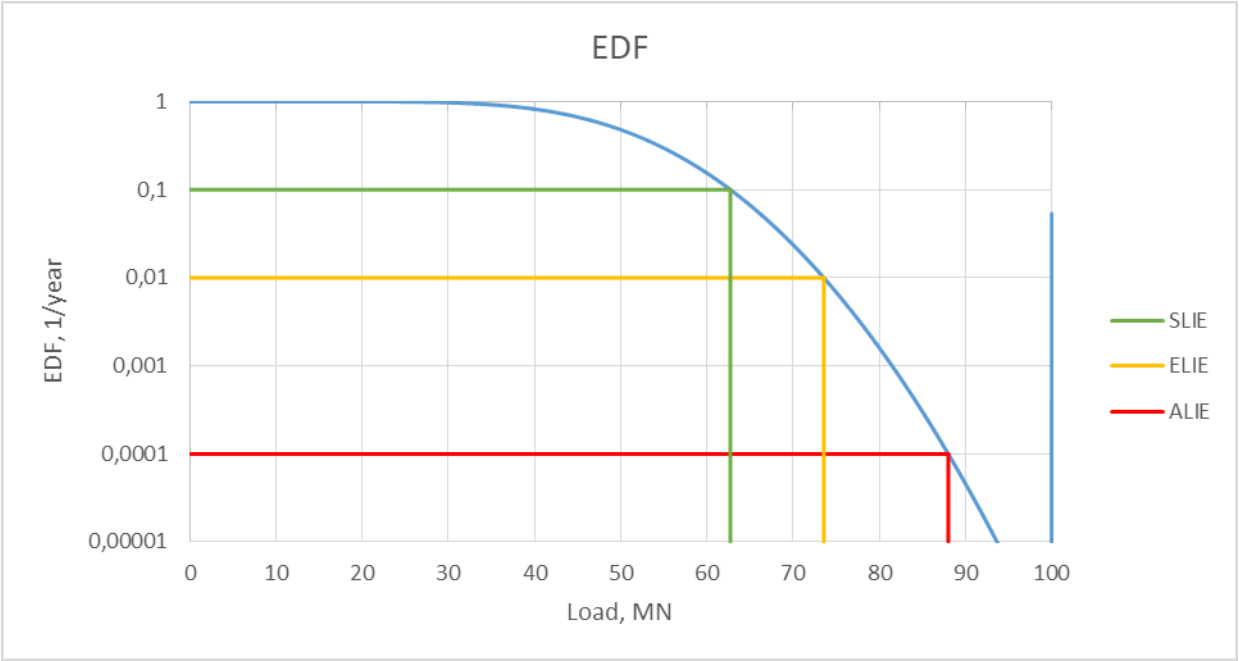

Figure 2-18. The exceedance distribution function (Global ice action)

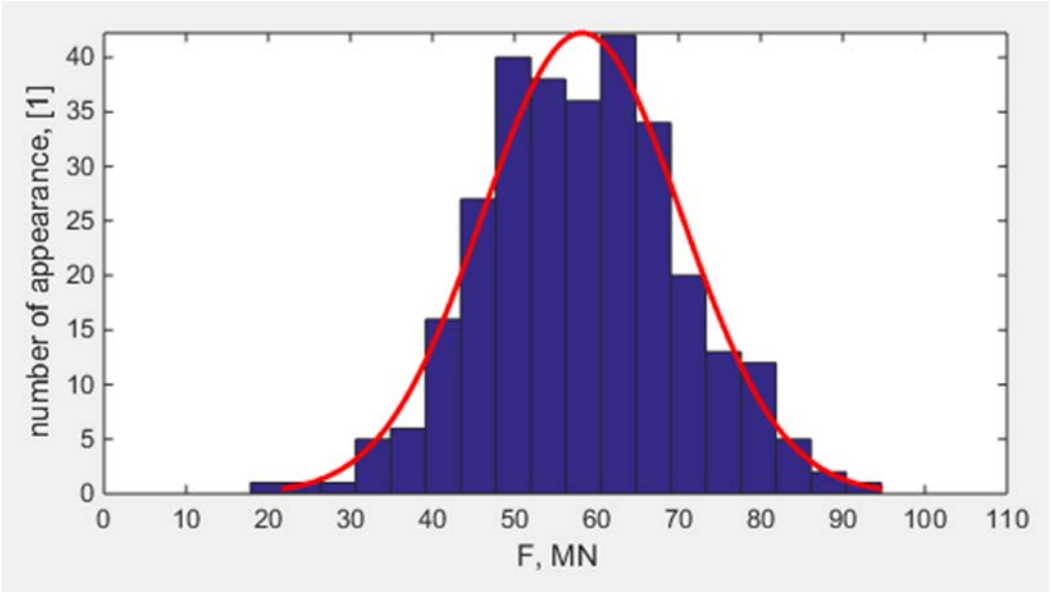

Figure 2-19. The probability density function of the ice load (Korzhavin)

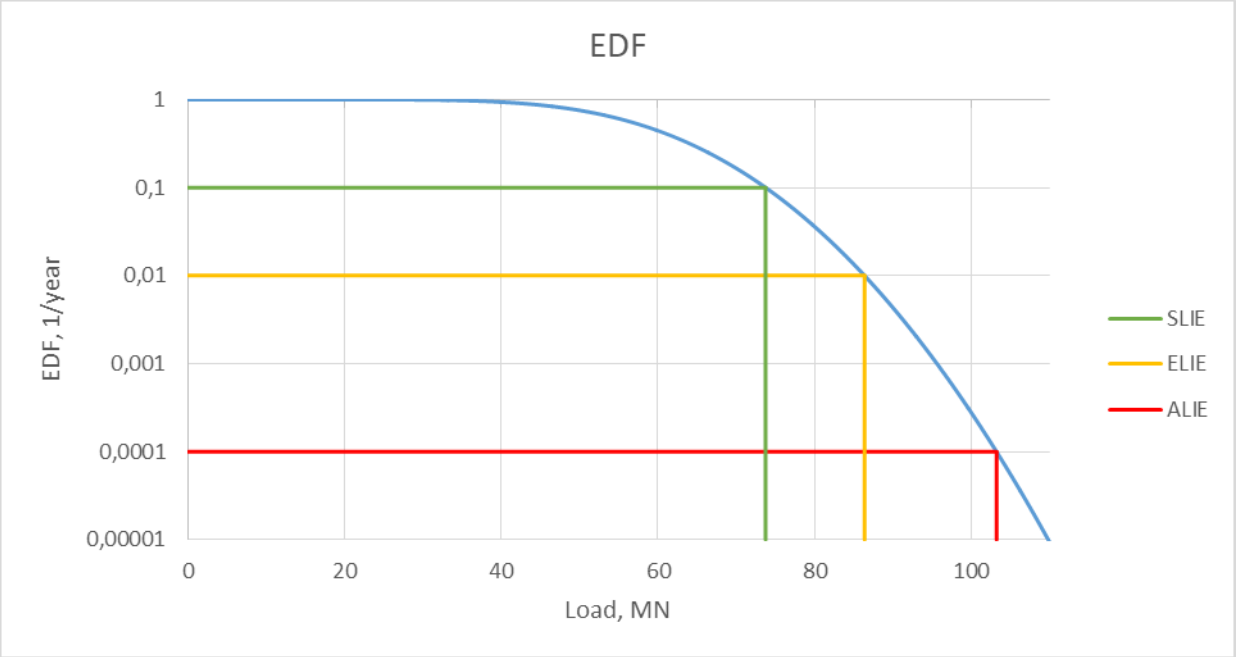

Figure 2-20. The exceedance distribution function (Korzhavin)

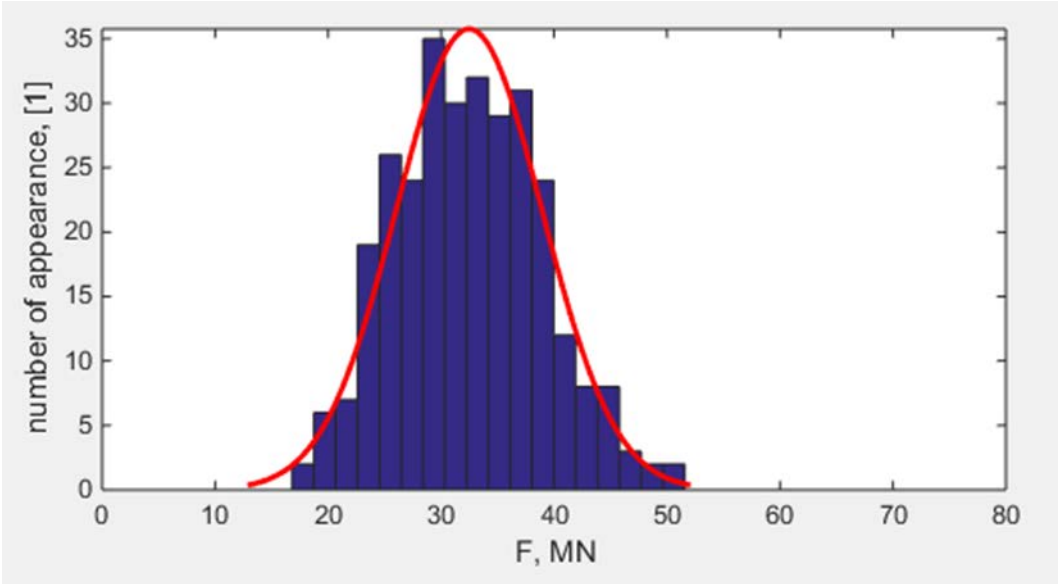

Figure 2-21. The probability density function of the ice load (ISO 19906)

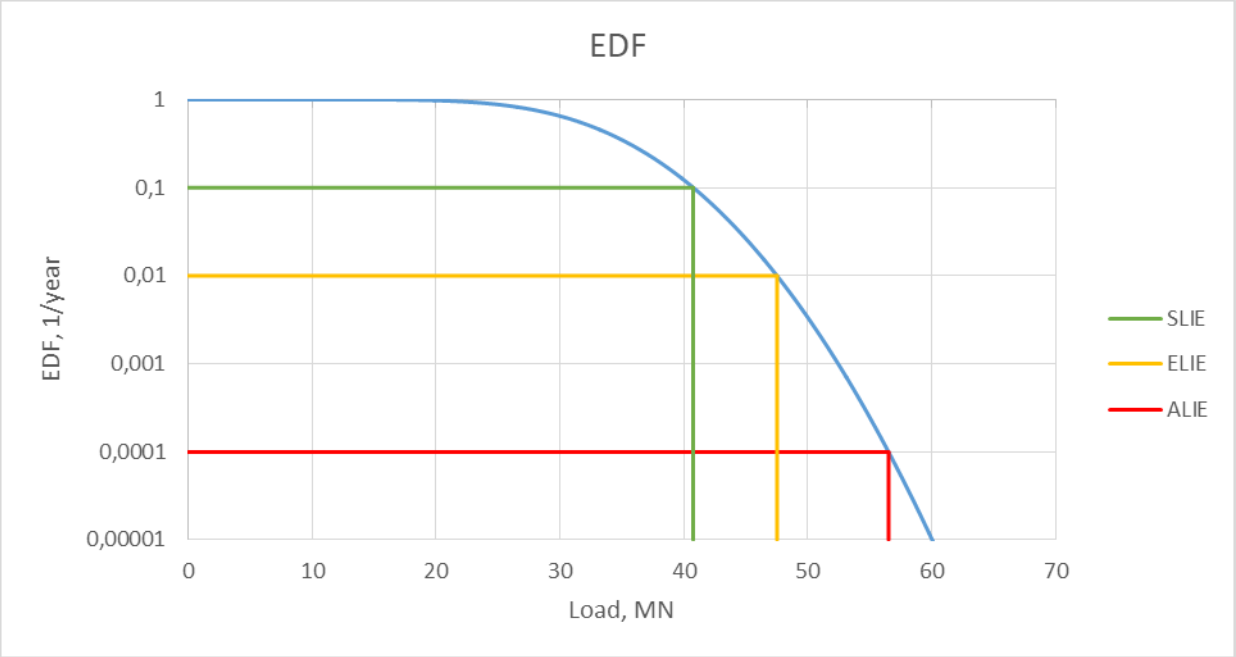

Figure 2-22. The exceedance distribution function (ISO 19906)

Table 2-7. Ice load results from MATLAB

Equation	Ice Event	Proportion	Load, MN
Global ice action	Serviceability	Once in ten years	62.72
	Extreme	Once in a hundred years	73.56
	Abnormal	Once in ten thousand years	88.01
Korzhavin	Serviceability	Once in ten years	73.74
	Extreme	Once in a hundred years	86.38
	Abnormal	Once in ten thousand years	103.23
ISO 19906	Serviceability	Once in ten years	40.96
	Extreme	Once in a hundred years	47.52
	Abnormal	Once in ten thousand years	56.52

As it was written before, estimation of ice load according to the ISO 19906 is preferable. The design load effects corresponding to the design loads could be written as:

$$S_{d\,SL} = \frac{F_{SL}}{A} = \frac{40.96}{A}\ MPa \qquad (2.39)$$

$$S_{d\ ELIE} = \frac{F_{ELIE}}{A} = \frac{47.52}{A}\ MPa \tag{2.40}$$

$$S_{d\ ALIE} = \frac{F_{ALIE}}{A} = \frac{56.52}{A}\ MPa \tag{2.41}$$

According to the data obtained from calculations, the design load effects S_d should not exceed the design resistances R_d:

$$S_{d\ SL} \leq R_{d\ SL} \tag{2.42}$$

$$S_{d\ ELIE} \leq R_{d\ ELIE} \tag{2.43}$$

$$S_{d\ ALIE} \leq R_{d\ ALIE} \tag{2.44}$$

2.3.2 Ice load on the monocone structure

When an ice sheet acts on a wide slope or cone, the flexural failure component can be evaluated considering the ice sheet as an elastic beam on elastic foundation. In addition, three-dimensional effects can be considered as well as the presence of rubble on the face of the structure in the model outlined below. This method can also be used for downward breaking slopes by replacing ice weight in air by ice buoyancy in water. The present model accounts approximately for axial forces in the ice sheet and other more comprehensive approaches, are recommended if they are to be dealt with correctly.

According to this model (ISO 19906:2010), the horizontal action component is determined as:

$$F_H = \frac{H_B + H_P + H_R + H_L + H_T}{1 - \frac{H_B}{\sigma_F l_c h}} \tag{2.45}$$

Where

H_B – breaking load

H_P – load component required to push the sheet ice through the ice rubble

H_R – load to push the ice blocks up the slope through the ice rubble

H_L – load required to lift the ice rubble on top of the advancing ice sheet prior to breaking

H_T – load to turn the ice block at the top of the slope

σ_F – flexural strength of the ice sheet

l_c – length of circumferential bending crack

The denominator-term is included to account for the compressive stress in the ice due to the horizontal load at the interface with the structure. The breaking component H_B is the main component, which is found as:

$$H_B = 0.68\xi\sigma_f l_c \left(\frac{\rho_w g h^5}{E}\right)^{0.25} \tag{2.46}$$

Where

$$\xi = \frac{\sin\alpha + \mu\cos\alpha}{\cos\alpha - \mu\sin\alpha}$$

ρ_w – water density

E – elastic modulus

Length of circumferential bending crack is obtained as:

$$l_c = w + \frac{\pi^2}{4} L_c \tag{2.47}$$

$$L_c = \left(\frac{Eh^3}{12\rho_w g(1-\nu^2)}\right)^{0.25} \tag{2.48}$$

Where

w – waterline diameter of the cone or width of a sloping structure

ν – Poisson ratio for ice, typically equal to 0.3

The load component H_P is expressed as given by equation

$$H_P = wh_r^2\mu_i\rho_i g(1-e)\left(1-\frac{\tan\theta}{\tan\alpha}\right)^2\frac{1}{2\tan\theta} \quad (2.49)$$

Where

h_r – rubble height

μ_i – ice-to-ice friction coefficient

e – porosity of the ice rubble

θ – angle the rubble makes with the horizontal

The load component H_R is given by:

$$H_R = \frac{w\rho_i g h_r}{\cos\alpha - \mu\sin\alpha}P \quad (2.50)$$

$$P = \left(0.5(\mu_i+\mu)(1-e)h_r\left(\mu_i\left(\frac{\sin\alpha}{\tan\theta}-\cos\alpha\right)+\frac{\cos\alpha}{\tan\alpha}\right)\left(1-\frac{\tan\theta}{\tan\alpha}\right)+h\frac{\sin\alpha+\mu\cos\alpha}{\sin\alpha}\right) \quad (2.51)$$

The load component H_L is given by:

$$H_L = wh_r\xi\left(1-\frac{\tan\theta}{\tan\alpha}\right)\left(0.5h_r\rho_i g(1-e)\left(\frac{1}{\tan\theta}-\frac{1}{\tan\alpha}+\tan\phi\left(1-\frac{\tan\theta}{\tan\alpha}\right)\right)+c\right) \quad (2.52)$$

Where

ϕ– friction angle of the ice rubble

c – cohesion of the ice rubble

The final load component H_T is given by a following Equation:

$$H_T = 1.5wh^2\rho_i g\frac{\cos\alpha}{\sin\alpha-\mu\cos\alpha} \quad (2.53)$$

Working Stress Design

The result of computing the equation (2.45) is given in Table below:

Table 2-8.Ice load on the monocone
(for ice: $D = 66\ m, \sigma_f = 0.52\ MPa, h = 1.2\ m$)

Ice load, MN
ISO 19906 Equation (2.45)
35.01

The stress corresponding to the force is given by:

$$\sigma = \frac{F}{A} = \frac{35.01}{A}\ MPa \tag{2.37}$$

Therefore, the monocone structure should be designed in such a way as to withstand stress equal or less than stress due to ice force.

$$\sigma \leq f_d\ \sigma_{required}$$
$$\frac{35.01}{A} MPa \leq f_d\ \sigma_{required} \tag{2.38}$$

Limit State Design and Load Resistance Factor Design

The results of the Monte Carlo simulation from the MATLAB are plotted in Figures 2-21 and 2-22. The Table 2-9 shows the load values for different events. Due to lack of information, there was implemented semi-probabilistic approach. The flexural strength is constant and equal to 0.5 MPa, while the ice thickness is vary.

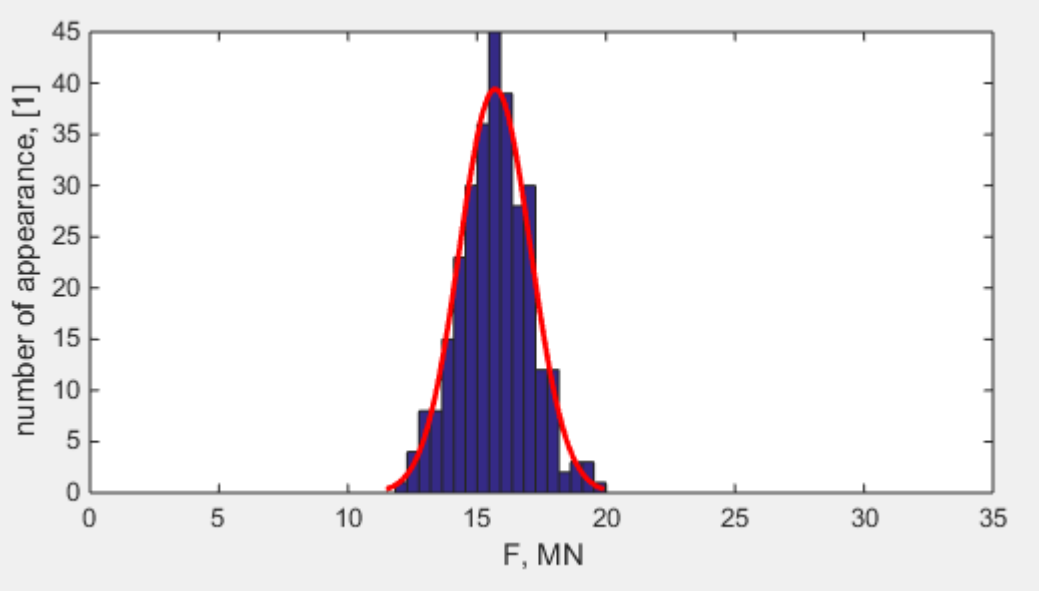

Figure 2-23. The probability density function of the ice load

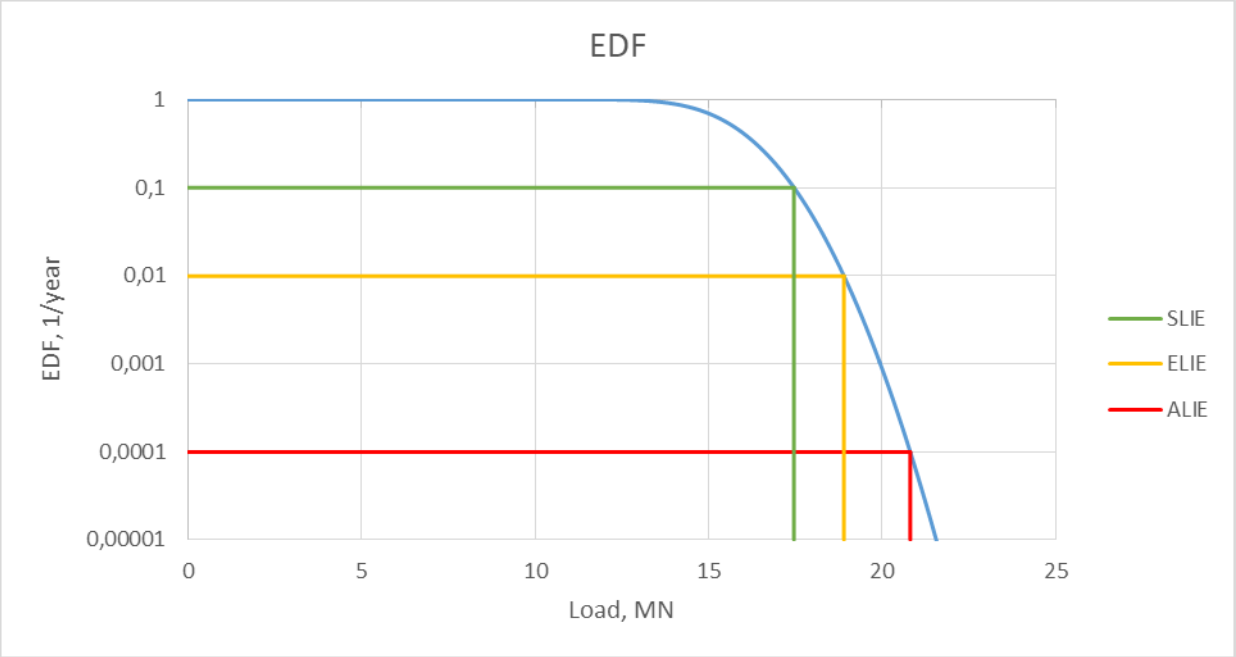

Figure 2-24. The exceedance distribution function

Table 2-9.Ice load on the monocone

Ice event	**Proportion**	**Load, MN**
Serviceability	Once in ten years	17.46
Extreme	Once in a hundred years	18.90
Abnormal	Once in ten thousand years	20.81

2.3.3 Preliminary conclusions

The tables presented below summarizes all the results of calculations carried out above.

Table 2-10. Comparison of wave loads on the platforms

Wave load, MN							
Monopod platform (D=35 m)				Monocone platform (D=43.83 m)			
WSD	LSD			WSD	LSD		
	SLS	ULS	ALS		SLS	ULS	ALS
28.73	23.04	26.01	29.95	39.06	34.83	39.50	45.74

Table 2-11. Comparison of ice loads on the platforms (Global ice action – ISO 19906)

Ice load, MN	
Monopod platform (D=35 m)	Monocone platform (D=43.83 m)

Global ice action				ISO 19906			
WSD	LSD			WSD	LSD		
	SLS	ULS	ALS		SLS	ULS	ALS
59.45	62.72	73.56	88.01	35.01	17.46	18.90	20.81

Table 2-12. Comparison of ice loads on the platforms (Korzhavin – ISO 19906)

Ice load, MN							
Monopod platform (D=35 m) Korzhavin				Monocone platform (D=43.83 m) ISO 19906			
WSD	LSD			WSD	LSD		
	SLS	ULS	ALS		SLS	ULS	ALS
58.84	73.74	86.38	103.23	35.01	17.46	18.90	20.81

Table 2-13. Comparison of ice loads on the platforms (ISO 19906)

Ice load , MN							
Monopod platform (D=35 m) ISO 19906				Monocone platform (D=43.83 m) ISO 19906			
WSD	LSD			WSD	LSD		
	SLS	ULS	ALS		SLS	ULS	ALS
32.80	40.96	47.52	56.52	35.01	17.46	18.90	20.81

According to the data obtained from the calculations, the following conclusions are drawn:

1) Deterministic calculations are more conservative than probabilistic calculations, which is certainly a drawback of this method.
2) Probabilistic calculations using the Monte Carlo method are more complicated, since a large amount of statistical data is required for modeling.
3) LSD is more efficient compare to WSD, because probabilistic calculations are more realistic and hence the requirements for the strength characteristics of the material are smaller, which leads to lower construction costs.
4) Wave load on the monocone platform is much greater than on the monopod platform due to the difference in the diameter. Ice load on the monopod platform is two times higher than on the monocone structure. Difference

between ice load on the monopod and monocone platforms is not significant, while difference of wave load is relatively high. Therefore, it is difficult to conclude which of the suggested technical solutions is preferable in terms of the loads resistance.

5) The further numerical and analytical studies are to be carried out to make the reliable conclusion.

3. Main Subsea Projects

In order to understand and choose the subsea concept it is necessary to analysis the best practices of the main subsea projects located in similar conditions with Dolginskoye oil field are considered. The list of these fields are presented in Table 3-1. These projects are divided into two categories:

- Subsea oil fields located in the Arctic and sub-Arctic zones
- Projects in shallow water

Table 3-1. Subsea projects located in the similar conditions with Dolginskoye field

Arctic and sub-Arctic zones		**Shallow water**	
Field	**Region**	**Field**	**Region**
Goliat	Barents Sea	Deep Panuke	Atlantic Ocean
Snohvit	Barents Sea	Medway	North Sea
Sakhalin III	Okhotsk Sea	NS377	Red Sea
Terra Nova	Atlantic Ocean	K5F	North Sea
White Rose	Atlantic Ocean	K18	North Sea
Aasta Hansteen	Norwegian Sea	K4Z	North Sea

In this section, only Arctic projects are considered, analysis related to the shallow water projects will be held later in the master's thesis. The existing subsea facilities implemented in the Arctic projects depending on the water depth are presented in the Figure 3-1. According to this figure, subsea facilities were used more than once in the Arctic Zone.

3.1 Subsea production and transportation

The following projects have the subsea productions systems:

- Sakhalin III – Sea of Okhotsk, Russia
- White Rose – Atlantic Ocean, Canada
- Terra Nova – Atlantic Ocean, Canada
- Snohvit – Barents Sea, Norway
- Goliat – Barents Sea, Norway

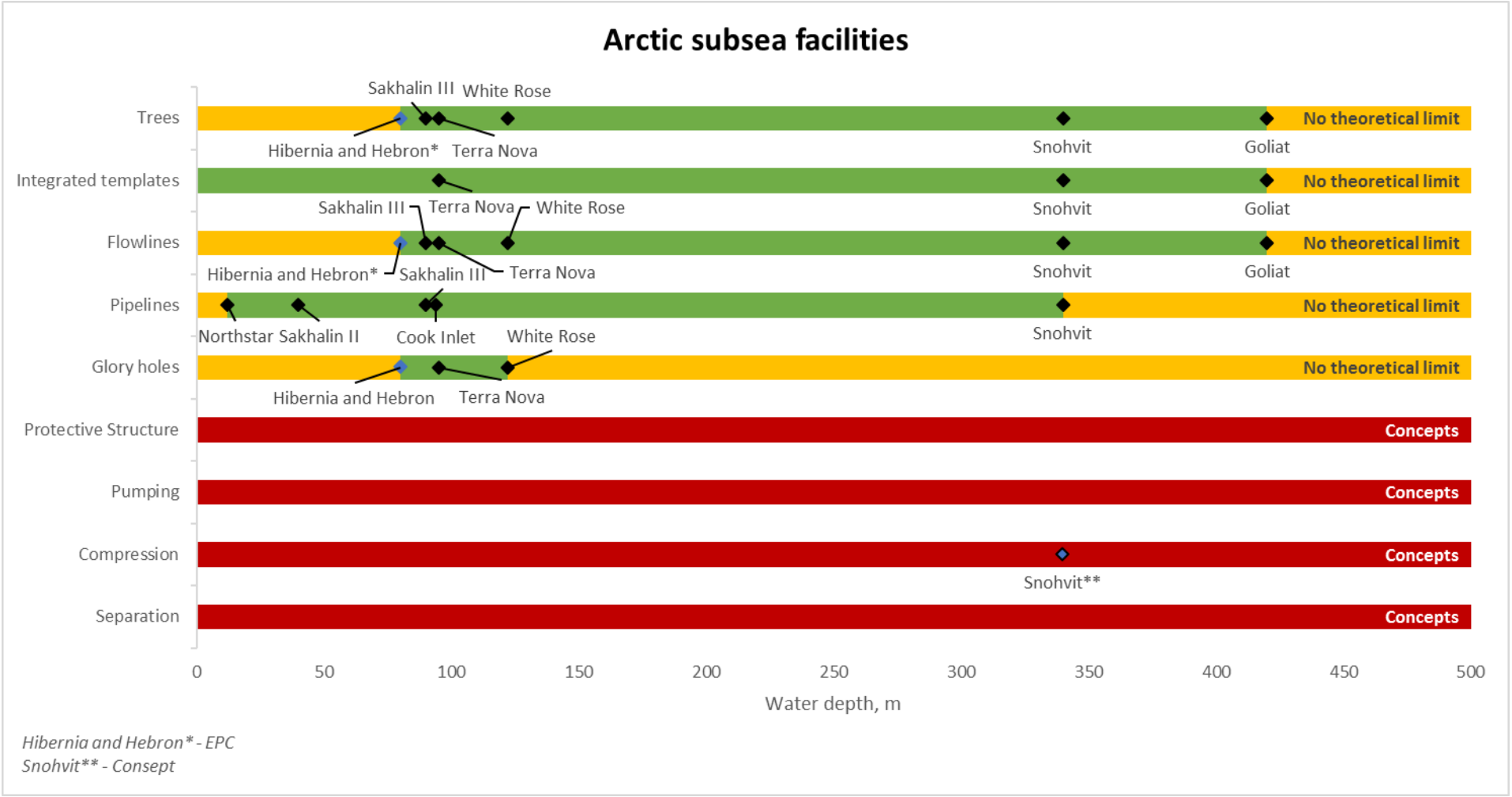

Figure 3-1. Arctic subsea facilities (Egorov, 2017)

Moreover, oil or gas in the following fields flows through the subsea pipeline to the shore:

- Sakhalin II – Sea of Okhotsk, Russia
- Sakhalin III – Sea of Okhotsk, Russia
- Northstar – Prudhoe Bay, USA
- Cook Inlet – Gulf of Alaska, USA
- Snohvit – Barents Sea, Norway

Note that the subsea production system can be installed in the future on the Hebron and Hibernia projects. At the moment, EPC (engineering, procurement, construction) contracting is taking place (Hebron project, 2015).

3.2 Protection of subsea equipment

One of the main challenges in the application of the subsea production systems is the protection of equipment from the ice load. This problem can be solved by using the "glory holes" technology that was used on two projects – Terra Nova in 1999 and White Rose in 20003. The purpose of these "glory holes" is to protect the subsea wellheads from keels ridges or icebergs. However, it is possible to use another technology, which is currently at the stage of conceptual study. This technology implies the use of the protective dome shaped concrete structures as illustrated in Figure 3-2 (Prescott et al., 2016).

According to Prescott et al. (2016), by using a glory hole with a protection structure approach, it is feasible to install a subsea wellhead facility in Arctic and Sub-Arctic shallow water conditions and flow the productions to shore via a subsea pipeline.

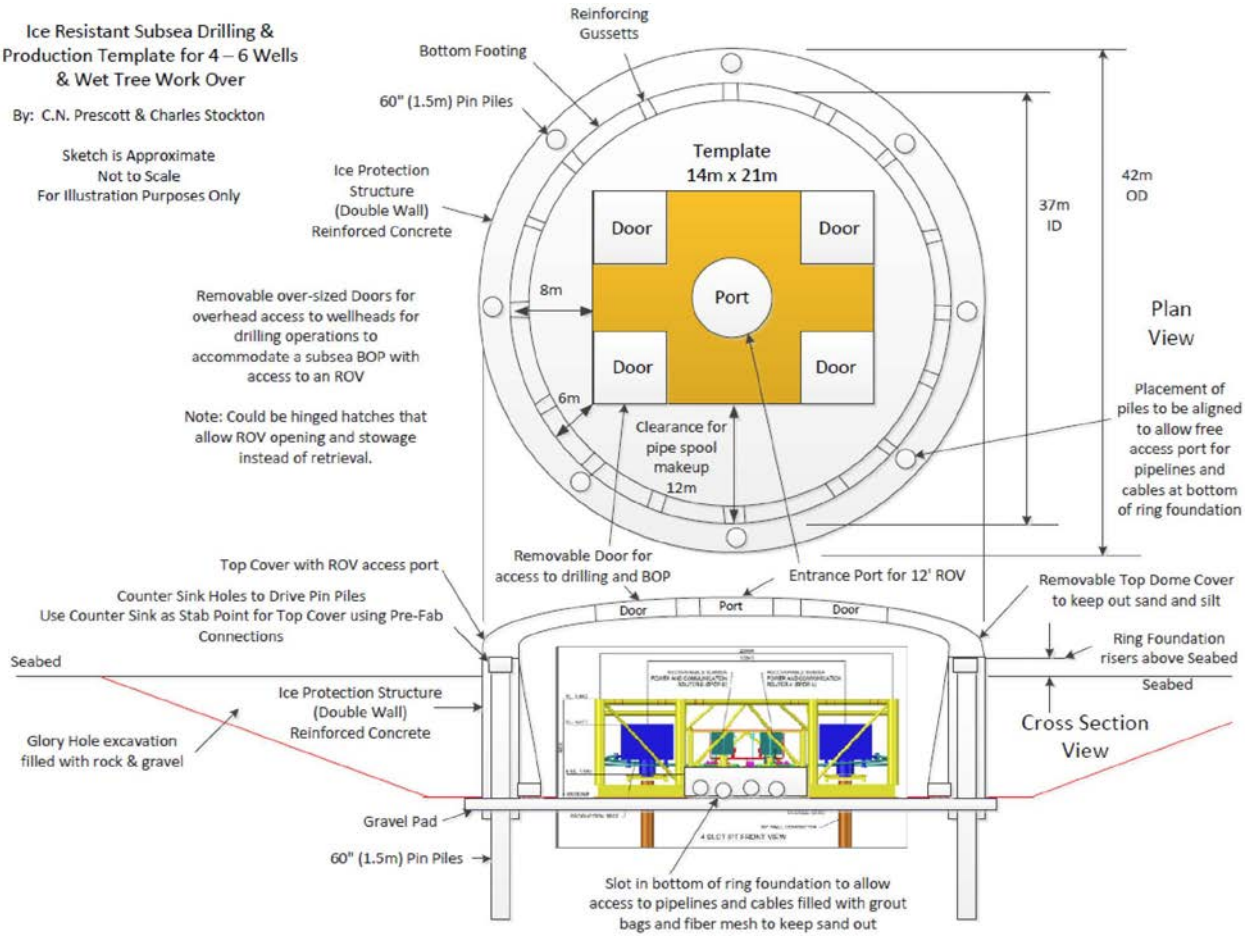

Figure 3-2. Proposed Glory Hole Protective Structure with Gravel/Rock Fill and Protective Dome with Access Ports and Doors for Drilling and Maintenance

3.3 Subsea processing

The subsea compression facilities are planned on the Snohvit unit. Subsea gas compression systems are based on subsea separation systems utilizing marinized dry gas compressor with upstream well-stream processing and liquid pumps. The multiphase compressor will handle unprocessed well stream comprising, condensate and water (Hjelmeland, 2011).

3.4 Best practice - the Goliat

It is necessary to pay attention to the modern subsea projects in the Arctic. The Goliat is the newest project located in the Baretns Sea. The technical analysis of the subsea field development is given below.

3.4.1 General information

The Goliat field was discovered in 2000 and owned by ENI Norge. It is located approximately 50 km southeast of the Snøhvit field and 88 km northwest of Hammerfest. The water depth in the Goliat field area is 360-420 m (NPD, n.d.).

Goliat comprises of two individual reservoirs – the Kobbe formation and the Realgrunnen group. Oil and thin gas caps are accumulated in Triassic sandstone in the Kapp Toscana Group (Realgrunnen subgroup) and the Kobbe Formation. The depth of Realgrunnen group is 1100, while the Kobbe formation lies at 1800 meters beneath the sea surface. Hydrostatic pressure of the reservoirs – 120 bar for the Realgrunnen and 190 bar for the Kobbe. Oil production started on 12 March 2016. Goliat will produce 100,000 barrels of oil per day. The field is assessed to contain around 180 million barrels of oil (NPD, n.d.).

3.4.2 Subsea Concept

Main challenge of the Goliad field development is to take into account the climatic conditions of the Arctic zone (Rekdal, n.d.):

- Severe conditions – winterization is needed;
- Impact of ice;
- Sensitive Arctic environment.

It is also necessary to ensure good environmental solutions and safeguard framework conditions:

- Prevent acute emissions;
- Minimize operational emissions;
- Establish a proper oil spill preparedness.

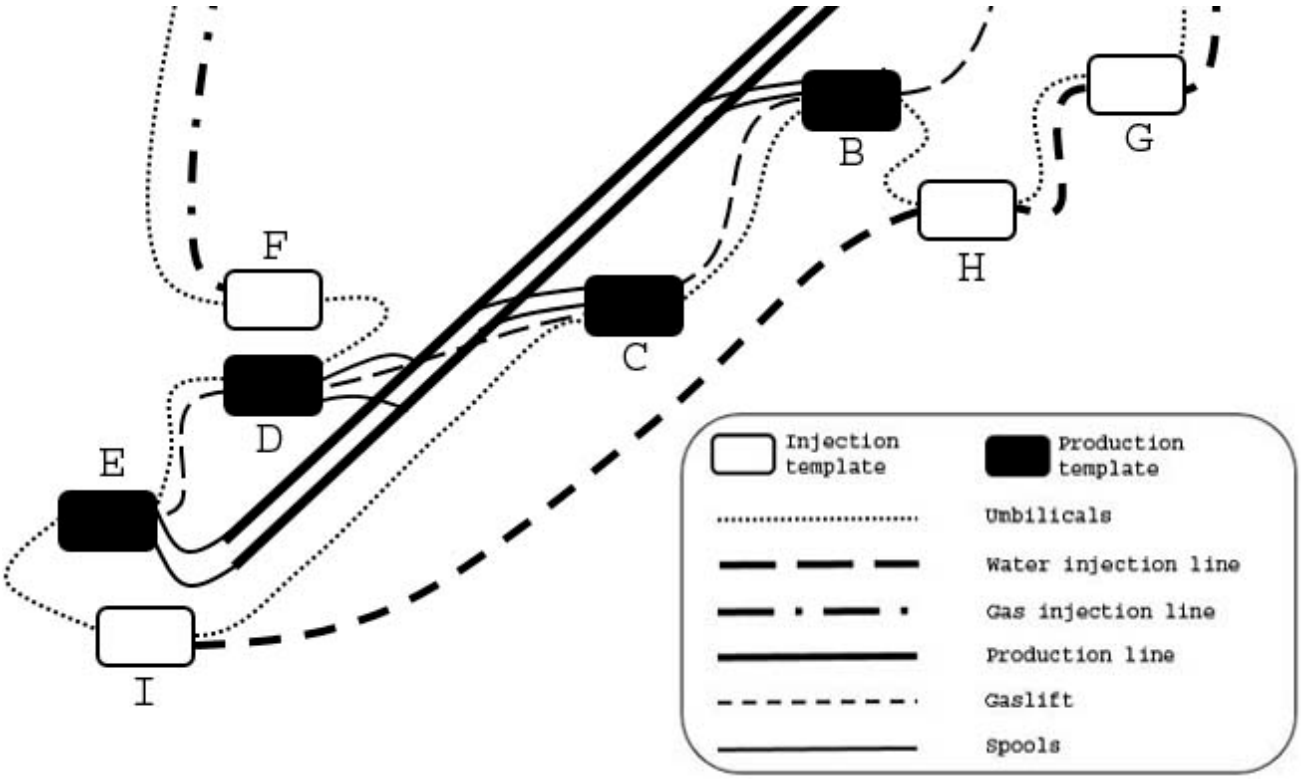

Figure 3-3. Top view of the subsea facilities (Egorov, 2017)

A unique subsea development concept was chosen as the answer to these challenges. Illustration of the subsea facilities is given in Figure 3-3. Goliat subsea concept comprises of eight subsea templates with a total of 32 well slots, infield flowlines and a cylindrical production, storage and offloading unit -Sevan 1000 FPSO (ENI, n.d.). The subsea templates are tied-back to the FPSO, which has an integrated storage and loading system. The Goliat FPSO is powered from Hammerfest substation onshore through 1065 km of subsea power cable. There are 29 wells: 16 producers, 9 water injectors, 3 gas injectors and an observation well.

The two rigid flowlines create a loop from the Sevan 1000 FPSO to template E and back. Due to this, it is possible to perform the round-trip pigging. Templates B,C and D are connected to the production flowlines via flexible jumpers being tied in to in-line Tee structures on the flowlines. The rigid expansion spools are used to tie-in to template E. Templates B, C, D and E have access to the gas lift flowline for artificial lift purposes. Flexible water injection flowlines are routed from the FPSO

in a "daisy-chain" configuration through template G and H to I. The gas injection flowline is a rigid line which starts at the FPSO and ends at template F (Tangvald, 2009).

3.4.3 Special Features

Related to the subsea facilities in this field there are three main features that are special: Direct Electrical Heating (DEH) system for flow assurance. It is necessary to avoid hydrate, wax and scale formation in flowlines and risers.

- Leakage monitoring system for oil spills detecting. This is a very urgent challenge in the Arctic.
- Integrated Template Structures (ITS). Applying of ITS is cost effective.

The production flowlines are fitted with a Direct Electrical Heating (DEH) system. The pipe is heated by running alternating current through the steel in the pipe. It is used to maintain temperature in flowline above hydrate, wax or ice appearance temperature, either by intermittent or continuous heating and to warm the fluid contents during a shutdown. The DEH system consists of three different kinds of the cables (Heggdal, n.d.):

- 4x 500m feeder cables - 1x1200mm^2;
- 2x 7,487m piggyback cable - 1x1200mm^2;
- 1x 1,266m DEH riser cable - 4x1600mm^2.

A piggy-back cable that runs along the entire length of each flow line with connection points and current transition zones at the flowline ends. A separate DEH cable riser connects the FPSO topside DEH equipment to the piggy-back cables. In addition to the DEH system, the production flowlines is coated with a wet insulation coating.

The SPS is provided with leakage monitoring systems in order to increase the environmental protection. Goliat remote sensing system should (Bjornbom, 2012):

- Provide early detection of acute spills of significance according to regulation and requirements in discharge permit;
- Be able to classify and to track the movement of acute spills;
- Give decision support during spill combating (no action/mechanical recovery/dispersion).

According to Bjornbom et al. (2012), all types of templates (production, gas injection, water injection) are designed with two different subsea retrievable sensor technologies:

1. Capacitive sensors (Phaze) - positioned beneath the subsea tree hatches. Each hatch functions as a collector covering:
    - Subsea tree and well head;
    - Flow control module;
    - Subsea tree to manifold connection point.
2. Acoustic sensors (Naxys) - installed on the manifolds.

The development of the field includes the installation of eight Integrated Template Structures (ITS). The templates each accommodate one manifold and four well slots. The height of each template is 25 meters, 33 meters long and 23 meters wide. The structure enables tie-in operations either before or after drilling the wells. According to NORSOK requirements, the ITS is designed for loads from dropped objects (Tangvald, 2009).

Wells are drilled through the slots, where the conductors are hung off during cementing of the conductor to the soil. Each of the four slots contains an integrated foundation and protection structure. The objective of the template structure is to provide seabed support for the manifold and well slot arrangement that provides

adequate support, guiding and alignment for the drilling and completion of the wells and interface to the manifold module. The purpose of the template structure is to provide seabed support for the manifold and well slot arrangement that provides adequate support for the drilling and completion of the wells and interface to the manifold module.The main structural elements ensure the protection of trees, manifold system and tie-in areas from dropped objects or impact from fishing activities.

3.4.4 Alternative Subsea Solution

The field development concept was using by first Arctic FPSO with subsea production system. The FPSO consists of a circular facility including a processing plant, oil storage capacity and accommodation facilities. The produced water is re-injected into the reservoir. Produced oil is stored on the facility prior to onward transport by shuttle tankers to the market.

According to Rekdal (n.d.), the alternative solutions that could have been considered are:

1. Offshore processing on the semi-submersible platform and onshore oil storage. In this concept, oil production using subsea production system, processing on a semi-submersible platform and transportation of processed oil through a pipeline to land are considered.
2. Onshore processing and storage. In this case, subsea production, separation and boosting systems are elaborated with the transportation of hydrocarbons via oil and gas pipelines. In addition, there is water injection pipeline.

There are several reasons to consider this concept the best such as:

- The selected technical solutions are inherently safe with a low level of risk and comply with the requirements of the Barents Sea with respect to emissions to air and discharges to sea;

- The facilities provide an elaborate working environment and meet the challenges associated with the harsh climate;
- A floating production facility offshore provides the best opportunity for tie-ins to other discoveries in the area;
- This concept is considered as a most cost effective.

3.4.5 Key Risks Identification Related to Subsea Development

Oil spills. The main key risks in Goliat field development, the spills in a “fragile” Arctic environment can lead that one to an ecological disaster with irreparable consequences. The elimination of spills in the Arctic zone is also complicated by:

- The presence of ice and ice drifts;
- Low temperatures;
- Strong winds and etc.

The leakage monitoring system is applied to reduce the risk of oil spills.

The risk of plugging of flowlines by hydrates, wax and scale formation in the subsea fields is high. It is necessary to avoid it and ensure a flow of crude oil with the required flow rate and pressure. This risk was reduced by the following measures:

- The production flowlines are fitted with a Direct Electrical Heating (DEH) system.
- The subsea production system provides the means for injecting chemicals to prevent hydrate, wax and scale formation.

3.5 Preliminary conclusion

Based on the foregoing, it can be concluded that the subsea production systems can be used in the Arctic, namely Dolginskoye field. There are several successful subsea Arctic projects in the world such as Goliat, Snøhvit, White Rose and Sakhalin III. Moreover, the subsea production system can be installed in the future on the Hebron and Hibernia projects. This proves that environmental problems can be solved, for instance with implementation of the leakage monitoring systems as in the Goliat project.

The problem associated with shallow water and risk of gouging can also be solved by using the “glory holes” technology that was used on two projects – Terra Nova in 1999 and White Rose in 20003. Also, it could be combined with the special protective structures.

3.6 Analysis of possible vessels for the template installation

The installation of the templates is one of the challenges for the Dolginskoye oil field development. This chapter describes how to select the vessel that can be used in the Pechora Sea.

Vessel motions can be defined by the six degrees of freedom: three translational - heave, surge, sway and three rotational - yaw, , pitch (Gudmestad, 2015). Heave is considered to be most important for template installation operation. The wave period in the Pechora Sea is varied from 8.6 to 9.5 seconds. It is necessary to avoid resonance therefore the natural period of the vessel in heave should be less than 8.6 s or larger than 9.5 s. (Russian Maritime Register of Shipping, 2003).

Installation of the subsea templates can be performed by multi-purpose service vessels, heavy lift vessel and crane barges. Several types of vessels and the possibility of using them for installation process are discussed in this chapter.

3.6.1 Multipurpose service vessels

Multipurpose service vessel (MPSV) is one of the types of offshore support vessels and performs maintenance and supply functions in the offshore oil industry (MikroMarket Monitor, n.d.). They are typically up to 125 m long and displacement of this vessels are varied from 8-15,000 tons (Gudmestad, 2015). They are able to carry out a variety of activities including supply duties, lifting operations, ROV and survey activities, platform maintenance, diving, light well intervention and support for accommodation (Daleel, n.d.)

Installation of templates at the Snohvit field was carried out from the "BOA Deep C" multipurpose vessel (Rigzone, 2014). The length of the vessel is 119.3 m and the width is 27.32 m. The maximum draft is 8.8 m. "BOA Deep C" is equipped with a 250 tons crane (BOA, 2016).

3.6.2 Heavy lift vessels

Semi-submersible crane vessels (SSCV) are heavy lift vessels equipped with the heavy lift cranes that can perform lifts up to 14200 tons. The vessels are intended to perform installation and removal of subsea equipment, decommissioning services and heavy lifting operations. One of the world's biggest heavy lift vessels, Heerema's semi-submersible DCV Thialf, is used for the template installation at the Ormen Lange field. The vessel is 165 meters long, 201 meter over all, and 88 meters wide. The draft can be between 11.8 and 31.8 meters. It is equipped with two equally sized cranes giving it a lifting capability of 14200 tones. Thialf is a deepwater construction vessel with both anchor mooring and dynamic positioning station keeping (Heerema, n.d.).

3.6.3 Construction vessel

Vessels are used in the construction of various structures are known as offshore construction vessels. Other vessels of this type also include those that provide

fastening and transport assistance and those types of vessels that help in the positioning of deep sub-water cable and piping lines. Main types are:

- Diving Support Vessel
- Crane Vessel
- Pipe Laying Vessel

Some vessels can be used for various operations, for instance the Seven Arctic vessel is used both for pipe laying and for installing heavy constructions. The Seven Arctic is a highly capable construction vessel suitable for worldwide operations. The main crane is an active heave compensated (AHC) subsea construction crane with and has been specifically selected and developed to give outstanding flexibility and capability for a range of different operational requirements. The vessel is 162.3 m long and 32.0 m wide, the crane capacity is 1,000 t (Subsea 7, 2015).

3.6.4 Barges

Barges are a cheap way to transport offshore facilities. They are cheap to build, but they can transport a small amount of equipment. Barges have a flat bottom housing, where the body is divided into compartments for both structural and ballast purposes. The barges have high limitations: the waterline area is large, which gives a low heave period. For instance, the barge natural period in heave should be less than 4 seconds or larger than 10 s to be operative on a typical North Sea day. (Gudmestad, 2015)

3.6.5 Heave period calculation

According to Gudmestad (2015), heave motion is the vertical up and down motion of a vessel along the vertical axis. To obtain the Eigen period in heave, some assumptions are used. The damping is assumed to be 0 and initial conditions are defined as $z(t=0)=0$ and $\dot{z}(t=0)=(H/2)(1/\omega)$.

The equation of motion is given by:

$$m\ddot{z}(t)+c\dot{z}(t)+kz(t)=F(t) \tag{3.1}$$

Where

m – mass

c – damping coefficient

k – stiffness constant

F – external force

The solution can be written as:

$$z(t) = z_h(t) + z_p(t) \tag{3.2}$$

Where

$z_h(t)$ – the solution of the homogeneous equation, $F(t) = 0$

$z_p(t)$ – a particular solution of the full equation (3.1)

Taking into account the assumptions, the solution for the homogeneous equation can be revised as:

$$z_h(t) = \frac{H}{2}\sin(\omega_0 t) \tag{3.3}$$

Where

$\frac{H}{2}$ – amplitude

ω_0 – Eigen frequency, $\omega_0 = \sqrt{\frac{k}{m}}$

Hence, in order to find the natural period of the heave we need to know the stiffness k and the mass m. The mass consists of two components: the mass of the vessel is m_v and the added mass is m_a. The stiffness is determined as the resistance against the vertical motion:

$$k = A_w \rho g \tag{3.4}$$

Where

A_w – area in waterline

ρ – water density

Eigen frequency can be rewritten as follows:

$$\omega_0 = \sqrt{\frac{k}{m}} = \sqrt{\frac{A_w \rho g}{m_v + m_a}} \tag{3.5}$$

Therefore Eigen period:

$$T_0 = \frac{2\pi}{\omega_0} = 2\pi \sqrt{\frac{m_v + m_a}{A_w \rho g}} \tag{3.6}$$

Let us consider different cases:

- Case A – MPSV BOA Deep C
- Case B – SSCV Thialf
- Case C – CV Seven Arctic
- Case D – BOA Barge 43/44

Case A

Assume the MPSV is a rectangular body shape vessel. Taking into account the assumption, the added mass can be defined as follows (DNV, 2010):

$$m_a^{MPSV} = \rho C_A \frac{\pi}{4} a^2 b \tag{3.7}$$

Where

ρ – water density, $\rho = 1025\ kg/m^3$

C_A – added mass coefficient, $C_A = 0.872$ (DNV, 2010)

a – width, $a = 27.32\ m$

b – length, $b = 119.3\ m$

For the MPSV the natural period in heave is:

$$T_{heave}^{MPSV} = 2\pi \sqrt{\frac{m_v + \rho C_A \frac{\pi}{4} a^2 b}{ab\rho g}} \tag{3.8}$$

$$T_{heave}^{MPSV} = 2\pi\sqrt{\frac{9000\cdot 10^3 + 1025\cdot 0.872\cdot\frac{\pi}{4}\cdot 27.32^2\cdot 119.3}{27.32\cdot 119.3\cdot 1025\cdot 9.81}} = 9.28\ s \qquad (3.9)$$

Case B

Assume SSCV columns are the square prisms and two pontoons are the rectangular plates. Taking into account the assumption, the added mass can be defined as follows (DNV, 2010):

$$m_a^{SSCV} = N\rho C_A\frac{\pi}{4}a^2 b \qquad (3.10)$$

Where

N – number of pontoons, $N = 2$

ρ – water density, $\rho = 1025\ kg/m^3$

C_A – added mass coefficient for pontoons, $C_A = 0.934$ (DNV, 2010)

a – width of the pontoons, $a = 25\ m$

b – length of the pontoons, $b = 200\ m$

For the SSCV the natural period in heave is:

$$T_{heave}^{SSCV} = 2\pi\sqrt{\frac{m_v + N\rho C_A\frac{\pi}{4}a^2 b}{ab\rho g}} \qquad (3.11)$$

$$T_{heave}^{SSCV} = 2\pi\sqrt{\frac{129221\cdot 10^3 + 2\cdot 1025\cdot 0.934\cdot\frac{\pi}{4}\cdot 25^2\cdot 200}{25\cdot 200\cdot 1025\cdot 9.81}} = 15.77\ s \qquad (3.12)$$

Case C

Assume the construction vessel Seven Arctic is a rectangular body shape vessel. Taking into account the assumption, the added mass can be defined as follows (DNV, 2010):

$$m_a^{CV} = \rho C_A\frac{\pi}{4}a^2 b \qquad (3.13)$$

Where

ρ – water density, $\rho = 1025\ kg/m^3$

C_A – added mass coefficient, $C_A = 0.897$ (DNV, 2010)

a – width, $a = 32\ m$

b – length, $b = 162.3\ m$

For the construction vessel the natural period in heave is:

$$T_{heave}^{CV} = 2\pi\sqrt{\frac{m_v + \rho C_A \frac{\pi}{4} a^2 b}{ab\rho g}} \tag{3.14}$$

$$T_{heave}^{CV} = 2\pi\sqrt{\frac{13574 \cdot 10^3 + 1025 \cdot 0.897 \cdot \frac{\pi}{4} \cdot 32^2 \cdot 162.3}{32 \cdot 162.3 \cdot 1025 \cdot 9.81}} = 10.04\ s \tag{3.15}$$

Case D

Assume the barge is a rectangular body shape vessel. Taking into account the assumption, the added mass can be defined as follows (DNV, 2010):

$$m_a^{barge} = \rho C_A \frac{\pi}{4} a^2 b \tag{3.16}$$

Where

ρ – water density, $\rho = 1025\ kg/m^3$

C_A – added mass coefficient, $C_A = 0.83$ (DNV, 2010)

a – width, $a = 30\ m$

b – length, $b = 91\ m$

For the barge the natural period in heave is:

$$T_{heave}^{barge} = 2\pi\sqrt{\frac{m_v + \rho C_A \frac{\pi}{4} a^2 b}{ab\rho g}} \tag{3.17}$$

$$T_{heave}^{barge} = 2\pi\sqrt{\frac{10866 \cdot 10^3 + 1025 \cdot 0.83 \cdot \frac{\pi}{4} \cdot 30^2 \cdot 91}{30 \cdot 91 \cdot 1025 \cdot 9.81}} = 9.7\ s \tag{3.18}$$

3.6.6 Selection of vessel

The wave period in the Pechora Sea is varied from 8.6 to 9.5 seconds. The heave period should not coincide with the period of waves in the sea in order to avoid resonance. The results of calculations are contained in the following table:

Table 3-2. The heave period of the installation vessels

Case	*Vessel*	T_{heave}
A	MPSV BOA Deep C	9.28
B	SSCV Thialf	15.77
C	CV Seven Arctic	10.04
D	BOA Barge 43/33	9.7

There is as assumption that the heave period does not change so much when the installation vessel get the ITS on board. According to the data obtained from calculations, the MPSV BOA Deep C could get in resonance with waves according to the Pechora Sea environmental conditions. It is necessary to change the natural period of the vessel to the greater value increase the deadweight, or choose another crane – SSCV Thaif or CV Seven Arctic. Transportation can be performed by BOA Barge 43/33.

Moreover, there is another solution – heave compensation system. There are three types of heave compensators typically used in marine operations:

- Passive heave compensator(PHC),
- Active heave compensator(AHC)
- Combined heave compensator.

PHC is designed to maintain a constant line tension, while in the AHC a simple mechanical feedback system is used to regulate the ship heave motions.

4. Analysis of the different field development concepts

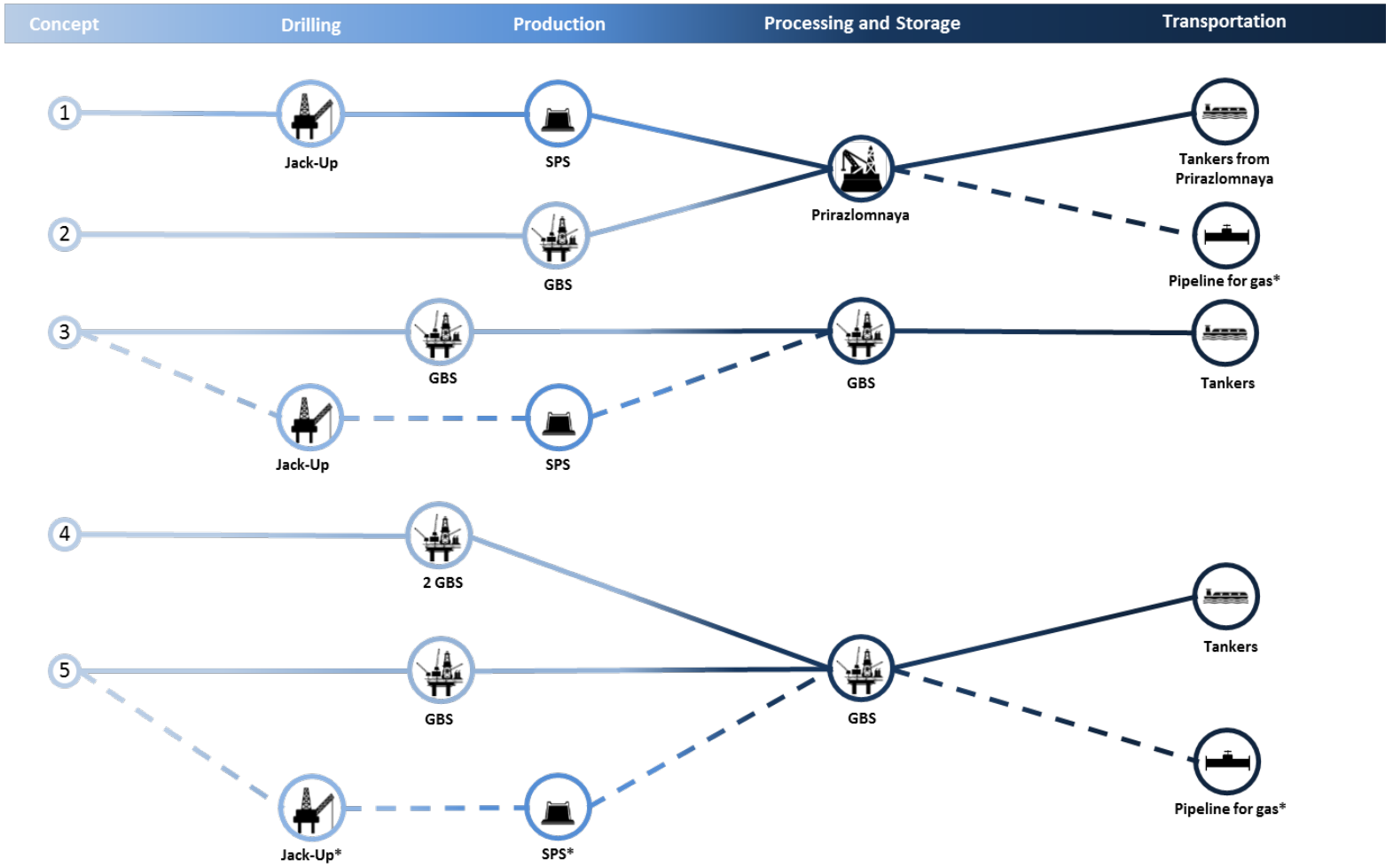

** It is necessary to clarify the gas reserves for assessing the economic feasibility of developing the gas-condensate part of the field*

Figure 4-1. Possible concepts of the Dolginskoye oil field development

The main purpose of the concepts comparison was to determine the most rational concept of field development based on the assessment of technical risks and costs. The initial data for the conceptual study was used in the course of the generalized expert evaluation of the required functionality. After determining the list of possible development concepts, a shortened list was selected, consisting of five different options for further evaluation.

There are two main categories of the development concepts such as Prirazlomnaya-dependent and independent.

- Dependent:
    - Concept №1:
        - Jack-Up rig is used for drilling;
        - Fully subsea development and production;
        - SPS is connected to the Prirazlomnaya via pipeline;
        - Prirazlomnaya is used for processing and storage;
        - Transportation of oil by tankers from Prirazlomnaya;
    - Concept №2:
        - Drilling and production at the GBS;
        - GBS and Prirazlomnaya are connected by pipeline;
        - Prirazlomnaya is used for processing and storage;
        - Transportation of oil by tankers from Prirazlomnaya;

- Independent:
    - Concept №3:
        - Drilling at the Northern part of the filed by Jack-Up for further SPS installation;
        - SPS is used for gas injection and oil production;
        - Drilling and production at the Southern part by technological platform (GBS);
        - Technological platform is used for processing and storage;

        - Transportation of oil by tankers from technological platform;
    - Concept №4:
        - Drilling, production, processing and storage at the GBS A (Northern part);
        - Drilling and production at the GBS B (Southern part);
        - Platforms are connected via pipeline;
        - Oil is transported by tankers;
    - Concept №5:
        - Drilling, production, processing and storage at the GBS (Southern part);
        - Jack-Up rig is used for drilling at the Northern part;
        - SPS is installed at the Northern part for oil and gas production, injection of gas;
        - Subsea installations are connected to the GBS by pipeline;
        - Processing and storage at the GBS;
        - Tankers are used for oil transportation while pipeline to shore should be used for gas transportation;

Each concept was compared for the following parameters:

- Capital expenditure (0 – low cost; 5 – high cost);
- Technical feasibility (0 – feasible; 5 – not feasible);
- Operational and environmental risks (0 – no risks; 5 – high risk);

Parameter	Concept №1	Concept №2	Concept №3	Concept №4	Concept №5
CAPEX	4	5	2	3	2
Technical feasibility	4	3	3	2	3
Risk	5	1	3	1	4

Also, there is a large uncertainty in capital expenditures at the current stage of the analysis. Dependent concepts require a significant modification of the

Prirazlomnaya platform. Costs and scope of work to modify the platform is difficult to assess. Therefore, this issue should be considered separately and in more detail.

It was assumed that the modernization of the platform in the case of the first and second concept is economically inefficient and technically difficult to implement.
Concept №5 is feasible from a technical point of view, but the feasibility of developing the gas part of the field is questionable. This concept is not considered in this work, but it is the subject of further research.
Therefore the following concepts is discussed in more detail below:

- Concept №3 – Scenario A;
- Concept №4 – Scenario B;

4.1 Scenario A

4.1.1 Drilling and maintenance of the wells

The general view of the field arrangement in this scenario is shown in Figure 4-2. This option is the development of the field with the SPS at point B and the technological gravity based platform at point A. This platform is designed for the production and full processing of crude oil as well as storage and oil offloading to tankers. In this scenario, the following parameters for field development have been adopted: laying of the pipeline from the SPS at point B to the platform and laying the pipeline for water injection into the formation and umbilical from platform to SPS. Drilling, maintenance and repair of wells at this point should be carried out from Jack-Up rig.

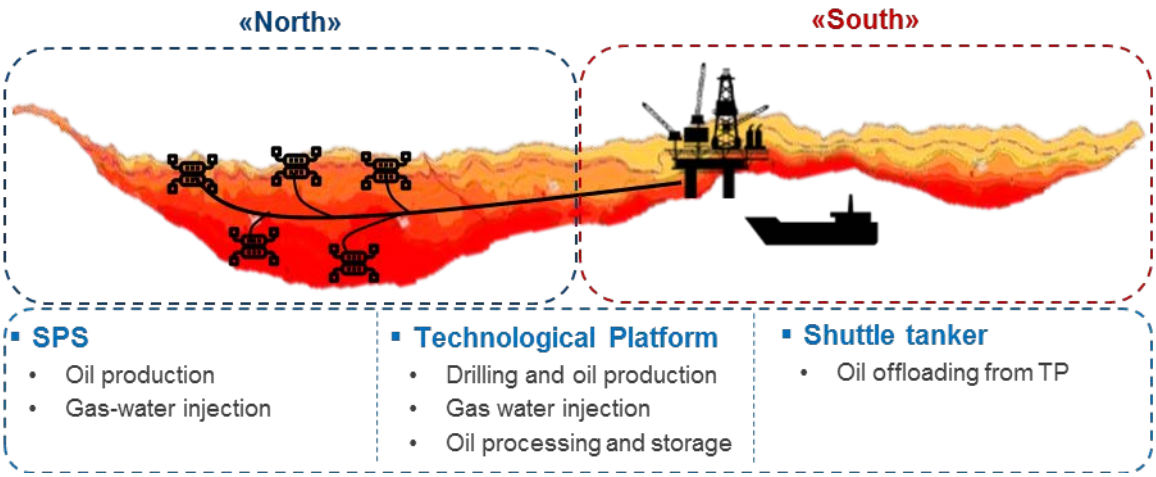

Figure 4-2. Scenario A

The drilling schedule is shown in the figure below.

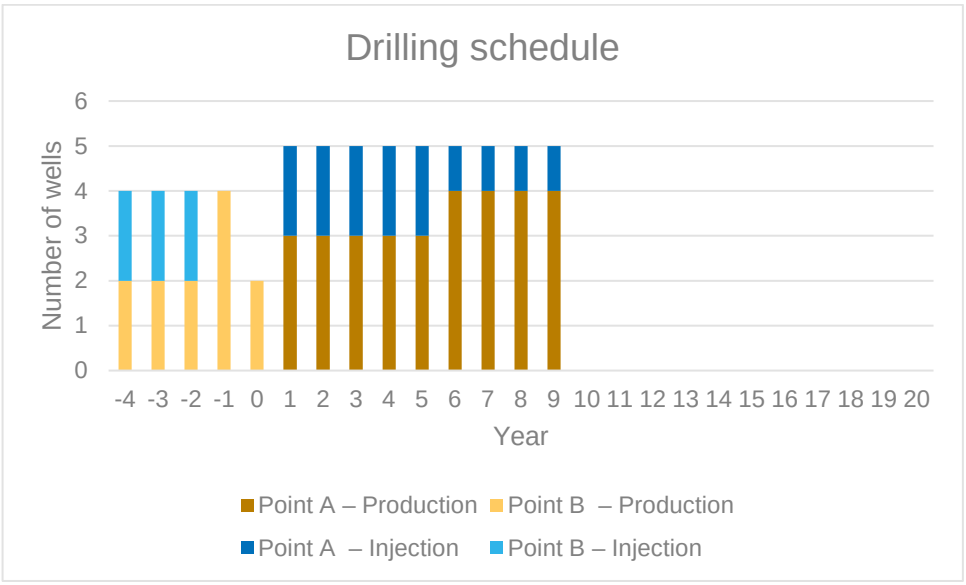

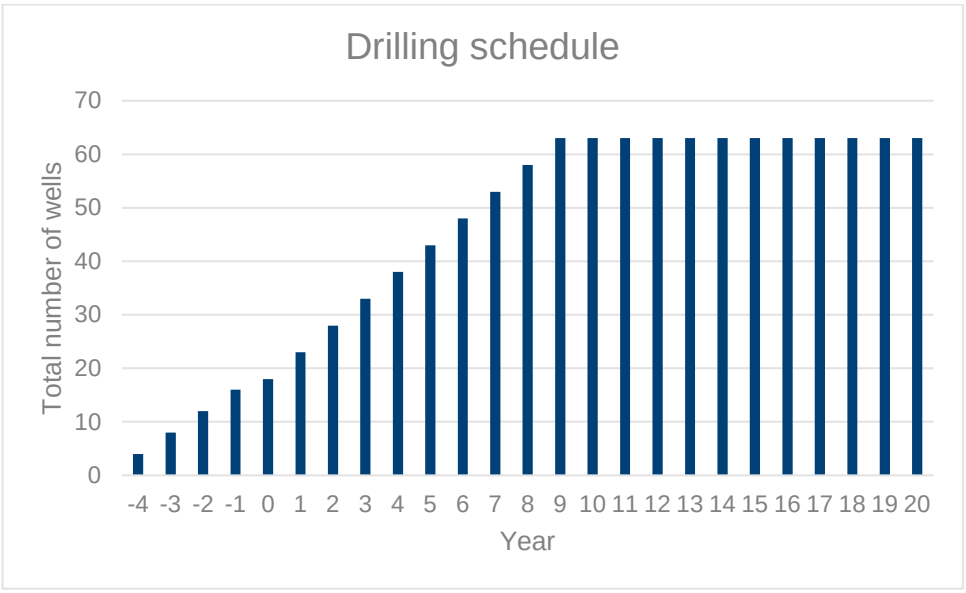

Figure 4-3. Drilling schedule for Scenario A.

According to the drilling schedule, the wells in the northern part of the field are being drilled while the platform is not yet installed. This optimizes costs and creates an early cash flow for operators with only a minimum cash outlay.

The use of Jack-Up drilling rigs is only possible during the ice-free period, i.e. not more than 5 months a year. The drilling time of one well is usually 2 months including completion of the well. Thus, one Jack-Up drilling rig can drill a maximum of two wells per year at the Dolginskoye field.

Considering the fact that it is planned to install 3 production modules (12 production wells) and 2 injection modules (6 injection wells) and that only two wells can be drilled in a year, it is necessary to use 2 drilling rigs. Also, these drilling rigs must be of Arctic design.

One of the main problems in this case is maintenance and repair of wells in the ice season. At this moment, there is no technology that allows such work, therefore it is necessary to carry out repairs only during the ice-free period. This leads to a greater risk of downtime in case of failure. Also, there is a risk of losses in oil production and accordingly the risk of potential negative impact on the overall oil recovery factor in the field.

4.1.2 Oil production, processing and storage

The use of electric submersible pumps to increase oil production was considered as one of the operational options, as well as operation without the use of Artificial Lift System (ALS). However, the use of such pumps entails the following problems:

- Power supply for the ESP from the platform;
- ESP maintenance and repair.

The exploitation of the wells without the use of ALS is possible, but it will lead to lower production rates and to lower revenues from the sale of oil.

It is suggested to use Integrated Template Structures. A centrally positioned manifold is connected to 4 X-mas trees and the structure serves as foundation and protection structure for manifold and trees. The scheme of such a ITS is shown in the figure 4-4.

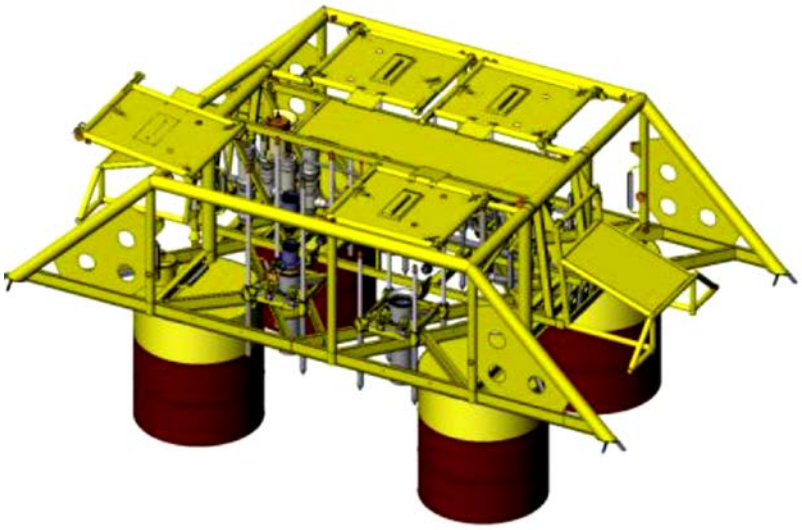

Figure 4-4. Integrated Template Structure (DNV GL, 2014)

The required number of ITS:

- Producers – 3 templates (12 production wells);
- Injectors – 2 templates (6 injection wells).

These five templates are connected to the platform via a 20 km long pipelines:

- Insulated production line (inside diameter about 8 inches);
- Injection line (ID ~12 inches).

The platform is a conical concrete structure considered in Chapter 2. This type of platform was chosen due to the low value of ice load, which is prevail in the conditions of the Pechora Sea. The platform includes the following parts:

- 50 well slots:
    - 31 production wells;
    - 14 injection wells;
    - 5 reserve;
- Stationary drilling facility;
- Technological facilities:
    - Stabilization, dehydration and export of oil;
    - Processing and injection of produced water and seawater into the formation;
    - Compression of associated gas for re-injection into the reservoir;
    - Reception and processing of the well fluid from SPS;
    - Oil storage;
- Living Quarters for crew;
- Other accessory systems;

4.1.3 Production profile

It is necessary to use horizontal long-distance wells to increase the initial oil production rate in the well. In the practice of operating horizontal wells, there are a number of expressions for calculating the flow rate of a liquid. The most used is the Joshi equation:

$$q_h = \frac{2\pi K h \Delta P}{\mu\beta\left(\ln\frac{\alpha+\sqrt{\alpha^2-\left(\frac{L}{2}\right)^2}}{\frac{L}{2}}+\frac{æh}{L}\ln\frac{æh}{2\pi r_{wb}}\right)} \quad (4.1)$$

$$\alpha = \frac{L}{2}\left(0{,}5+\left(0{,}25+\left(\frac{2R_d}{L}\right)^4\right)^{0{,}5}\right)^{0{,}5} \quad (4.2)$$

$$æ = \left(\frac{K}{K_z}\right)^{0{,}5} \quad (4.3)$$

Where

h – reservoir thickness;

K – coefficient of permeability by bedding;

ΔP – pressure drop;

μ – coefficient of oil dynamic viscosity;

β – formation volume factor;

L – length of horizontal part;

K_z – coefficient of permeability perpendicular to bedding;

æ – anisotropic factor;

r_{wb} – reduced wellbore radius;

R_d – radius of the drainage zone;

Using the formulas (4.1-4.3), the oil production was calculated for a horizontal well of the Dolginskoye field. The initial production rate of one production well is 1205 tons per day which is typical for similar wells at the Prirazlomnoye field. Further, the calculation of production by year was carried out, the results of calculation are shown in figures below.

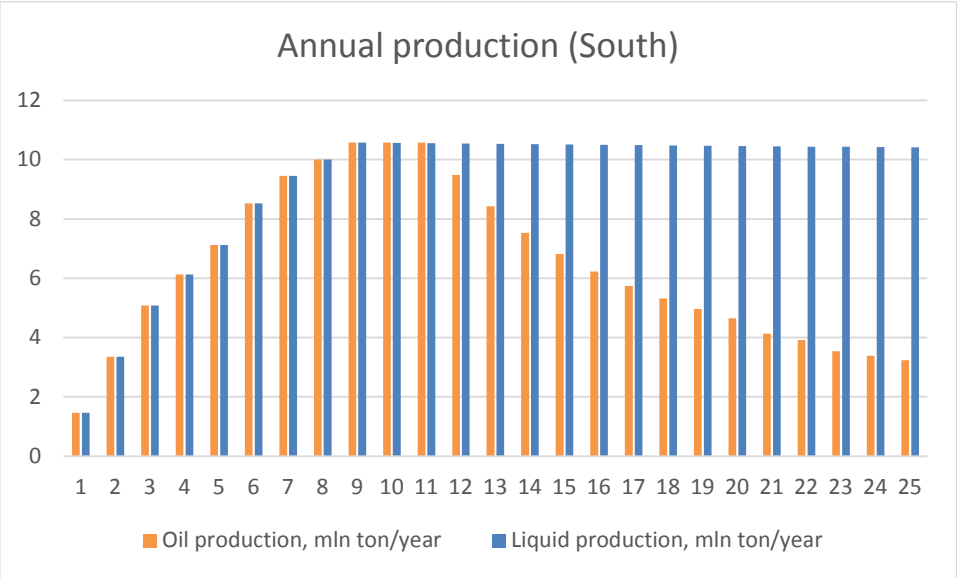

Figure 4-5. Annual production of oil and liquid at the Southern part of field

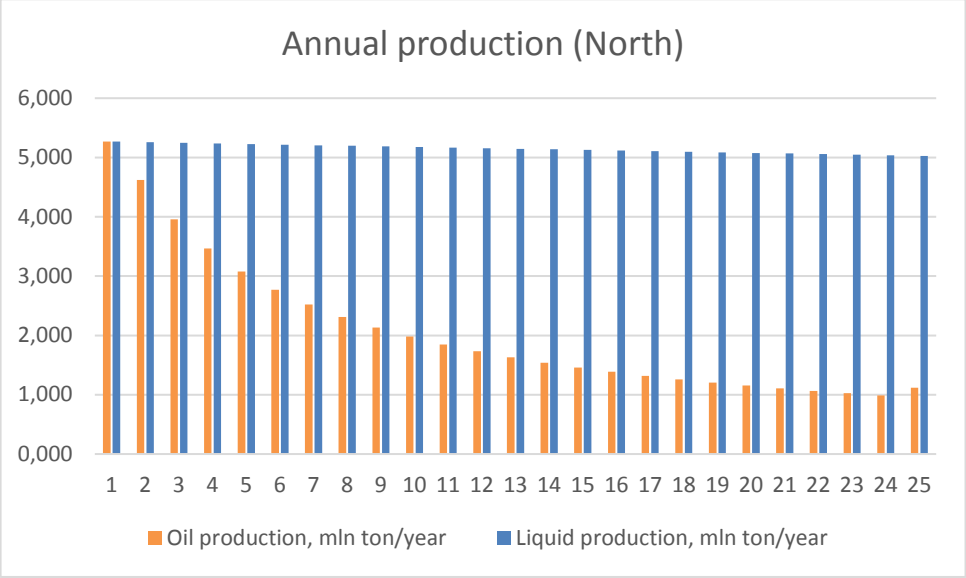

Figure 4-6. Annual production of oil and liquid at the Northern part of field

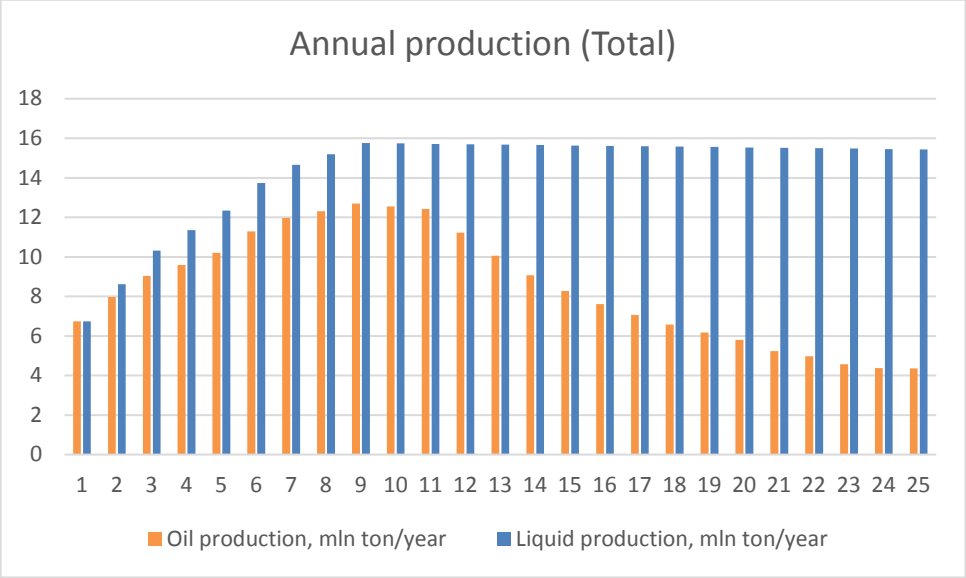

Figure 4-7. Annual production of oil and liquid

As can be seen from Figures 4-5, 4-6 and 4-7, the oil production from the northern part of the deposit begins simultaneously with the start of production on a platform located in the south. It is proposed to use early production systems and fast-track schedules. They can create an early cash flow for operators with only a minimum cash outlay. They also provide real-time production data for appraising reservoir performance before more-expensive long-term facilities are installed (Schlumberger, n.d.).

4.1.4 Transportation

The offloading operation carried out from the platform is provided by means an integrated system of direct oil offloading similar to system which is used on the Prirazlomnaya project. Transportation of oil from the platform requires two new shuttle tankers and an icebreaking vessel for ensuring safe offloading of oil on shuttle tankers.

4.1.5 Economic Efficiency

In the economic evaluation of the project, a cash flow model was constructed, consisting of the following parameters:

- Income from oil sales;
- Expenditure, consisting of operating and investment activities:
    - Operating activities – operational expenditures for oil production and subsequent taxes;
    - Investment activities - capital expenditures for the development and operation of the field;
- Economic indicators:
- Cash flow (CF);
- Discounted cash flow (DCF);
- Net present value (NPV).

The revenue part is formed by the sale of commercial oil and is calculated based on the volume of oil production and the price of one barrel. Production volumes were calculated earlier in paragraph 4.1.3. As for the selling price, it was assumed that the barrel of oil is sold for $ 75 (at a rate of 60 rubles per dollar).

To calculate the operating costs, it is desirable to have special software or conduct a deep analysis-benchmarking similar projects. Since there are not so many similar

projects, and carrying out this analysis requires a large amount of data and information, it was assumed on the basis of an expert assessment that the production of one barrel of oil requires $ 20 costs.

In addition to operating expenditures, it is necessary to take into account the main taxes that form the tax burden on the project:

- The mineral extraction tax depends on factors such as:
    - Kc - the dynamics of world oil prices;
    - Dm - features of oil production (Federal Tax Service, 2018);
- The mineral extraction tax was adopted at 3,000 rubles per ton of oil produced based on a similar Prirazlomnaya Arctic project;
- Property tax is 2.2% of the residual value of funds (Chapter 30 of the Tax Code)
- Unified social tax - is about 30% of the wage fund;
- Other taxes are not considered because their order is insignificant compared to the main taxes.

Investment activity is the cost of the following components:

- Engineering, procurement, construction and installation costs (EPCI) of a topside - $ 1.640 billion (according to Wood Mackenzie);
- Costs for the EPCI of a GBS are $ 1.110 billion (according to Wood Mackenzie);
- The following items are included in the well construction budget:
    - Drilling wells:
        - Preparatory work;
        - Provision of drilling crew;
        - Conductor, Technical Column, Production Column, Shank;
        - Output to the mode;
        - Testing;

- Hydrochloric acid treatment;
- Descent of the ESP;
- Project office;

- Services:
  - Directional drilling;
  - Bits;
  - Core sampling;
  - Drilling fluids;
  - Cementing of wells;
  - Lower completion of wells;
  - Hydrochloric acid treatment;
  - Geotechnical surveys;
  - Logging service;
  - Utilization of drilling waste;
  - Geonavigation;
- Rent of equipment:
  - Lease of containers;
  - Leasing of fishing tools;
  - Equipment for screwing and lowering pipes and tubing;
  - Hand tools, small mechanization tools, BHA elements, etc .;
  - Cable-rope installation;
  - Installation of the column head;
  - Installation of a Christmas tree;
- Materials:
  - Casing;
  - Tubing;
  - Column head;
  - Downhole equipment;
  - Christmas tree;
  - Hydrochloric acid;

- Direct costs:
  - Air transportation;
  - Providing anti-futnal security;
  - Author's supervision;
  - Development of design estimates;
  - Expertise of design estimates;
  - Insurance;
  - Storage of hydrochloric acid;
  - Expenses on the loan;
  - Defectoscopy;
  - Accommodation, meals and staff maintenance;
  - FEED;
  - Research and development centre;
  - Neutralization of drilling wastes;
- Spendable costs:
  - Platform services;
  - Administrative and management personnel (salary, payments, business trips);
  - Procurement.

- Thus, based on the experience of a similar Arctic project, the cost of building a single well was estimated at 1.315 billion rubles;
- The cost of construction of a single injection well was estimated at 1.184 billion rubles;
- The cost of building a well from a Jack-Up rig (without taking into account the lease of the rig itself) will be significantly lower than the cost of drilling a well from the platform. This is justified by the fact that wells drilled from the Jack-Up are more "simple" in technical terms, that is, the well trajectory is simplified and does not require large waste from the vertical and,

consequently, the depth along the trunk is also smaller, which leads to a reduction in the construction period of the well;

- The costs for the construction of a production well from Jack-Up platform are estimated at 855 million rubles, and the injection costs of 769 million rubles;
- The cost of the Jack-Up leasing is $ 100 thousand / day;
- According to Wood Mackenzie, the costs for the EPCI of the 4-slot integrated template are estimated at 7.2 billion rubles;
- The cost of constructing a pipeline from the subsea production system to the platform. The cost of construction of 1 km of the pipeline is estimated at $ 2 million.

Thus, an economic model of the Dolginskoye field development project was developed on the basis of scenario A. A more detailed table of the economic model is presented in the Appendix. The table below summarizes this model:

Table 4.2 Economical model of Concept A

Parameter, million rubles	Concept A
Revenues	**6 998 428**
CAPEX	**281 487**
Topside	98 400
GBS	66 000
Drilling	78 687
Subsea production system	36 000
Pipeline	2 400
OPEX	**2 528 848**
Operating costs of production	1 866 247
Taxes	661 608
NPV, billion rubles	**992**
IRR	**43%**
PI	**3.53**

4.2 Scenario B

4.2.1 Drilling and maintenance of the wells

The general view of the field arrangement in this scenario is shown in Figure 4-8. Two gravity based platforms (first – technological platform at point A and second – wellhead platform at point B) are used to develop Dolginskoye field. The purpose of wellhead platform is to drill wells and extract oil and then transport it to technological platform. The technological platform is the same as in the previous concept.

In this scenario, the following parameters for field development have been adopted: laying of the pipeline from the wellhead platform at point B to the technological platform at point A. Drilling, maintenance and repair of wells at both points should be carried out from platforms.

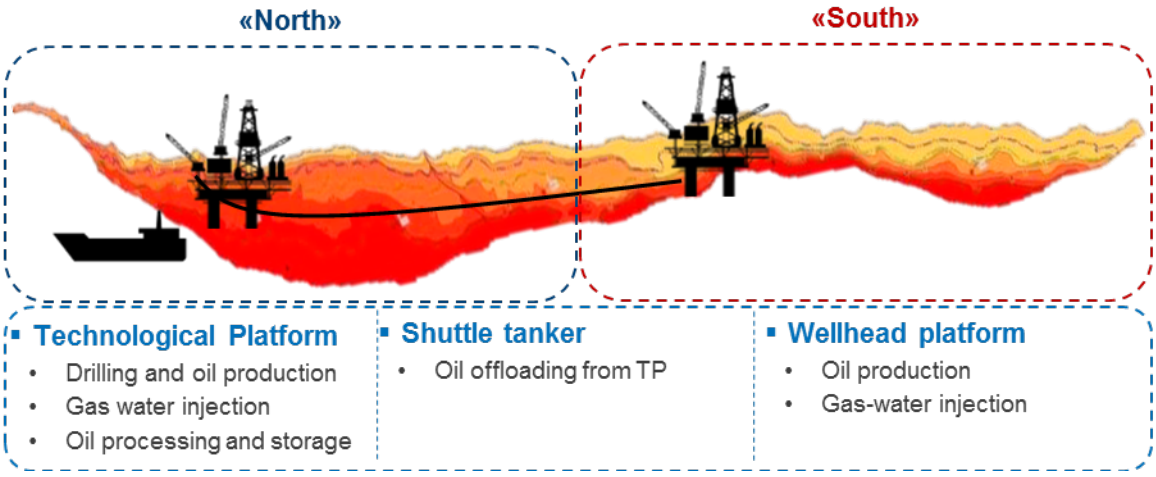

Figure 4-8. Scenario B

The drilling schedule is shown in the figure below.

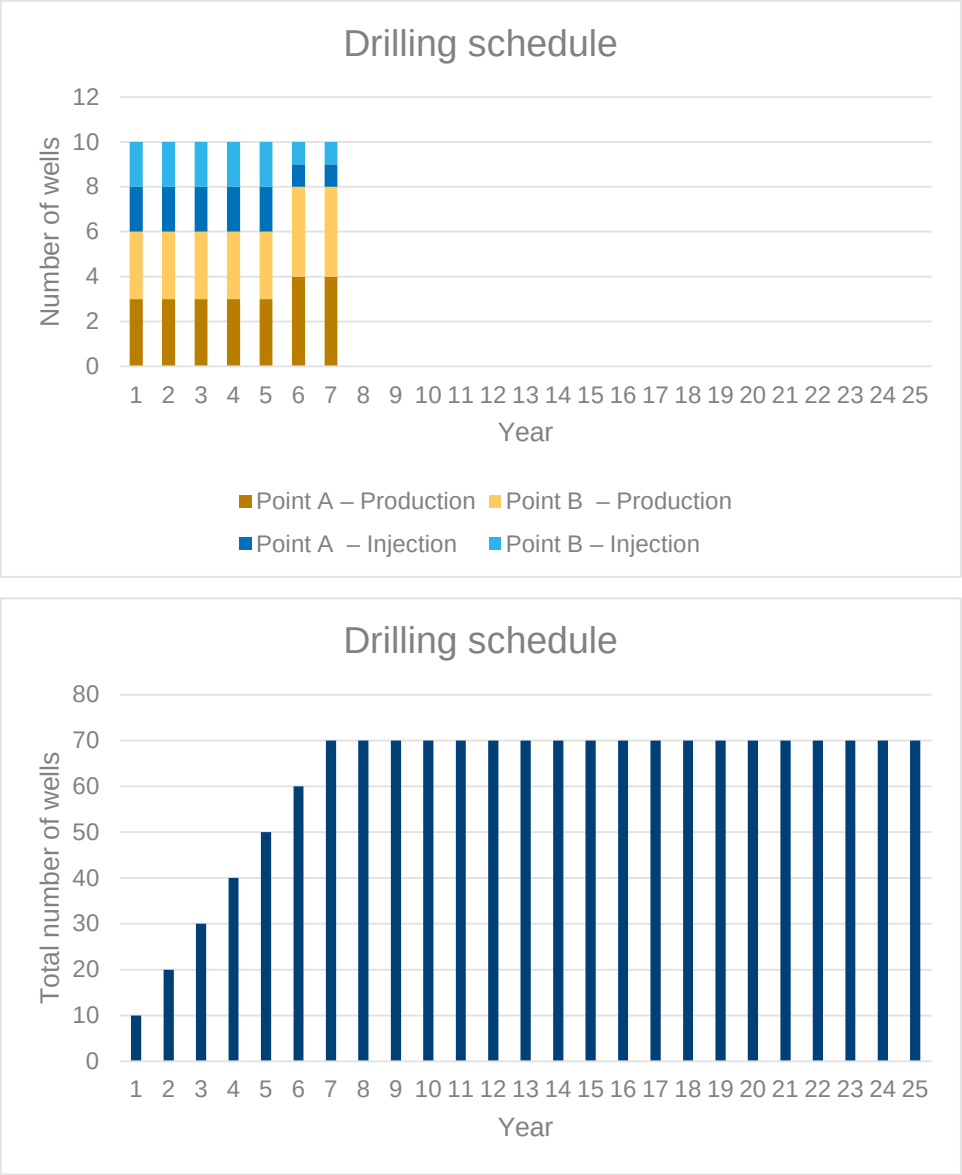

Figure 4-9. Drilling schedule for Scenario B.

Ice conditions do not affect to the drilling and maintenance, so they are year-round processes. According to the drilling schedule it is planned to drill 23 production wells and 12 injection wells on each platform. It is assumed that the average drilling speed, taking into account the repair of wells, is five wells per year for each platform. Also, coiled tubing technology can be used for well maintenance and repair. This makes it possible not to use the drilling rig for repair, so it can be used only for drilling. Hence, the number of wells drilled per year could be increased.

4.2.2 Oil production, processing and storage

It is envisaged to install two platforms for oil production and gas-water injection, one of which also includes the processing facilities and oil storage tanks. The platform is a conical concrete structure considered in Chapter 2. This type of platform was chosen due to the best resistance to the ice load, which is prevail in the conditions of the Pechora Sea. The wellhead platform includes the following parts:

- 40 well slots:
    - 23 production wells;
    - 12 injection wells;
    - 5 reserve;
- Stationary drilling facility;
- Collection of well fluid and transfer to the technological platform;
- Reception of formation water from the technological platform for injection into the reservoir;
- Reservoir pressure maintenance system;
- Living Quarters for crew;
- Other accessory systems;

The functions and facilities of the technological platform:

- 40 well slots:
    - 23 production wells;
    - 12 injection wells;
    - 5 reserve;
- Stationary drilling facility;
- Technological facilities:
    - Stabilization, dehydration and export of oil;
    - Processing and injection of produced water and seawater into the formation;

- Compression of associated gas for re-injection into the reservoir;
- Reception and processing of the well fluid from SPS;
- Oil storage;

- Receiving and processing of the well fluid from the wellhead platform;
- Transport of formation water for injection into the reservoir from a wellhead platform;
- Living Quarters for crew;
- Other accessory systems;

There is also a need for a pipeline between these platforms 20 km long, consisting of two branches:

- Insulated production line (inside diameter about 12 inches);
- Injection line (ID ~12 inches).

4.2.3 Production profile

In this case, the initial production rate is equal to 1205 tons per day. It is planned that both platforms will produce approximately the same amount of oil, therefore, the production profiles will be similar. The figures below shows the production profile for the field:

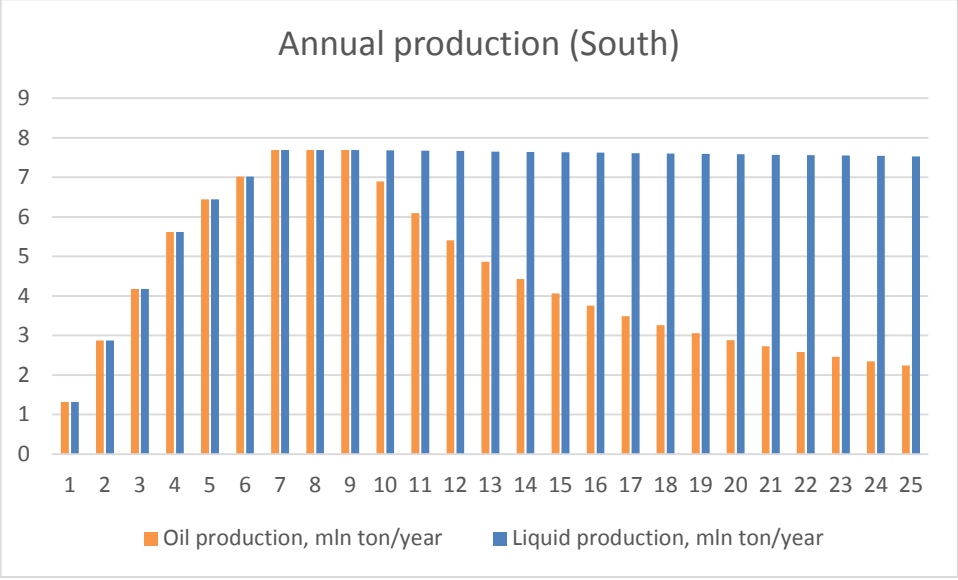

Figure 4-10. Annual production of oil and liquid at the Southern part of field

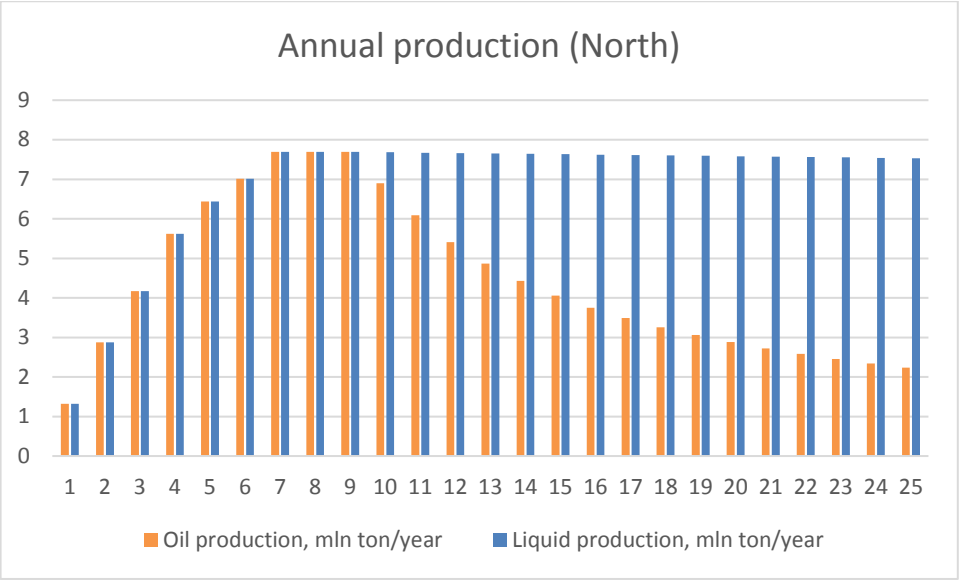

Figure 4-11. Annual production of oil and liquid at the Northern part of field

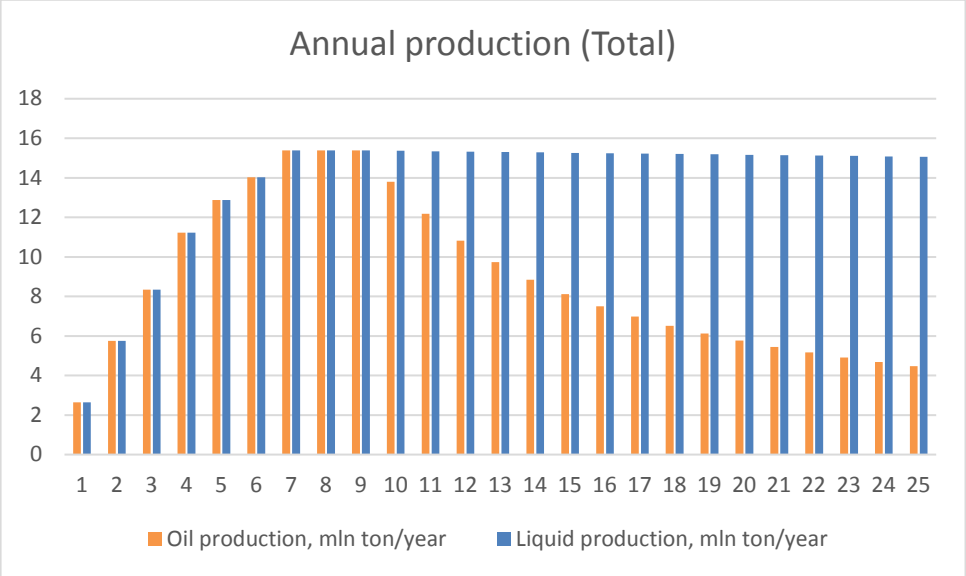

Figure 4-12. Annual production of oil and liquid

4.2.4 Transportation

The offloading system is the same as the system considered in scenario A. Given that the technological platform is located in the northern part of the field and that the intended place of delivery of the oil is Rotterdam (Holland).

4.3 Economic Efficiency

In this section, an economic evaluation of the scenario for the development of the Dolginskoye field is carried out. Below are the items that differ from the economic model of scenario A:

- EPCI - $ 1.640 billion for a technology platform, $ 1.420 billion for a wellhead platform (according to Wood Mackenzie);
- EPCI for gravity-type bases are $ 1.110 billion for each platform (according to Wood Mackenzie);

Thus, an economic model of the Dolginskoye field development project was developed on the basis of scenario B. A more detailed table of the economic model is presented in the Appendix. The table below summarizes this model:

Table 4.3 Economical model of Concept B

Parameter, million rubles	Concept A
Revenues	**7 328 133**
CAPEX	**406 894**
Topside	183 600
GBS	132 000
Drilling	88 894
Pipeline	2 400
OPEX	**2 659 721**
Operating costs of production	1 954 169
Taxes	704 741
NPV, billion rubles	**808**
IRR	**32%**
PI	**1.99**

Summary

The purpose of this work is to prepare technical proposals for industrial development and a conceptual scheme for the development of the Dolginskoye field. A list of possible concepts for field development was considered, followed by a preliminary analysis and screening. As a result, a list of five possible scenarios was formed. Within the scope of this thesis two scenarios independent of the platform Prirazlomnaya was considered and compared. The main purpose of the concepts comparison was to determine the most rational concept of field development based on the assessment of technical risks and costs.

Based on the calculations and analysis of the field development scenarios, the field development concept consisting of a technological platform located on the Southern part and the subsea production system located at the Northern part of the field was adopted as the most effective. The subsea facilities are connected to the technological platform where the construction of the wells and production of oil with the following processing, storage and offloading are performed. This concept is the most technically and economically feasible due to the lower capital expenditures for this development option and due to the early oil production which gives early income.

Also, an analysis of the optimal gravity based structure design for the conditions of the Dolginskoye water area was carried out. According to the calculations, a conical platform was chosen due to the lower ice and wave loads acting on the structure. These calculations were carried out in accordance with the international standard (ISO 19906) and the Norwegian standard (DNV-RP-C205) using the Monte Carlo method for more accurate results.

In addition, various scenarios for subsea equipment installation in the water area of the Dolginskoye field are considered. Based on the calculations carried out, basic scenarios for the installation of modules are proposed.

References

Bellendir, E. N., Toropov, E.E. (2000). *Analysis of Various Designs of the Stationary Platform Substructures For the Pechora Sea Shelf*: International Society of Offshore and Polar Engineers. Paper presented at the The Tenth International Offshore and Polar Engineering Conference. Seattle, Washington, USA.

Bjornbom, E. (2012). *Report - Leak detection and monitoring from template to satellite*.

Bjornbom, E., Hansen, O. and Engen, F. (2012). *Implementation of the oil spill preparedness for the Goliat offshore oil field development*. Paper presented at the SPE/APPEA International Conference on Health, Safety and Environment in Oil and Gas Exploration and Production. Perth, Australia.

BOA. (2016). *Specification - Boa Deep C.* Available at: http://www.boa.no/Admin/Public/DWSDownload.aspx?File=%2fFiles%2fFiler%2fBrochures%2fBOA+Deep+C+Brochure+Final+v4.pdf [Accessed November, 2017]

Daleel. (n.d.). Webpage. *Daleel oil and gas supply chain portal - Multi-Purpose Support Vessel (MPSV).* Available at: http://www.scmdaleel.com/category/multi-purpose-support-vessel-mpsv/209 [Accessed November, 2017]

DNV GL. (2014). *Introduction to Subsea Production Systems.* Available at: http://www.uio.no/studier/emner/matnat/math/MEK4450/h14/undervisningsmateriale/module-2/mek4450-dnvgl-05-templates-and-manifolds.pdf [Accessed May 2018]

DNV. (2010). Recommended practice DNV-RP-C205. *Environmental conditions and environmental loads*.

DNV. (2011). Offshore standard DNV-OS-C101. *Design of offshore steel structures, general (LRFD method).*

DNV. (2012). Offshore standard DNV-OS-C201. *Structural design of offshore units (WSD Method).*

Dymov, V. I., Zubakin, G.K., Klervantsov, Y.P., Rozhkov, V.A., Skutina, E.A. (2012). *Wind and waves in the Pechora Sea*. Journal: Problems of the Arctic and Antarctic, (4(94)),23-40

Egorov, Y. (2017). *Course project - The Goliat field subsea development,*University of Stavanger

ENI. (n.d.). Webpage. *Eni Norge AS. Facts regarding to the Goliat field.* Available at: http://www.eninorge.com/en/Field-development/Goliat [Accessed November, 2017]

Fadeev A.M. (2014). *Report - Dolginskoye field: status and prospects*. Saint Petersburg. Gazpromneft-Sakhalin.

Gazpromneft. (2014). *Report - Development of the Dolginskoye field*. Saint Petersburg. Gazpromneft.

Gazpromneft-Sakhalin internal data, n.d., *Information regarding the Dolginskoye field was obtained during the internship*.

Gudmestad, O. T. (2015). Marine technology and operations : theory & practice. Southampton: WIT Press.

Gudmestad, O. T., Zolotukhin, A. B., Ermakov, A. I. , Jakobsen R. A. , Michtenko I. T. , Vovk V. A. , Løset S. and Shkhinek K.N. (1999). *Basics of Offshore Petroleum Engineering and Development of Marine Facilities - With Emphasis on the Arctic Offshore*. Moscow: Neft i gas publishing house.

Hebron project. (2011). *Report - Comprehensive Study Report.* Available at: http://www.ceaa.gc.ca/050/documents_staticpost/46144/52565-eng.pdf [Accessed November, 2017]

Hebron project. (2015). Webpage. *Pool 3 Phase 1 Project*. Available at: http://www.hebronproject.com/procurement/pool3_strat.aspx [Accessed November, 2017]

Hebron project. (2015). Webpage. *The project.* Available at: http://www.hebronproject.com/project/index.aspx [Accessed November, 2017]

Heerema. (n.d.). Webpage. *Heerema Marine Contractors - Fleet - Thialf.* Available at: https://hmc.heerema.com/fleet/thialf/ [Accessed November, 2017]

Heggdal, O. (n.d.). *Report - Cost efficient subsea tie-back development concept in 1000m water depth and mitigation of hydrate challenges,* Presented at MCE Deepwater Development 2016.

Hibernia. (n.d.). Webpage. *About Hibernia*. Available at: http://www.hibernia.ca/index.html [Accessed November, 2017]

Hjelmeland, M., Olsen, A.B. and Marjohan, R. . (2011). *Advances in subsea wet gas compression technologies*. Paper presented at the International Petroleum Technology Conference. Bangkok, Thailand.

ISO. (2010). ISO 19906:2010 Preview Petroleum and natural gas industries - Arctic offshore structures.

Karunakaran, D.N. (2017). *Course - OFF520_1 Rørledninger og stigerør, University of stavanger.*

KBR. (n.d.). *Report - Hibernia Project Profile*. KBR, Inc. Available at: https://www.kbr.com/Documents/Project%20Profiles/ProjectProfile_Hibernia.pdf [Accessed November, 2017]

Løset, S. (2017). *Course - AT327_Arctic Offshore Engineering, UNIS, Svalbard.*

Løset, S., Shkhinek, K. N., Gudmestad, O. T., & Høyland, K. V. (2006). Actions from ice on arctic offshore and coastal structures. LAN, St Petersburg.

MicroMarket Monitor. (n.d.). *Report - Multi-purpose Service vessels Market Research,* Available at: http://www.micromarketmonitor.com/market-report/mpsv-multi-purpose-service-vessels-reports-2313317039.html [Accessed May, 2018].

Novikov, A. Y. (2014). *Report - Studies of stability of the drilling unit "Arcticheskaya" on the soil of Dolginskoye license* sector Saint Petersburg. Gazpromneft.

NPD. (n.d.). Webpage. *Norwegian Petroleum Directorate - Project "Factpages"*. Available at: http://factpages.npd.no [Accessed November, 2017]

Palmer, A., & Croasdale, K. (2013). Arctic offshore engineering. World Scientific Publishing.

Prescott, N., Mejia, F., Erford, J. and Bhardwaj, R. . (2016). *Shallow Water Subsea Drilling and Production Structure to Resist Sand and Ice Keel Intrusion in Arctic Environments*. Paper presented at the Arctic Technology Conference. St. John's, Newfoundland and Labrador, Canada.

Rekdal, O. (n.d.). *Report - Forebygging av akutte utslipp i prosjekterings- og designfase. Eksempel fra Goliat*, Presented at ENI Norge.

Rigzone. (2014). Webpage. *Statoil Begins Installation of First Template for Snohvit.* Available at: http://www.rigzone.com/news/oil_gas/a/13585/statoil_begins_installation_of_first_template_for_snohvit/ [Accessed November, 2017]

Sakhalin Energy. (n.d.). Webpage. *About the company - Company Assets - Piltun-Astokhskoye-B platform (PA-B).* Available at: http://www.sakhalinenergy.ru/en/company/company_assets/platforma_piltun_astokhskaya_b.wbp [Accessed November, 2017]

Selvadurai, A. P. S., & Boulon, M. J. (Eds.). (1995). Mechanics of Geomaterial Interfaces. Studies in Applied Mechanics. Elsevier Science & Technology.

Shestov, A. (2017). *Course - AT327_Arctic Offshore Engineering, UNIS, Svalbard.*

SNIP. (1986). Construction Codes and Regulations. *Loads and Forces of Hydrotechical Facilities SNIP 2.06.04-82*. Mosstroy, Moscow.

Subsea 7. (2015). *Specification – Seven Arctic construction vessel.* Available at: https://www.subsea7.com/content/dam/subsea7/documents/whatwedo/fleet/constructionvertical/Seven%20Artic%20Booklet%202015-Reference.pdf [Accessed November, 2017]

Tangvald, T. B. and Kiste, K. (2009). *Goliat field development circular FPSO in harsh environment*. Paper presented at the Offshore Mediterranean Conference and Exhibition. Ravenna, Italy.

VNIIGAZ. (2008). Report. *Synergy of the Prirazlomnaya project with other projects*. All-Union Scientific Research Institute of Natural Gases and Gas Technologies (VNIIGAZ).

Widianto, J.K, Gus, T. and Knut, B. (2016). *Concrete Gravity-Based Structure. Construction of the Hebron offshore oil platform.* Concnrete international, 38. Available at http://wpstatic.idium.no/www.concretestructures.no/2016/09/GBS-ACI-Vol38No6_full.pdf [Accessed November, 2017]

ФНС (2018). *Налог на добычу полезных ископаемых (НДПИ)*. Available at: https://www.nalog.ru/rn77/taxation/taxes/ndpi/ [Accessed May 2018]

Appendix
A: Data for calculations

Water depth	d, m	50
Water denisty	ρ, kg/m^3	1025
Drag coefficient	Cd	1.05
Mass coefficient	Cm	1.2
Monopod diameter	D, m	35
Monocone diameter	D, m	66
Significant wave height	Hs, m	4.7
Peak period	Tp, sec	10.2
Wave height	H, m	Statistical data
Wave period	T, sec	Statistical data
Indentation factor	I	1.1
Shape factor	K1	0.9
Contact factor	K2	1.0
Compressive strength	σ_c, MPa	1.415 (Mean value) Statistical data
Ice thickness	h, m	1.2 (Mean value) Statistical data
Flexural strength	σ_f, MPa	0.5 MPa
Young`s modulus of ice	E, GPa	8.7
Ice friction coefficient	μ	0.3
Slope angle	α, °	52
Height of the rubble*	hr, m	5
Ice density	ρ_{ice}, kg/m^3	910
Poisson ratio for ice	v	0.3
Ice-to-ice friction coefficient * *	μ_i	0.3
Porosity of the ice rubble***	e	0.4
Angle the rubble makes with the horizontal***	θ, °	42
Friction angle of the ice rubble***	ϕ, °	45
Cohesion of the ice rubble***	c, kPa	4

*Assumption according to Loset, S.
** Assumption based on the Doctoral thesis of Sukhorukov, S. (2013) – "Ice-Ice and Ice-Steel Friction in Field and in Laboratory"
*** Assumptions according to Kulyakhtin and Hoyland (2015) - "Ice rubble frictional resistance by critical state theories".

B: MATLAB transcripts

Wave load on the monopod platform

```
clear all;
close all;

d=50;
po=1025;
Cd=1.05;
Cm=1.2;
D=35;
x1=0;
syms z
data=load('tempWave.dat');
waveheight=data(:,2);
waveperiod=data(:,3);
xxx=0:0.01:2.5;
pd_height=fitdist(waveheight,'Normal');
pd_period=fitdist(waveperiod,'Normal');
iterations=1000;
hFig = figure('units','normalized','outerposition',[0 0 1 1]);


for i=1:iterations
    H(i,1)=random(pd_height);
    T(i,1)=random(pd_period);
    t(i,1)=0;
    psi(i,1)=H(i,1)/2;
    w(i,1)=2*3.14/T(i,1);
    k(1,1)=0.0415;
    l(i,1)=tanh(d)*9.81*T(i,1)^2/(2*(3.14));
    k(i,1)=3.14*2/l(i,1);

U(i,1)=(psi(i,1)*k(i,1)*9.81/w(i,1))*(cosh(k(i,1)*(z+d))/cosh(k(i,1)*d))*sin(
w(i,1)*t(i,1)-k(i,1)*x1);

acr(i,1)=psi(i,1)*k(i,1)*9.81*(cosh(k(i,1)*(z+d))/cosh(k(i,1)*d))*cos(w(i,1)*
t(i,1)-k(i,1)*x1);
    fd(i,1)=0.5*po*Cd*D*U(i,1)*abs(U(i,1));
    fm(i,1)=0.25*3.14*D^2*po*Cm*acr(i,1);
    F(i,1)=((double(int(fd(i,1),z,-d,psi(i,1))))+(double(int(fm(i,1),z,-
d,psi(i,1)))))/10^6;
    pdf_height=pdf(pd_height,xxx);
    cdf_height=cdf(pd_height,xxx);
    pdf_period=pdf(pd_period,xxx);
    cdf_period=cdf(pd_period,xxx);

    if i>5
        subplot(2,2,1);
            histfit(F);
                xlabel('F, MN');
                ylabel('number of appearance, [1]');
                axis([0 120 0 inf]);

        subplot(2,2,2);
            f=0:0.01:120;
            pd_F=fitdist(F,'Normal');
            pdf_F=pdf(pd_F,f);
            cdf_F=cdf(pd_F,f);
            plot(i,pd_F.sigma/pd_F.mu*100,'.r'); hold on;
```

```
            grid on;
            axis([0 iterations 0 inf] )
            xlabel('iteration number');
            ylabel('\sigma / \mu, %');

        subplot(2,2,3);
        plot(f, cdf_F);
            xlabel('F, MN');
            ylabel('CDF(F), [1]');
            grid on;


        subplot(2,2,4);
            if i>6
                set(h1,'Visible','off');
                set(h2,'Visible','off');
                set(h3,'Visible','off');
                set(h4,'Visible','off');
                set(h5,'Visible','off');
                set(h6,'Visible','off');
                set(h7,'Visible','off');
            end
            edf_F=1-cdf_F;
            h1=plot(f, edf_F);hold on;
            set(gca, 'YScale', 'log');
            axis([0 120 10^-5 1]);
            xlabel('F, MN');
            ylabel('EDF(F), [1]');
            grid on;

            SL=max(find(edf_F>10^-1));
            a=SL;
            h2=stem(f(a),edf_F(a),'.g');
            xx=[0 f(a)]; yy=[edf_F(a) edf_F(a)];
            h3=plot(xx,yy,'g');

            ELIE=max(find(edf_F>10^-2));
            a=ELIE;
            h4=stem(f(a),edf_F(a),'.r');
            xx=[0 f(a)]; yy=[edf_F(a) edf_F(a)];
            h5=plot(xx,yy,'r');


            ALIE=max(find(edf_F>10^-4));
            a=ALIE;
            h6=stem(f(a),edf_F(a),'.black');
            xx=[0 f(a)]; yy=[edf_F(a) edf_F(a)];
            h7=plot(xx,yy,'black');

        pause(0.001);
    end
end
```

Wave load on the monocone platform

```
clear all;
close all;

d=50;
po=1025;
Cd=1.05;
Cm=1.2;
D=66.25;
x1=0;
syms z
data=load('tempWave.dat');
waveheight=data(:,2);
waveperiod=data(:,3);
xxx=0:0.01:2.5;
pd_height=fitdist(waveheight,'Normal');
pd_period=fitdist(waveperiod,'Normal');
iterations=1000;
hFig = figure('units','normalized','outerposition',[0 0 1 1]);


for i=1:iterations
    H(i,1)=random(pd_height);
    T(i,1)=random(pd_period);
    t(i,1)=0;
    psi(i,1)=H(i,1)/2;
    w(i,1)=2*3.14/T(i,1);
    k(1,1)=0.0415;
    l(i,1)=tanh(d)*9.81*T(i,1)^2/(2*(3.14));
    k(i,1)=3.14*2/l(i,1);

U(i,1)=(psi(i,1)*k(i,1)*9.81/w(i,1))*(cosh(k(i,1)*(z+d))/cosh(k(i,1)*d))*sin(
w(i,1)*t(i,1)-k(i,1)*x1);

acr(i,1)=psi(i,1)*k(i,1)*9.81*(cosh(k(i,1)*(z+d))/cosh(k(i,1)*d))*cos(w(i,1)*
t(i,1)-k(i,1)*x1);
    fd(i,1)=0.5*po*Cd*D*U(i,1)*abs(U(i,1));
    fm(i,1)=0.25*3.14*D^2*po*Cm*acr(i,1);
    F(i,1)=((double(int(fd(i,1),z,-d,psi(i,1))))+(double(int(fm(i,1),z,-
d,psi(i,1)))))/10^6;
    pdf_height=pdf(pd_height,xxx);
    cdf_height=cdf(pd_height,xxx);
    pdf_period=pdf(pd_period,xxx);
    cdf_period=cdf(pd_period,xxx);

    if i>5
        subplot(2,2,1);
            histfit(F);
                xlabel('F, MN');
                ylabel('number of appearance, [1]');
                axis([0 120 0 inf]);

        subplot(2,2,2);
            f=0:0.01:120;
            pd_F=fitdist(F,'Normal');
            pdf_F=pdf(pd_F,f);
            cdf_F=cdf(pd_F,f);
            plot(i,pd_F.sigma/pd_F.mu*100,'.r'); hold on;
                grid on;
                axis([0 iterations 0 inf] )
```

```
            xlabel('iteration number');
            ylabel('\sigma / \mu, %');

        subplot(2,2,3);
        plot(f, cdf_F);
            xlabel('F, MN');
            ylabel('CDF(F), [1]');
            grid on;


        subplot(2,2,4);
            if i>6
                set(h1,'Visible','off');
                set(h2,'Visible','off');
                set(h3,'Visible','off');
                set(h4,'Visible','off');
                set(h5,'Visible','off');
                set(h6,'Visible','off');
                set(h7,'Visible','off');
            end
            edf_F=1-cdf_F;
            h1=plot(f, edf_F);hold on;
            set(gca, 'YScale', 'log');
            axis([0 120 10^-5 1]);
            xlabel('F, MN');
            ylabel('EDF(F), [1]');
            grid on;

            SL=max(find(edf_F>10^-1));
            a=SL;
            h2=stem(f(a),edf_F(a),'.g');
            xx=[0 f(a)]; yy=[edf_F(a) edf_F(a)];
            h3=plot(xx,yy,'g');

            ELIE=max(find(edf_F>10^-2));
            a=ELIE;
            h4=stem(f(a),edf_F(a),'.r');
            xx=[0 f(a)]; yy=[edf_F(a) edf_F(a)];
            h5=plot(xx,yy,'r');


            ALIE=max(find(edf_F>10^-4));
            a=ALIE;
            h6=stem(f(a),edf_F(a),'.black');
            xx=[0 f(a)]; yy=[edf_F(a) edf_F(a)];
            h7=plot(xx,yy,'black');

        pause(0.001);
    end
end
```

Ice load on the monopod structure (Global ice action)

```
clear all;
close all;

nu=0.3; %friction coefficient
alpha=30; %angle
C1=0.68*(sind(alpha)+nu*cosd(alpha))/(cosd(alpha)-nu*sind(alpha));
C2=(sind(alpha)+cosd(alpha)*nu)*((sind(alpha)+nu*cosd(alpha))/(cosd(alpha)-
nu*sind(alpha))+cotd(alpha));
pow=1025; %water density
E=8.7*10^9; %Young`s modulus of ice
hr=5; %Height of the rubble on the structure’s slope
poi=910

D=35;
I=1.1;
K1=0.9;
K2=1;

data=load('temp.dat');
apr=data(:,4);
x=0:0.01:2.5;
pd_ice=makedist('Normal','mu', 1.201, 'sigma',0.1021);
pd_sigmaC=makedist('Normal','mu', 1.41541, 'sigma',0.2690041);
iterations=300;
hFig = figure('units','normalized','outerposition',[0 0 1 1]);


for i=1:iterations
    h(i,1)=random(pd_ice);
    sigmaC(i,1)=random(pd_sigmaC);
    F(i,1)=sigmaC(i,1)*D*h(i,1);
    pdf_ice=pdf(pd_ice,x);
    cdf_ice=cdf(pd_ice,x);
    pdf_sigmaC=pdf(pd_sigmaC,x);
    cdf_sigmaC=cdf(pd_sigmaC,x);

    if i>5
        subplot(2,2,1);
            histfit(F);
                xlabel('F, MN');
                ylabel('number of appearance, [1]');
                axis([0 150 0 inf]);

        subplot(2,2,2);
            f=0:0.01:250;
            pd_F=fitdist(F,'Normal');
            pdf_F=pdf(pd_F,f);
            cdf_F=cdf(pd_F,f);
            plot(i,pd_F.sigma/pd_F.mu*100,'.r'); hold on;
                grid on;
                axis([0 iterations 0 inf] )
                xlabel('iteration number');
                ylabel('\sigma / \mu, %');

        subplot(2,2,3);
        plot(f, cdf_F);
            xlabel('F, MN');
            ylabel('CDF(F), [1]');
            grid on;
```

```
        subplot(2,2,4);
            if i>6
                set(h1,'Visible','off');
                set(h2,'Visible','off');
                set(h3,'Visible','off');
                set(h4,'Visible','off');
                set(h5,'Visible','off');
                set(h6,'Visible','off');
                set(h7,'Visible','off');
            end
            edf_F=1-cdf_F;
            h1=plot(f, edf_F);hold on;
            set(gca, 'YScale', 'log');
            axis([0 150 10^-5 1]);
            xlabel('F, MN');
            ylabel('EDF(F), [1]');
            grid on;

            SL=max(find(edf_F>10^-1));
            a=SL;
            h2=stem(f(a),edf_F(a),'.g');
            xx=[0 f(a)]; yy=[edf_F(a) edf_F(a)];
            h3=plot(xx,yy,'g');

            ELIE=max(find(edf_F>10^-2));
            a=ELIE;
            h4=stem(f(a),edf_F(a),'.r');
            xx=[0 f(a)]; yy=[edf_F(a) edf_F(a)];
            h5=plot(xx,yy,'r');


            ALIE=max(find(edf_F>10^-4));
            a=ALIE;
            h6=stem(f(a),edf_F(a),'.black');
            xx=[0 f(a)]; yy=[edf_F(a) edf_F(a)];
            h7=plot(xx,yy,'black');

        pause(0.001);
    end
end
```

Ice load on the monopod structure (Korzhavin equation)

```
clear all;
close all;

D=35;
I=1.1;
K1=0.9;
K2=1;

data=load('temp.dat');
apr=data(:,4);
x=0:0.01:2.5;
pd_ice=makedist('Normal','mu', 1.201, 'sigma',0.1021);
pd_sigmaC=makedist('Normal','mu', 1.41541, 'sigma',0.2690041);
iterations=300;
hFig = figure('units','normalized','outerposition',[0 0 1 1]);


for i=1:iterations
    h(i,1)=random(pd_ice);
    sigmaC(i,1)=random(pd_sigmaC);
    F(i,1)=I*K1*K2*sigmaC(i,1)*D*h(i,1);
    pdf_ice=pdf(pd_ice,x);
    cdf_ice=cdf(pd_ice,x);
    pdf_sigmaC=pdf(pd_sigmaC,x);
    cdf_sigmaC=cdf(pd_sigmaC,x);

    if i>5
        subplot(2,2,1);
            histfit(F);
                xlabel('F, MN');
                ylabel('number of appearance, [1]');
                axis([0 150 0 inf]);

        subplot(2,2,2);
            f=0:0.01:150;
            pd_F=fitdist(F,'Normal');
            pdf_F=pdf(pd_F,f);
            cdf_F=cdf(pd_F,f);
            plot(i,pd_F.sigma/pd_F.mu*100,'.r'); hold on;
                grid on;
                axis([0 iterations 0 inf] )
                xlabel('iteration number');
                ylabel('\sigma / \mu, %');

        subplot(2,2,3);
        plot(f, cdf_F);
            xlabel('F, MN');
            ylabel('CDF(F), [1]');
            grid on;


        subplot(2,2,4);
            if i>6
                set(h1,'Visible','off');
                set(h2,'Visible','off');
                set(h3,'Visible','off');
                set(h4,'Visible','off');
                set(h5,'Visible','off');
                set(h6,'Visible','off');
                set(h7,'Visible','off');
```

```
            end
            edf_F=1-cdf_F;
            h1=plot(f, edf_F);hold on;
            set(gca, 'YScale', 'log');
            axis([0 250 10^-5 1]);
            xlabel('F, MN');
            ylabel('EDF(F), [1]');
            grid on;

            SL=max(find(edf_F>10^-1));
            a=SL;
            h2=stem(f(a),edf_F(a),'.g');
            xx=[0 f(a)]; yy=[edf_F(a) edf_F(a)];
            h3=plot(xx,yy,'g');

            ELIE=max(find(edf_F>10^-2));
            a=ELIE;
            h4=stem(f(a),edf_F(a),'.r');
            xx=[0 f(a)]; yy=[edf_F(a) edf_F(a)];
            h5=plot(xx,yy,'r');


            ALIE=max(find(edf_F>10^-4));
            a=ALIE;
            h6=stem(f(a),edf_F(a),'.black');
            xx=[0 f(a)]; yy=[edf_F(a) edf_F(a)];
            h7=plot(xx,yy,'black');

        pause(0.001);
    end
end
```

Ice load on the monopod structure (ISO 19906)

```
clear all;
close all;

m=-0.16;
h1=1;
D=35;

data=load('temp.dat');
apr=data(:,4);
x=0:0.01:2.5;
pd_ice=makedist('Normal','mu', 1.201, 'sigma',0.1021);
pd_sigmaC=makedist('Normal','mu', 1.41541, 'sigma',0.2690041);
iterations=300;
hFig = figure('units','normalized','outerposition',[0 0 1 1]);


for i=1:iterations
    h(i,1)=random(pd_ice);
    sigmaC(i,1)=random(pd_sigmaC);
    if h(i,1)<1
        n(i,1)=-0.5+h(i,1)/5;
    else
        n(i,1)=-0.3;
    end;
    F(i,1)=D*h(i,1)*sigmaC(i,1)*(h(i,1))^n(i,1)*(D/h(i,1))^m;
    pdf_ice=pdf(pd_ice,x);
    cdf_ice=cdf(pd_ice,x);
    pdf_sigmaC=pdf(pd_sigmaC,x);
    cdf_sigmaC=cdf(pd_sigmaC,x);

    if i>5
        subplot(2,2,1);
            histfit(F);
                xlabel('F, MN');
                ylabel('number of appearance, [1]');
                axis([0 100 0 inf]);

        subplot(2,2,2);
            f=0:0.01:250;
            pd_F=fitdist(F,'Normal');
            pdf_F=pdf(pd_F,f);
            cdf_F=cdf(pd_F,f);
            plot(i,pd_F.sigma/pd_F.mu*100,'.r'); hold on;
                grid on;
                axis([0 iterations 0 inf] )
                xlabel('iteration number');
                ylabel('\sigma / \mu, %');

        subplot(2,2,3);
        plot(f, cdf_F);
            xlabel('F, MN');
            ylabel('CDF(F), [1]');
            grid on;


        subplot(2,2,4);
            if i>6
                set(h1,'Visible','off');
```

```
                set(h2,'Visible','off');
                set(h3,'Visible','off');
                set(h4,'Visible','off');
                set(h5,'Visible','off');
                set(h6,'Visible','off');
                set(h7,'Visible','off');
            end
            edf_F=1-cdf_F;
            h1=plot(f, edf_F);hold on;
            set(gca, 'YScale', 'log');
            axis([0 150 10^-5 1]);
            xlabel('F, MN');
            ylabel('EDF(F), [1]');
            grid on;

            SL=max(find(edf_F>10^-1));
            a=SL;
            h2=stem(f(a),edf_F(a),'.g');
            xx=[0 f(a)]; yy=[edf_F(a) edf_F(a)];
            h3=plot(xx,yy,'g');

            ELIE=max(find(edf_F>10^-2));
            a=ELIE;
            h4=stem(f(a),edf_F(a),'.r');
            xx=[0 f(a)]; yy=[edf_F(a) edf_F(a)];
            h5=plot(xx,yy,'r');


            ALIE=max(find(edf_F>10^-4));
            a=ALIE;
            h6=stem(f(a),edf_F(a),'.black');
            xx=[0 f(a)]; yy=[edf_F(a) edf_F(a)];
            h7=plot(xx,yy,'black');

        pause(0.001);
    end
end
```

Ice load on the monocone structure (ISO 19906)

```
clear all;
close all;

m=-0.16;
h1=1;
D=66;
sigmaF=0.52*10^6;%Pa
pow=1025; %water density
E=8.7*10^9; %Young`s modulus of ice
v=0.3;
g=9.81;
mu=0.3; %friction coefficient
alpha=52; %angle
xi=(sind(alpha)+mu*cosd(alpha))/(cosd(alpha)-mu*sind(alpha));
hr=5; %Height of the rubble on the structure’s slope
poi=910;
mui=0.3;
e=0.4;
teta=alpha-10;
fi=45;
C=4*10^3; %Pa

data=load('temp.dat');
apr=data(:,4);
x=0:0.01:2.5;
pd_ice=makedist('Normal','mu', 1.201, 'sigma',0.1021);
iterations=300;
hFig = figure('units','normalized','outerposition',[0 0 1 1]);


for i=1:iterations
    h(i,1)=random(pd_ice);
    Lc(i,1)=(E*h(i,1)^3/(12*pow*g*(1-v^2)))^0.25;
    lc(i,1)=D+3.14^2/4*Lc(i,1);
    Hb(i,1)=0.68*xi*sigmaF*lc(i,1)*(pow*g*h(i,1)^5/E)^0.25;

    Hp(i,1)=D*hr^2*mui*poi*g*(1-e)*(1-
tand(teta)/tand(alpha))^2*(1/(2*tand(teta)));

    P(i,1)=(0.5*(mui+mu)*(1-e)*hr*(mui*((sind(alpha)/tand(teta))-
cosd(alpha))+cosd(alpha)/tand(alpha))*(1-
tand(teta)/tand(alpha))+h(i,1)*(sind(alpha)+mu*cosd(alpha))/sind(alpha));
    Hr(i,1)=P(i,1)*(D*poi*g*hr/(cosd(alpha)-mu*sind(alpha)));

    Hl(i,1)=D*hr*xi*(1-tand(teta)/tand(alpha))*(0.5*hr*poi*g*(1-
e)*(1/tand(teta)-1/tand(alpha)+tand(fi)*(1-tand(teta)/tand(alpha)))+C);

    Ht(i,1)=1.5*D*h(i,1)^2*poi*g*(cosd(alpha)/(sind(alpha)-mu*cosd(alpha)));

    F(i,1)=(Hb(i,1)+Hp(i,1)+Hr(i,1)+Hl(i,1)+Ht(i,1))/(1-
(Hb(i,1)/(sigmaF*lc(i,1)*h(i,1))))/10^6;

    pdf_ice=pdf(pd_ice,x);
    cdf_ice=cdf(pd_ice,x);


    if i>5
        subplot(2,2,1);
```

```
            histfit(F);
                xlabel('F, MN');
                ylabel('number of appearance, [1]');
                axis([0 50 0 inf]);

        subplot(2,2,2);
            f=0:0.01:250;
            pd_F=fitdist(F,'Normal');
            pdf_F=pdf(pd_F,f);
            cdf_F=cdf(pd_F,f);
            plot(i,pd_F.sigma/pd_F.mu*100,'.r'); hold on;
                grid on;
                axis([0 iterations 0 inf] )
                xlabel('iteration number');
                ylabel('\sigma / \mu, %');

        subplot(2,2,3);
        plot(f, cdf_F);
            xlabel('F, MN');
            ylabel('CDF(F), [1]');
            grid on;

        subplot(2,2,4);
            if i>6
                set(h1,'Visible','off');
                set(h2,'Visible','off');
                set(h3,'Visible','off');
                set(h4,'Visible','off');
                set(h5,'Visible','off');
                set(h6,'Visible','off');
                set(h7,'Visible','off');
            end
            edf_F=1-cdf_F;
            h1=plot(f, edf_F);hold on;
            set(gca, 'YScale', 'log');
            axis([0 150 10^-5 1]);
            xlabel('F, MN');
            ylabel('EDF(F), [1]');
            grid on;

            SL=max(find(edf_F>10^-1));
            a=SL;
            h2=stem(f(a),edf_F(a),'.g');
            xx=[0 f(a)]; yy=[edf_F(a) edf_F(a)];
            h3=plot(xx,yy,'g');

            ELIE=max(find(edf_F>10^-2));
            a=ELIE;
            h4=stem(f(a),edf_F(a),'.r');
            xx=[0 f(a)]; yy=[edf_F(a) edf_F(a)];
            h5=plot(xx,yy,'r');

             ALIE=max(find(edf_F>10^-4));
            a=ALIE;
            h6=stem(f(a),edf_F(a),'.black');
            xx=[0 f(a)]; yy=[edf_F(a) edf_F(a)];
            h7=plot(xx,yy,'black');

        pause(0.001);
    end
end
```